

HIGH HYDROSTATIC PRESSURE INDUCED INACTIVATION KINETICS
OF *E. COLI* O157:H7 AND *S. AUREUS* IN CARROT JUICE AND ANALYSIS
OF CELL VOLUME CHANGE

A THESIS SUBMITTED TO
THE GRADUATE SCHOOL OF NATURAL AND APPLIED SCIENCES
OF
MIDDLE EAST TECHNICAL UNIVERSITY

BY

MUTLU PİLAVTEPE

IN PARTIAL FULFILLMENT OF THE REQUIREMENTS
FOR
THE DEGREE OF DOCTOR OF PHILOSOPHY
IN
FOOD ENGINEERING

DECEMBER 2007

Approval of the thesis:

HIGH HYDROSTATIC PRESSURE INDUCED INACTIVATION KINETICS
OF *E. COLI* O157:H7 AND *S. AUREUS* IN CARROT JUICE AND ANALYSIS
OF CELL VOLUME CHANGE

submitted by **MUTLU PİLAVTEPE** in partial fulfillment of the requirements for
the degree of **Doctor of Philosophy in Food Engineering Department, Middle
East Technical University** by,

Prof. Dr. Canan Özgen
Dean, Graduate School of **Natural and Applied Sciences** _____

Prof. Dr. Zümrüt Begüm Ögel
Head of Department, **Food Engineering** _____

Assoc. Prof. Dr. Hami Alpas
Supervisor, **Food Engineering Dept., METU** _____

Prof. Dr. Faruk Bozoğlu
Co-Supervisor, **Food Engineering Dept., METU** _____

Examining Committee Members

Prof. Dr. Levent Bayındırlı
Food Engineering Dept., METU _____

Assoc. Prof. Dr. Hami Alpas
Food Engineering Dept., METU _____

Prof. Dr. Alev Bayındırlı
Food Engineering Dept., METU _____

Prof. Dr. Yaşar Kemal Erdem
Food Engineering Dept., Hacettepe University _____

Assoc.Prof.Dr. Dilek Sivri Özay
Food Engineering Dept., Hacettepe University _____

Date: December 27th, 2007

I hereby declare that all information in this document has been obtained and presented in accordance with academic rules and ethical conduct. I also declare that, as required by these rules and conduct, I have fully cited and referenced all material and results that are not original to this work.

Name, Last name : Mutlu Pilavtepe

Signature :

ABSTRACT

HIGH HYDROSTATIC PRESSURE INDUCED INACTIVATION KINETICS OF *E. COLI* O157:H7 AND *S. AUREUS* IN CARROT JUICE AND ANALYSIS OF CELL VOLUME CHANGE

Pilavtepe, Mutlu

Ph.D., Department of Food Engineering

Supervisor: Assoc. Prof. Dr. Hami Alpas

Co-Supervisor: Prof. Dr. Faruk Bozođlu

December 2007, 182 pages

The main objective of this study was to determine the pressure induced inactivation mechanism of pressure-resistant *Escherichia coli* O157:H7 933 and *Staphylococcus aureus* 485 in a low acid food.

Firstly, inactivation curves of pathogens were obtained at 200 to 400 MPa at 40°C in peptone water and carrot juice. First-order and Weibull models were fitted and Weibull model described the inactivation curves of both pathogens more accurately than first-order model, revealing that food systems could exhibit either protective or sensitizing effect on microorganisms. Carrot juice had a protective effect on *E. coli* O157:H7 whereas it had a sensitizing effect on *S. aureus*, due to

the naturally occurring constituents or phytoalexins in carrot roots that could have a toxic effect.

Secondly, scanning electron microscopy (SEM) and fluorescent microscopy images of studied pathogens were taken. Developed software was used to analyze SEM images to calculate the change in the view area and volume of cells. Membrane integrity of pressurized cells was also examined using fluorescent microscopy images.

The increase in average values of the view area and volume of both pathogens was significant for the highest pressure levels studied.. The increase in volume and the view area could be explained by the modification of membrane properties, i.e., disruption or increase in permeability, lack of membrane integrity, denaturation of membrane-bound proteins and pressure-induced phase transition of membrane lipid bilayer. The change in volume and the view area of microorganisms added another dimension to the understanding of inactivation mechanisms of microbial cells by HHP.

Keywords: High Hydrostatic Pressure, *Escherichia coli* O157:H7, *Staphylococcus aureus*, Weibull Model, Image Analysis.

ÖZ

***E. COLI* O157:H7 VE *S. AUREUS*'UN HAVUÇ SUYUNDA YÜKSEK HİDROSTATİK BASINCA BAĞLI İNAKTİVASYON KİNETİĞİ VE HÜCRESEL HACİM DEĞİŞİKLİĞİ ANALİZİ**

Pilavtepe, Mutlu

Doktora, Gıda Mühendisliği Bölümü

Tez Yöneticisi: Doç. Dr. Hami Alpas

Ortak Tez Yöneticisi: Prof. Dr. Faruk Bozoğlu

Aralık 2007, 182 sayfa

Bu tezin ana amacı, basınca dirençli *Escherichia coli* O157:H7 933 ve *Staphylococcus aureus* 485' in düşük asitli bir gıdada basınca bağlı inaktivasyon kinetiğini ve mekanizmasını belirlemektir.

Çalışmanın birinci bölümünde, çalışılan patojenlerin inaktivasyon eğrileri 200-400 MPa ve 40°C'de peptonlu su ve havuç suyunda elde edilmiştir. Mikrobiyal inaktivasyon, birinci derece reaksiyon kinetiği ve Weibull dağılımı ile modellenmiştir. Weibull dağılımının inaktivasyon eğrilerini daha iyi betimlediği belirlenmiştir. Havuç suyunun *E. coli* O157:H7 üzerine koruyucu etkisi varken, *S. aureus* üzerine inhibe edici etkisi olduğu gözlenmiştir. Bu etkinin, havuç köklerinde doğal olarak bulunan bileşiklerin veya fitoaleksinlerin *S. aureus*

üzerindeki toksik etkisinden kaynaklanabileceği bulunmuştur. Yüksek hidrostatik basınç (YHB) ve fitoaleksinlerin kombine kullanımı, basınca direçli *S. aureus* ve diğer Gram- pozitif bakterilere karşı potansiyel antibakteriyel uygulama olabilir.

Çalışmanın ikinci bölümünde, farklı basınç uygulamalarında her iki patojenin taramalı elektron ve floresans mikroskopu ile görüntüleri elde edilmiştir. SEM mikrografikleri kullanılarak görüntü analizi metodu ile bakteri hücrelerinin yüzey alanını ve hacmini hesaplamak için bir bilgisayar programı geliştirilmiştir. Basınçlanmış hücrelerin membran bütünlüğü de floresans mikroskopu görüntüleri ile incelenmiştir.

Her iki patojenin yüzey alanı ve hacmi çalışılan en yüksek basınç değerlerinde önemli bir artış göstermiştir. *E. coli* O157:H7 hücreleri 200 MPa basınç değerinde de yüzey alanı ve hacim olarak önemli bir artış göstermiştir. Bu basınçlar altında yüzey alanı ve hacimdeki artışlar membranın yapısındaki bir takım değişiklikler, örneğin, geçirgenliğin kaybolması veya artması, membran bütünlüğünün bozulması, membrana bağlı proteinlerin denatürasyonu ve membran yağ tabakasındaki faz değişimi ile açıklanabilmektedir. Mikroorganizmaların yüzey alanı ve hacimlerdeki değişikliklerin hesaplanarak basınç inaktivasyon mekanizmasının irdelenmesi literatüre yeni bir boyut eklemiştir.

Anahtar Kelimeler: Yüksek Hidrostatik Basınç, *Escherichia coli* O157:H7, *Staphylococcus aureus*, , Weibull Modeli, Görüntü Analizi.

To My Family

ACKNOWLEDGEMENTS

I wish to express my deepest gratitude to my supervisor Assoc. Prof. Dr. Hami Alpas and co-supervisor Prof. Dr. Faruk Bozođlu for their guidance, advice, criticism, encouragements and insight throughout the research.

I want to extent my thanks to Prof. Dr. Murat Balaban and Prof. Dr. Ahmed Yousef for their help and encouragement during my research experience at University of Florida, Gainesville, Florida, USA and Ohio State University, Columbus, Ohio, USA. I would also like to thank Prof. Dr. Levent Bayındırlı and Prof. Dr. Yaşar Kemal Erdem for their suggestions and comments.

I would like to express my thanks to Brian Kemmenoe and Kathy Wolken at the Campus Facility and Imaging Facility, Ohio State University, OH, USA for their assistance with the SEM studies.

This study was supported through a grant from METU- BAP-08-11DPT2002K120510-GT-4.

My special thanks go to my research group friend, Sencer Buzrul for his support during all parts of this study. I would also like to express my thanks to my roommate Özlem Ergezer for her great support during hard times of this study.

Knowing that whenever I am in trouble there is a friend ready to help me makes everything easier, I want to thank Erkan Karacabey for his great support and patience.

My thanks are attended to my other office-mates, especially Özge Şakıyan and Nadide Seyhun. Sharing both bad and good moments with friends is the best part of the life.

Finally, I would like to express my deepest gratitude to my family; my fiancé, Cenk Çelik, my mother Filiz Pilavtepe, my father Halil Pilavtepe, and my sister Müge Pilavtepe for their love, endless patience and encouragement. Any word is not enough to express my appreciation to them. With love, I dedicate this work to them.

TABLE OF CONTENTS

ABSTRACT.....	iv
ÖZ.....	vi
DEDICATION.....	viii
ACKNOWLEDGEMENTS.....	ix
TABLE OF CONTENTS.....	xi
LIST OF TABLES.....	xv
LIST OF FIGURES.....	xx
CHAPTER	
1. INTRODUCTION.....	1
1.1 History of HHP.....	2
1.2 Working Principle of HHP.....	3
1.3 HHP Systems.....	4
1.4 Commercial Applications of HHP.....	10
1.5 Effect of HHP on Molecules.....	13
1.5.1 Effect of HHP on Proteins.....	13
1.5.2 Effect of HHP on Lipids.....	15
1.5.3 Effect of HHP on Starch.....	16
1.5.4 Effect of HHP on Water.....	17
1.6 Effect of HHP on Microorganisms.....	19
1.6.1 Bacterial Cells.....	20
1.6.2 Bacterial Spores.....	22
1.6.3 Fungi.....	24

1.6.4	Viruses.....	24
1.7	Mechanisms of Microbial Inactivation by HHP.....	25
1.7.1	HHP Effects on Cell Morphology.....	25
1.7.2	HHP Effects on Cellular Components.....	26
1.8	Injury due to HHP.....	28
1.9	The Hurdle Concept.....	29
1.9.1	HHP and Low pH.....	30
1.9.2	HHP and Antimicrobial Agents.....	30
1.9.3	HHP and Mild Heat.....	31
1.9.4	HHP and Water Activity (a_w).....	31
1.10	Effect of HHP on Microorganisms in Food Systems.....	32
1.11	HHP Inactivation Kinetics of Microorganisms.....	33
1.11.1	First-order Model.....	33
1.11.2	Non-linear Models.....	36
1.12	Aim of the Study.....	40
2.	MATERIALS AND METHODS.....	43
2.1	Materials.....	43
2.1.1	High Hydrostatic Pressure (HHP) Equipment.....	43
2.1.2	Cultures and Media.....	44
2.1.3	Raw Material.....	45
2.2	Methods.....	45
2.2.1	Determination of Early Stationary Growth Phase.....	45
2.2.2	Preparation and Inoculation of Carrot Juice and Model System.....	46
2.2.3	Determination of pH.....	46
2.2.4	HHP Treatment.....	47
2.2.5	Enumeration of Viable Cells.....	47

2.2.6	Modeling of the Inactivation Curves.....	48
2.2.6.1	First-order Kinetics.....	48
2.2.6.2	Weibull Model.....	48
2.2.7	SEM Analysis.....	49
2.2.8	Fluorescent Microscopy.....	50
2.2.9	Machine Vision Analysis.....	51
2.2.10	Data Analysis.....	56
2.2.10.1	Model Evaluation.....	56
2.2.10.2	Statistical Analysis.....	57
3.	RESULTS AND DISCUSSION.....	58
3.1	Inactivation of <i>Escherichia coli</i> O157:H7 933 and <i>Staphylococcus aureus</i> 485 by High Hydrostatic Pressure (HHP) in Carrot Juice.....	58
3.1.1	Pressure Inactivation Curves of Foodborne Pathogens.....	58
3.1.2	Modeling of Inactivation Kinetics.....	63
3.1.3	Parameters of the Models.....	69
3.1.4	Pressure Dependence of Model Parameters.....	74
3.1.5	Effect of External Factors on Inactivation Curves.....	78
3.2	Morphological Changes.....	80
3.3	Membrane Integrity.....	88
3.4	Machine Vision Based Quantification of Bacterial Volume Change with HHP.....	91
3.4.1	View Area and Volume Distributions with Pressure..	91
3.4.2	Volume Change Related Inactivation Mechanism.....	97
4.	CONCLUSIONS AND RECOMMENDATIONS.....	101
	REFERENCES.....	103

APPENDICES

A.	GROWTH CURVES.....	114
B.	EFFECT OF VARIABLES ON MACHINE VISION ANALYSIS	117
B.1	Effect of Software Variables on Volume Calculations.....	117
B.2	Effect of SEM Magnification on Calculation of View Area..	119
C.	MODELING AND REGRESSION RESULTS.....	126
C.1	First Order Modeling of Inactivation Curves.....	126
C.2	Regression Results of First Order and Weibull Models.....	130
D.	TABLE OF EQUATIONS.....	149
E.	VIEW AREA AND VOLUME CALCULATIONS.....	168
F.	ANOVA AND TUKEY'S COMPARISON TABLES.....	175
	CURRICULUM VITAE.....	180

LIST OF TABLES

TABLE

1.1	Current Applications of HHP.....	12
1.2	Temperature change due to adiabatic compression for selected substances.....	19
3.1	Comparison of the first-order and Weibull models for the inactivation curves of foodborne pathogens in peptone water (PW) and carrot juice (CJ) at 40°C.....	68
3.2	Parameters of the Weibull and first-order models in peptone water (PW) and carrot juice (CJ) at 40°C.....	70
3.3	Process times calculated to accomplish 5-log ₁₀ reduction in peptone water (PW) and carrot juice (CJ) at 40°C by using Weibull distribution and first-order kinetics.....	73
3.4	Antibacterial activities of 6- methoxymellein.....	79
3.5	Average values of view area and volume of <i>E. coli</i> O157:H7 933 and <i>S. aureus</i> 485 for each pressure treatment at 40°C.....	95
B.1.1	Error analysis of the volume calculation of test image.....	118
B.2.1	View area results of <i>S. aureus</i> 485 cells calculated by LenseEye Software from Fig. B.2.2.....	120
B.2.2	View area results of <i>S. aureus</i> 485 cells calculated by LenseEye Software from Fig. B.2.4.....	121
B.2.3	View area results of <i>S. aureus</i> 485 cells calculated by LenseEye Software from Fig. B.2.6.....	123

B.2.4	View area results of <i>S. aureus</i> 485 cells calculated by LenseEye Software from Fig. B.2.8.....	124
B.2.5	Error analysis of magnification level for the view area calculations (common cells at different magnification levels are indicated as bold in Tables B.1.1-B.1.4).....	125
C.2.1	Regression results from Sigma Plot for <i>E. coli</i> O157:H7 933 in peptone water for first-order model at 200 MPa.....	130
C.2.2	Regression results from Sigma Plot for <i>E. coli</i> O157:H7 933 in peptone water for first-order model at 250 MPa.....	131
C.2.3	Regression results from Sigma Plot for <i>E. coli</i> O157:H7 933 in peptone water for first-order model at 275 MPa.....	131
C.2.4	Regression results from Sigma Plot for <i>E. coli</i> O157:H7 933 in peptone water for first-order model at 300 MPa.....	132
C.2.5	Regression results from Sigma Plot for <i>E. coli</i> O157:H7 933 in peptone water for first-order model at 325 MPa.....	132
C.2.6	Regression results from Sigma Plot for <i>E. coli</i> O157:H7 933 in carrot juice for first-order model at 200 MPa.....	133
C.2.7	Regression results from Sigma Plot for <i>E. coli</i> O157:H7 933 in carrot juice for first-order model at 250 MPa.....	133
C.2.8	Regression results from Sigma Plot for <i>E. coli</i> O157:H7 933 in carrot juice for first-order model at 275 MPa.....	134
C.2.9	Regression results from Sigma Plot for <i>E. coli</i> O157:H7 933 in carrot juice for first-order model at 300 MPa.....	134
C.2.10	Regression results from Sigma Plot for <i>E. coli</i> O157:H7 933 in carrot juice for first-order model at 325 MPa.....	135
C.2.11	Regression results from Sigma Plot for <i>E. coli</i> O157:H7 933 in peptone water for Weibull model at 200 MPa.....	135

C.2.12	Regression results from Sigma Plot for <i>E. coli</i> O157:H7 933 in peptone water for Weibull model at 250 MPa.....	136
C.2.13	Regression results from Sigma Plot for <i>E. coli</i> O157:H7 933 in peptone water for Weibull model at 275 MPa.....	136
C.2.14	Regression results from Sigma Plot for <i>E. coli</i> O157:H7 933 in peptone water for Weibull model at 300 MPa.....	137
C.2.15	Regression results from Sigma Plot for <i>E. coli</i> O157:H7 933 in peptone water for Weibull model at 325 MPa.....	137
C.2.16	Regression results from Sigma Plot for <i>E. coli</i> O157:H7 933 in carrot juice for Weibull model at 200 MPa.....	138
C.2.17	Regression results from Sigma Plot for <i>E. coli</i> O157:H7 933 in carrot juice for Weibull model at 250 MPa.....	138
C.2.18	Regression results from Sigma Plot for <i>E. coli</i> O157:H7 933 in carrot juice for Weibull model at 275 MPa.....	139
C.2.19	Regression results from Sigma Plot for <i>E. coli</i> O157:H7 933 in carrot juice for Weibull model at 300 MPa.....	139
C.2.20	Regression results from Sigma Plot for <i>E. coli</i> O157:H7 933 in carrot juice for Weibull model at 325 MPa.....	140
C.2.21	Regression results from Sigma Plot for <i>S. aureus</i> 485 in peptone water for first-order model at 200 MPa.....	140
C.2.22	Regression results from Sigma Plot for <i>S. aureus</i> 485 in peptone water for first-order model at 250 MPa.....	141
C.2.23	Regression results from Sigma Plot for <i>S. aureus</i> 485 in peptone water for first-order model at 300 MPa.....	141
C.2.24	Regression results from Sigma Plot for <i>S. aureus</i> 485 in peptone water for first-order model at 350 MPa.....	142
	Regression results from Sigma Plot for <i>S. aureus</i> 485 in peptone	

C.2.25	water for first-order model at 400 MPa.....	142
C.2.26	Regression results from Sigma Plot for <i>S. aureus</i> 485 in carrot juice for first-order model at 300 MPa.....	143
C.2.27	Regression results from Sigma Plot for <i>S. aureus</i> 485 in carrot juice for first-order model at 350 MPa.....	143
C.2.28	Regression results from Sigma Plot for <i>S. aureus</i> 485 in carrot juice for first-order model at 400 MPa.....	144
C.2.29	Regression results from Sigma Plot for <i>S. aureus</i> 485 in peptone water for Weibull model at 200 MPa.....	144
C.2.30	Regression results from Sigma Plot for <i>S. aureus</i> 485 in peptone water for Weibull model at 250 MPa.....	145
C.2.31	Regression results from Sigma Plot for <i>S. aureus</i> 485 in peptone water for Weibull model at 300 MPa.....	145
C.2.32	Regression results from Sigma Plot for <i>S. aureus</i> 485 in peptone water for Weibull model at 350 MPa.....	146
C.2.33	Regression results from Sigma Plot for <i>S. aureus</i> 485 in peptone water for Weibull model at 400 MPa.....	146
C.2.34	Regression results from Sigma Plot for <i>S. aureus</i> 485 in carrot juice for Weibull model at 300 MPa.....	147
C.2.35	Regression results from Sigma Plot for <i>S. aureus</i> 485 in carrot juice for Weibull model at 350 MPa.....	147
C.2.36	Regression results from Sigma Plot for <i>S. aureus</i> 485 in carrot juice for Weibull model at 400 MPa.....	148
D.1	Table Curve 3D equation list for <i>E. coli</i> O157:H7 933 pressurized in peptone water.....	149
D.2	Table Curve 3D equation list for <i>E. coli</i> O157:H7 933 pressurized in carrot juice.....	154

D.3	Table Curve 3D equation list for <i>S. aureus</i> 485 pressurized in peptone water.....	158
D.4	Table Curve 3D equation list for <i>S. aureus</i> 485 pressurized in carrot juice.....	163
E.1	View area results <i>E. coli</i> O157:H7 933 cells calculated by LenseEye Software from Fig. E.2.....	169
E.2	Volume results of <i>E. coli</i> O157:H7 933 cells calculated by LenseEye Software from Fig. E.2.....	171
E.3	View area results of <i>S. aureus</i> 485 cells calculated by LenseEye Software from Fig. E.8.....	172
E.4	Volume results of <i>S. aureus</i> 485 cells calculated by LenseEye Software from Fig. E.8.....	174
F.1	One-way ANOVA results for view area values of <i>E. coli</i> O157:H7 933.....	175
F.2	Tukey's pairwise comparisons for view area values of <i>E. coli</i> O157:H7 933.....	176
F.3	One-way ANOVA results for transformed volume (log volume) values of <i>E. coli</i> O157:H7 933.....	176
F.4	Tukey's pairwise comparisons for transformed volume (log volume) values of <i>E. coli</i> O157:H7 933.....	177
F.5	One-way ANOVA results for area values of <i>S. aureus</i> 485.....	177
F.6	Tukey's pairwise comparisons for area values of <i>S. aureus</i> 485.....	178
F.7	One-way ANOVA results for transformed volume (log volume) values of <i>S. aureus</i> 485.....	178
F.8	Tukey's pairwise comparisons for transformed volume (log volume) values of <i>S. aureus</i> 485.....	179

LIST OF FIGURES

FIGURE

1.1	A typical high-pressure processing system for treating pre-packaged foods.....	5
1.2	Direct pressure generator.....	6
1.3	Indirect pressure generator.....	7
1.4	A multivessel arrangement for semi-continuous high-pressure processing.....	9
1.5	Commonly observed types of survival curves. Left plot: Linear [A], Downward concave [B], Upward concave [C] and biphasic [D]. Right plot: Linear with a preceding shoulder [E], Sigmoidal I – starting with a downward concavity and ending up with an upward concavity [F], Sigmoidal II – starting with a upward concavity and ending up with an downward concavity [G], Linear with tailing [H].....	37
2.1	SEM micrograph of pressurized (325 MPa- 1 min- 40°C) <i>E. coli</i> O157:H7 933.....	51
2.2	Isolated organisms from Figure 1, with size reference square.....	52
2.3	An isolated organism, its perimeter and its curve of symmetry obtained by image analysis.....	53
2.4	Volume calculation details for the organism in Figure 3, with different number of volume slices.....	54
2.5	Test image to confirm volume calculation accuracy.....	55
2.6	Volume calculation details for different organisms.....	56

3.1	Inactivation curves of <i>E. coli</i> O157:H7 933 for 200 MPa and 250 MPa in peptone water (pH= 6.95) at 40 °C.....	59
3.2	Inactivation curves of <i>E. coli</i> O157:H7 933 for 275 MPa, 300 MPa and 325 MPa in peptone water (pH= 6.95) at 40 °C.....	60
3.3	Inactivation curves of <i>E. coli</i> O157:H7 933 for 200 MPa and 250 MPa in carrot juice (pH= 6.22) at 40 °C.....	60
3.4	Inactivation curves of <i>E. coli</i> O157:H7 933 for 275 MPa, 300 MPa and 325 MPa in carrot juice (pH= 6.22) at 40 °C.....	61
3.5	Inactivation curves of <i>S. aureus</i> 485 for 200 MPa and 250 MPa in peptone water (pH= 6.95) at 40 °C.....	61
3.6	Inactivation curves of <i>S. aureus</i> 485 for 300 MPa, 350 MPa and 400 MPa in peptone water (pH= 6.95) at 40 °C.....	62
3.7	Inactivation curves of <i>S. aureus</i> 485 for 300 MPa, 350 MPa and 400 MPa in carrot juice (pH= 6.22) at 40 °C.....	62
3.8	Inactivation curves of <i>E. coli</i> O157:H7 933 at different pressure levels (●, 200 MPa; ○, 250 MPa; ▼, 275 MPa; ▽, 300 MPa; ■, 325 MPa) in peptone water (pH= 6.95) at 40°C modeled with Weibull distribution.....	64
3.9	Inactivation curves of <i>E. coli</i> O157:H7 933 at different pressure levels (●, 200 MPa; ○, 250 MPa; ▼, 275 MPa; ▽, 300 MPa) in carrot juice (pH= 6.22) at 40°C modeled with Weibull distribution.....	65
3.10	Inactivation curves of <i>S. aureus</i> 485 at different pressure levels (●, 200 MPa; ○, 250 MPa; ▼, 275 MPa; ▽, 300 MPa; ■, 325 MPa) in peptone water (pH= 6.95) at 40°C modeled with Weibull distribution.....	66

3.11	Inactivation curves of <i>S. aureus</i> 485 at different pressure levels (●, 300 MPa; ○, 350 MPa; ▼, 400 MPa) in carrot juice (pH= 6.22) at 40°C modeled with Weibull distribution.....	67
3.12	Dependence of scale factor (α) on pressure (MPa) and shape factor (β) for <i>E. coli</i> O157:H7 933 in peptone water.....	75
3.13	Dependence of scale factor (α) on pressure (MPa) and shape factor (β) for <i>E. coli</i> O157:H7 933 in carrot juice.....	76
3.14	Dependence of scale factor (α) on pressure (MPa) and shape factor (β) for <i>S. aureus</i> 485 in peptone water.....	77
3.15	SEM micrograph of unpressurized <i>E. coli</i> O157:H7 933.....	81
3.16	SEM micrograph of pressurized (200 MPa- 1 min- 40°C) <i>E. coli</i> O157:H7 933.....	81
3.17	SEM micrograph of pressurized (250 MPa- 1 min- 40°C) <i>E. coli</i> O157:H7 933.....	82
3.18	SEM micrograph of pressurized (275 MPa- 1 min- 40°C) <i>E. coli</i> O157:H7 933.....	82
3.19	SEM micrograph of pressurized (300 MPa- 1 min- 40°C) <i>E. coli</i> O157:H7 933.....	83
3.20	SEM micrograph of pressurized (325 MPa- 1 min- 40°C) <i>E. coli</i> O157:H7 933.....	83
3.21	SEM micrograph of unpressurized <i>S. aureus</i> 485.....	84
3.22	SEM micrograph of pressurized (200 MPa- 5 min- 40 °C) <i>S. aureus</i> 485.....	85
3.23	SEM micrograph of pressurized (250 MPa- 5 min- 40 °C) <i>S. aureus</i> 485.....	86
3.24	SEM micrograph of pressurized (300 MPa- 5 min- 40 °C) <i>S. aureus</i> 485.....	86

3.25	SEM micrograph of pressurized (350 MPa- 5 min- 40 °C) <i>S. aureus</i> 485.....	87
3.26	SEM micrograph of pressurized (400 MPa- 5 min- 40 °C) <i>S. aureus</i> 485.....	87
3.27	Fluorecent microscopy image of (a) unpressurized, pressurized at (b) 200 MPa- 1 min- 40°C, (c) 250 MPa- 1 min- 40°C, (d) 275 MPa- 1 min- 40°C, (e) 300 MPa- 5 min- 40°C, (f) 325 MPa- 5 min- 40°C, <i>E. coli</i> O157:H7 933.....	89
3.28	Fluorecent microscopy image of (a) unpressurized, pressurized at (b) 200 MPa- 5 min- 40°C, (c) 250 MPa- 5 min- 40°C, (d) 300 MPa- 5 min- 40°C, (e) 350 MPa- 5 min- 40°C, (f) 400 MPa- 5 min- 40°C, <i>S. aureus</i> 485.....	90
3.29	Area distributions of <i>E. coli</i> O157:H7 933 cells under different pressure treatments at 40°C.....	92
3.30	Volume distributions of <i>E. coli</i> O157:H7 933 cells under different pressure treatments at 40°C.....	93
3.31	Area distributions of <i>S. aureus</i> 485 cells under different pressure treatments at 40°C.....	93
3.32	Volume distributions of <i>S. aureus</i> 485 cells under different pressure treatments at 40°C.....	94
A.1	Growth curve of <i>E. coli</i> O157:H7 933.....	114
A.2	Growth curve of <i>E. coli</i> O157:H7 933.....	115
A.3	Growth curve of <i>S. aureus</i> 485.....	115
A.4	Growth curve of <i>S. aureus</i> 485.....	116
B.1.1	Details of the volume calculation of test image. Zero degrees rotation, 80 points on the perimeter, and 15 slices.....	117

B.1.2	Details of the volume calculation of the test image. Rotation angle -5, 200 points on the perimeter, and 30 slices.....	117
B.2.1	SEM micrograph of unpressurized <i>S. aureus</i> 485 with a magnification of x 25 000.....	119
B.2.2	Isolated organisms from Figure B.2.1, with size reference square.....	119
B.2.3	SEM micrograph of unpressurized <i>S. aureus</i> 485 with a magnification of x 20 000.....	120
B.2.4	Isolated organisms from Figure B.2.3, with size reference square.....	121
B.2.5	SEM micrograph of unpressurized <i>S. aureus</i> 485 with a magnification of x 15 000.....	122
B.2.6	Isolated organisms from Figure B.2.5, with size reference square.....	122
B.2.7	SEM micrograph of unpressurized <i>S. aureus</i> 485 with a magnification of x 10 000.....	123
B.2.8	Isolated organisms from Figure B.2.7, with size reference square.....	124
C.1.1	Inactivation curves of <i>E. coli</i> O157:H7 933 in peptone water (0.1% peptone, pH 6.95) at different pressure levels (●, 200 MPa; ○, 250 MPa; ▼, 275 MPa; ▽, 300 MPa; ■, 325 MPa) at 40°C	126
C.1.2	Inactivation curves of <i>E. coli</i> O157:H7 933 in carrot juice (pH 6.22) at different pressure levels (●, 200 MPa; ○, 250 MPa; ▼, 275 MPa; ▽, 300 MPa; ■, 325 MPa) at 40°C.....	127
C.1.3	Inactivation curves of <i>S. aureus</i> 485 in peptone water (0.1% peptone, pH 6.95) at different pressure levels (●, 200 MPa; ○, 250 MPa; ▼, 300 MPa; ▽, 350 MPa; ■, 400 MPa) at 40°C.....	128
C.1.4	Inactivation curves of <i>S. aureus</i> 485 in carrot juice (pH 6.22) at different pressure levels (●, 300 MPa; ○, 350 MPa; ▼, 400 MPa) at 40°C.....	129

E.1	SEM micrograph of unpressurized <i>E. coli</i> O157:H7 933.....	168
E.2	Isolated organisms of unpressurized <i>E. coli</i> O157:H7 933 as area objects, with size reference square.....	169
E.3	Rotated (rotation angle= 0°) volume image of object 2 from Fig. E.2...	170
E.4	Rotated (rotation angle= -16°) volume image of object 3 from Fig. E.2	170
E.5	Rotated (rotation angle= -14°) volume image of object 4 from Fig. E.2	170
E.6	Rotated (rotation angle= 10°) volume image of object 5 from Fig. E.2.	170
E.7	SEM micrograph of pressurized (300 MPa- 5 min- 40°C) <i>S. aureus</i> 485.....	171
E.8	Isolated organisms of pressurized (300 MPa- 5 min- 40°C) <i>S. aureus</i> 485 as area objects, with size reference square.....	172
E.9	Rotated (rotation angle= 5°) volume image of object 2 from Fig. E.8.	173
E.10	Rotated (rotation angle= 1°) volume image of object 3 from Fig. E.8.	173
E.11	Rotated (rotation angle= 17°) volume image of object 4 from Fig. E.8.	173
E.12	Rotated (rotation angle= 14°) volume image of object 5 from Fig. E.8.	173

CHAPTER 1

INTRODUCTION

The effectiveness of most of the food processing and preservation methods currently used were recognized well before 2000 B.C. without any knowledge of the basic principles and the role of foodborne microorganisms in the spoilage and health hazards of food origin. These methods include heating, low temperature, drying, controlling water activity (a_w) and oxidation-reduction potential, low pH, and the use of some antimicrobial chemicals. Once the association of microorganisms with food spoilage and foodborne diseases was recognized, specific techniques to destroy them as well as to prevent or reduce their growth were developed in the early 20th century. The increase in urbanization and changes in the socio-economic pattern in developed countries resulted with the dependence of a large population to various processed foods with extended shelf-life (Ray et al., 2001). Today's consumers are also making their choices on the quality and safety of food products (Hogan et al., 2005).

Prolonged shelf-life in foods has traditionally been associated with thermal processing, alone or in combination with chemical or biochemical preservation methods (Ohlsson, 2002). Commercial food sterilization and preservation methods often result in a number of undesired changes in foods, such as loss of color, flavor, texture and nutritional value i.e., a reduction in the apparent freshness and quality of the final product (Hogan et al., 2005). In addition, the cumulative effect of consuming many additives has not been studied. There are

growing suspicions that some of these could be hazardous, especially due to long-term usage. The health conscious consumers are interested in foods that are less processed, almost natural and with no or very little preservative (Ray et al., 2001). Therefore, alternative or novel food processing technologies have been explored and implemented to provide safe, fresh-tasting nutritive foods without the use of heat or chemical preservatives (Hogan et al., 2005).

Novel processing methods are also called as minimal processing technologies where they ‘minimally influence the quality characteristics of a food whilst, at the same time, giving the food sufficient shelf-life during storage and distribution’. An even more precise definition, describe them as techniques that ‘preserve foods but also retain to a greater extent their nutritional quality and sensory characteristics by reducing the reliance on heat as the main preservative action’ (Ohlsson, 2002).

High hydrostatic pressure (HHP), ultrasound, pulsed electric fields, osmotic dehydration, thermal membrane processes, high intensity pulsed light, radio frequency electric fields, irradiation and new chemical and biochemical hurdles as nisin, lactoferrin, ozone and others, can minimally or non-thermally process-preserve foods. In the search of new processing methods, the application of HHP processing has shown considerable potential as an alternative technology to heat treatments, in terms of assuring safety and quality attributes (Hogan et al., 2005).

1.1 History of HHP

The technology of HHP processing has been known (e.g. Hite, 1899) to be a potential preservation technique for more than a century (Butz and Tauscher,

2002). Hite designed and constructed a high-pressure machine that could reach pressures of about 700 MPa and he and his co-workers examined the potential use of HHP processing for a wide range of foods and beverages, including the pressure inactivation of viruses. In 1899, Hite reported that pressures around 450 MPa or greater could improve the keeping the quality of milk. In 1914, he showed that yeasts and lactic acid bacteria associated with sweet, ripe fruit were more susceptible to pressure than other microorganisms, especially spores of bacteria associated with vegetables (Hogan et al., 2005). In 1914, Bridgman described the coagulation of egg white as a consequence of HHP treatment. In 1932, Basset and Machebouf studied the sensitivity of various living organisms and biological compounds and showed that it was impossible to destroy bacterial spores. The reason why microorganisms were affected by HHP was not completely clear. In 1994, Hayakawa developed a theory about the inactivation. Researchers are also trying to describe pressure-induced phenomena at the molecular level (Bertucco and Spilimbergo, 2001).

Although the potential for HHP processing of foods has been known since the late nineteenth century, its application has only recently been recognized. The use of HHP as a food preservation technique has gained momentum throughout the world as an alternative to traditional heat-based methods during the last decade in some areas (Hogan et al., 2005).

1.2 Working Principle of HHP

HHP processing involves exposing a packaged liquid or solid food submerged in a liquid (pressure-transmitting medium) or a liquid food in a closed chamber to pressure between 100 and 800 MPa for a desirable period of time at a desirable

temperature. This makes the process uniquely three-dimensional (Ray et al., 2001).

There are two general scientific principles of direct relevance of the use of high pressure in food processing. The first is the “Le Chatelier’s” principle, which applies to all physical processes and states that, when a system at equilibrium is disturbed the system responds in a way that tends to minimize the disturbance. This means that HHP stimulates reactions that result in a decrease in volume but opposes reactions that involve an increase in volume. Secondly, “The Isostatic Rule” states that pressure is instantaneously and uniformly transmitted throughout the sample under pressure, whether it is in direct contact with the pressure medium or hermetically sealed in a flexible package that transmits pressure (Hogan et al., 2005).

1.3 HHP Systems

The main components of a HHP system are a high-pressure steel cell for the sample to be treated, a high-pressure generating system, a temperature controller, and a loading system for the material to be treated (Figure 1.1). When the samples are inserted in the container, it is filled with a fluid that transmits the pressure (Bertucco and Spilimbergo, 2001). Water may be used as the pressure-transmitting fluid, but water containing castor oil, silicone oil, sodium benzoate, ethanol or glycol is also used. The ability of the pressure-transmitting fluid to protect the inner vessel surface from corrosion, the specific HHP system being used, the process temperature range and the viscosity of the fluid under pressure are some of the factors involved in selection of the fluid (Hogan et al., 2005).

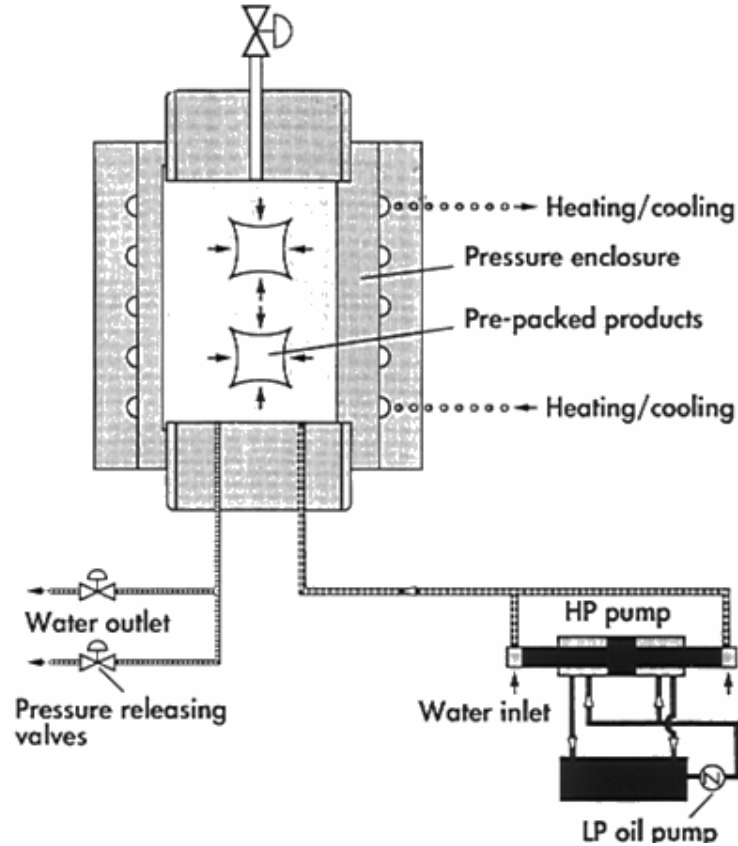


Figure 1.1 A typical high-pressure processing system for treating pre-packaged foods (Adapted from Olsson, 1995)

High pressures can be generated by direct or indirect compression or by heating the pressure-transmitting medium. In direct compression (Figure 1.2), a piston coaxial with the container is required and the compressions are particularly fast. This method is employed only in laboratory-scale equipments because of the leakage problem between the piston and the internal surface of the vessel (Bertucco and Spilimbergo, 2001).

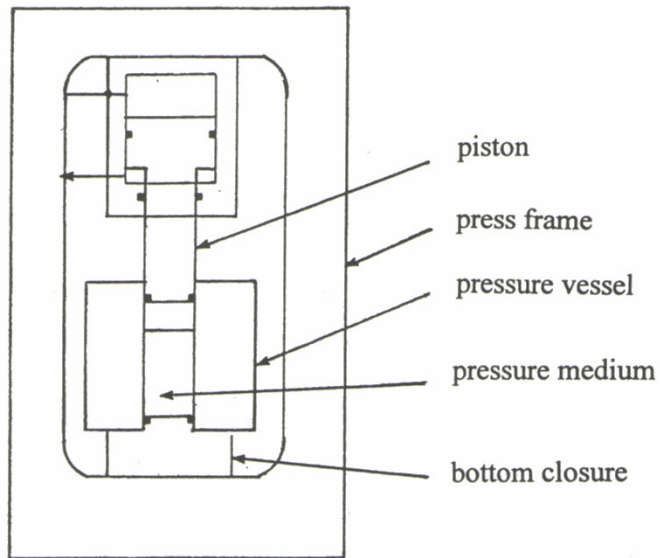


Figure 1.2 Direct pressure generator (Adapted from Deplace, 1995)

Indirect method: (Figure 1.3) is a more widespread method in which the pressurization fluid is pumped from the pressure medium tank to the pressure vessel by means of an intensifier. The purpose of such an intensifier (or possibly of a high-pressure pump) is to increase the pressure in the pressure vessel by compressing the fluid and the product to be pressurized. The liquid is pumped from the pressure-medium tank to the cell, until the desired pressure values is reached (Deplace, 1995; Bertuccio and Spilimbergo, 2001).

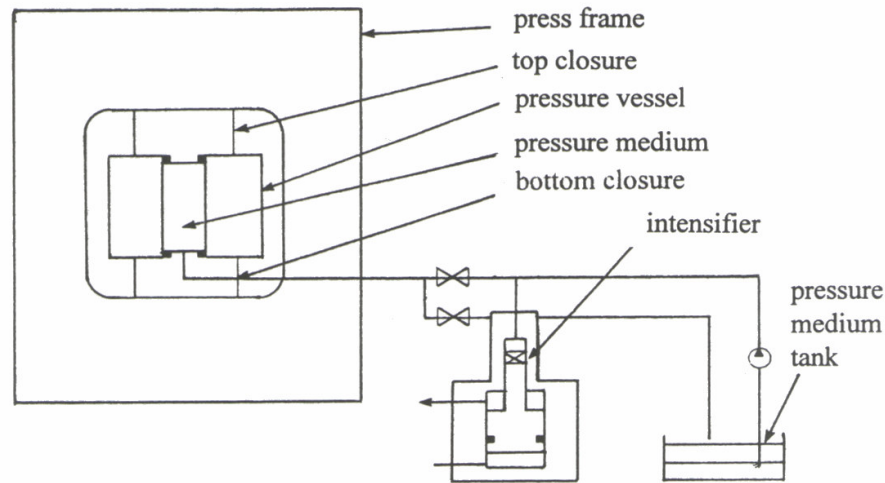


Figure 1.3 Indirect pressure generator (Adapted from Deplace, 1995)

Industrial HHP treatment is currently a batch or semi-continuous process. The selection of equipment depends on the kind of food product to be processed and to the process parameters. Solid food products or foods with large solid particles can only be treated in batch mode. Liquids, slurries and other pumpable products have the additional option of semi-continuous production (Hogan et al., 2005).

Batch processes: are necessary for packaged foods. Most HHP systems in industrial use for food processing are batch systems, whereby the product is placed in a high-pressure chamber and the vessel is closed, filled with pressure-transmitting medium and pressurized either by pumping medium into the vessel or by reducing the volume of the pressure chamber. Once the desired pressure is reached, the pump or piston is stopped, the valves are closed and the pressure is maintained without further energy input. After the required hold time has elapsed,

the system is depressurized, the vessel is opened and the product is unloaded. The system is then reloaded with product, by either operators or machines, depending on the degree of automation possible. The total time for pressurization, holding and depressurization is referred to as the 'cycle time'. In a commercial application, with this sort of batch process, a short holding time under pressure is desirable in order to maximize throughput of the product.

Direct introduction of the liquid to be processed into the high-pressure chamber has been seen as a promising alternative to batch processes. So far, this has been achieved industrially only in a semi-continuous mode, which means that the liquid to be treated is introduced periodically into the HHP chamber (Moreau, 1995). Current semi-continuous systems for treating liquids use a pressure vessel with a free piston to compress liquid foods. A low-pressure food pump is used to fill the pressure vessel and, as the vessel is filled, the free piston is displaced. When filled, the inlet port is closed and high-pressure process water is introduced behind the free piston to compress the liquid food. After an appropriate holding time, releasing the pressure on the high-pressure process water decompresses the system. The treated liquid is discharged from the pressure vessel to a sterile hold tank through a discharge port. A low-pressure water pump is used to move the free piston towards the discharge port. The treated liquid food can be filled aseptically into pre-sterilized containers (Hogan et al., 2005).

The combination of multiple cells, which work sequentially and which are fed by a central high-pressure compressor, can be seen to produce greater continuity in the process. This has been achieved in the Japanese Wakayama Plant for tangerine treatment. Another Japanese plant built for Pokka Corporation treats 600 lt/h of grapefruit juice. More chambers could be coupled together as shown in Figure 1.4 (Moreau, 1995).

Regardless of the method and system utilized to compress the food, HHP treatments are conducted in cycles of three differentiable steps. An initial time, designated as come-up time, is required to reach the selected working pressure. Pressure is then maintained for a selected time (holding time), after which pressure is usually released in a few seconds (release time). The come-up, holding and release times, the selected maximum pressure, the pressure-transmitting medium composition, and the initial temperature of the food and pressure transmitting medium, are the process engineering variables of control in HHP processing technology (Rodriguez, 2003).

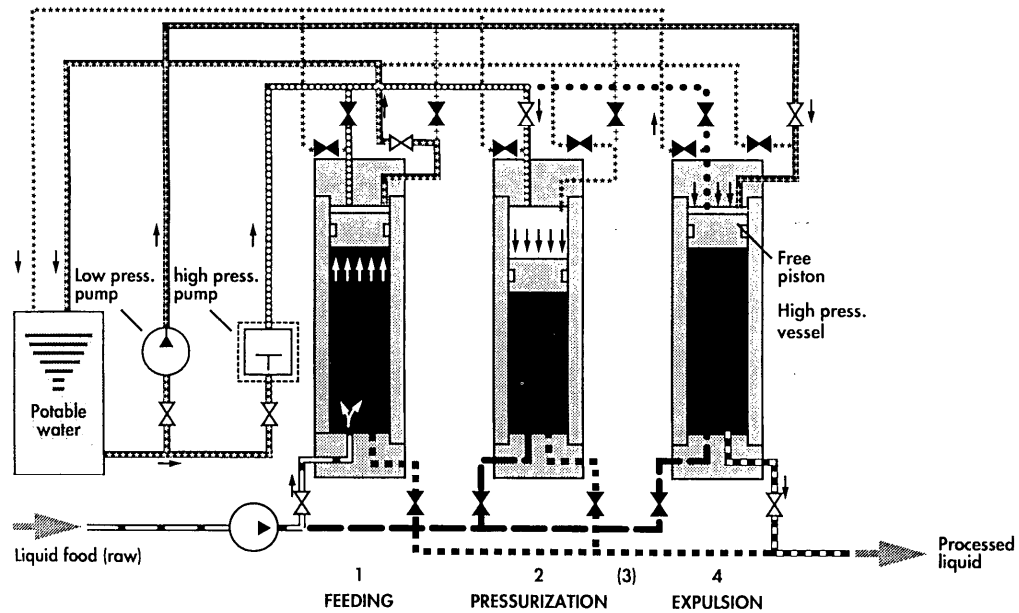


Figure 1.4 A multivessel arrangement for semi-continuous high-pressure processing (Adapted from Moreau, 1995)

1.4 Commercial Applications of HHP

Investigations on the applications of HHP for food processing started a century ago. Serious attempts to apply HHP to food preservation were initiated in the 1980s by the Japanese Ministry of Agriculture, Forestry, and Fisheries in collaboration with several food industries. Close to this development, the European Union initiated a collaborative program for the development of equipment for the processing. HHP treatment has been shown to produce shelf-stable foods with a pH of 4.2 or lower and extended shelf life of refrigerated foods. In the early 1990s high pressure processed fruit jams and grapefruit juice appeared in the Japanese market, representing commercial application of the process (Venugopal, 2006). A range of pressure-treated products (Table 1.1) has already been introduced into the markets of the Japan, France, Spain and USA (Butz and Tauscher, 2002). Currently HHP processed products are low pH fruit juices (grapefruit juice, mandarin juice, apple and orange juice), jams, jellies, fruit dressing, avocado, yoghurt, salted raw squid, fish sausages, oysters. In these foods, the major interest was to destroy pathogens, molds, yeasts and cells of some aciduric bacteria. At present, the effectiveness of this method for the destruction and growth inhibition of yeasts and molds and their spores, bacterial cells and spores, parasites and protozoa and viruses in low pH as well as high pH foods are being studied to produce high quality foods with enhanced shelf-life and safety (Ohlsson, 2002).

HHP has potential applications in other food commodities also, which include improvement of tenderness of pre-rigor beef muscle, removal of bitterness in orange juice, selective removal of β -lactoglobulin from whey concentrates, and acceleration of bovine milk curdling by rennet (Venugopal, 2006). Starch

molecules are similarly opened and partially degraded, to produce increased sweetness and susceptibility to amylase activity. Other research has found that the appearance, odor, texture and taste of soybeans and rice did not change after processing, whereas root vegetables, including potato and sweet potato, became softer, more pliable, sweeter and more transparent (Ohlsson, 2002).

Table 1.1 Current Applications of HHP (Ohlsson, 2002; Hogan et al., 2005)

Product	Manufacturer	Country
Jams, fruit dressing, fruit sauce topping, yoghurt, fruit jelly	Meidi-ya Company	Japan
Grapefruit juice	Pokka Corp.	Japan
Mandarin juice	Wakayama Food Ind.	Japan
Non-frozen tropical fruits	Nishin Oil Mills	Japan
Tenderized beef	Fuji Ciku Mutterham	Japan
Avocado puree, salsa dips, ready meals and fruit juices	Avomex	USA
Orange juice	UltiFruit	France
Bread ready pre-sliced meats (Ham, Turkey, Beef)	Hormel Foods Corp.	USA
Salsa	Simply Fresco	USA
Hummus	Hannah International	USA
Fruit and vegetable juices	Odwalla	USA
Processed poultry products	Purdue Farms	USA
Oysters	Motivatit Seafoods	USA
Oysters	Goose Point Oysters	USA
Oysters	Joey Oysters	USA
Fruit juices	Pampryl	France
Apple Juice	Frubaca	Portugal
Sliced ham and tapas	Espuna	Spain
Fruit juices and smoothies	Orchard House	UK
Broccoli- Apple Juice	Food Res. Inst. Prague	Czech Republic
Organic apple juice and cider	Lovitt Fresh	USA

1.5 Effect of HHP on Molecules

HHP only affects non-covalent bonds (the ionic, hydrophobic and H-bonds), leaving covalent bonds intact and consequently, induces alterations in the structure of secondary- and tertiary-bonded molecules (Ross et al., 2003). These changes cause the macromolecules to unfold. Especially proteins unfold due to disruption of weak bonds during pressurization and refold in different configurations following release of pressure. Large carbohydrate molecules also undergo, to some extent, similar changes (Ray et al., 2001). It has been generally known that HHP has very little effect on low molecular weight compounds such as flavor compounds, vitamins and pigments compared to thermal processes (Pandurangi and Balasubramaniam, 2005).

1.5.1 Effect of HHP on Proteins

Pressure effects on molecular systems are governed simply by the principle of Le Chatelier, which states that a pressure increase will shift a given equilibrium to the side that occupies the smallest volume (Meersman et al., 2006).

The effects of HHP on proteins can be described at different levels of the molecular structure, i.e. primary, secondary, tertiary and quaternary structural levels (Tauc et al., 2002). Primary level is the sequence of amino acids in the polypeptide chain. There is no report in the literature on the effect of pressure on the covalent bonds. The secondary structure is formed by hydrogen bonds within and between the peptide chains. In general one expects a stabilization of these structures by pressure. The specific packing of the secondary structures forms the tertiary level and several compact structures may assemble to form the quaternary

structure (Heremans, 1995). The interactions between amino acid residues in the tertiary and quaternary structures of proteins are similar (van der Waals forces and those of electrostatic nature), and similar responses to pressure are expected. The non-covalent interactions between the subunits are therefore quite sensitive to pressure (Silva and Weber, 1993).

When hydrostatic pressure is applied, the protein- solvent system evolves toward the global configuration that occupies the least volume. Since in the unfolded state the excluded volume of packing defects is eliminated and charges and hydrophobic residues are exposed to solvation, it is this form of the protein that is favored by pressure. Based on the criteria of intrinsic packing and hydration, denatured protein species can be conceptually divided into three classes: compact intermediate states (such as molten globules), partially unfolded states, and the fully unfolded state. The volume of the protein- solvent system in the transition state (molten globule- like) is significantly larger than in the unfolded state and somewhat larger than in the folded state. It is reasonable to interpret the large increase in volume between unfolded and transition states as resulting from collapse of the unfolded polypeptide chain to a loosely packed globule from which solvent is excluded. The decrease in volume observed between the transition state and the folded state most likely arises from more efficient packing in the final folded structure (Vidugiris et al., 1995; Chalikian, 2003).

Based on studies of the transfer of small hydrophobic compounds to water, the volume change of unfolding proteins is predicted to be negative and very large. The volume change for this transfer will become positive with increasing pressure. This contradiction is called the protein volume paradox: “the liquid hydrocarbon model fails almost completely when one attempts to extend it to the effects of pressure on protein denaturation” (Meersman et al., 2006).

Enzyme activity is an important parameter affecting quality, particularly of cut fruits and vegetables. Since enzymes are proteins, it is expected that application of pressure changes the structural conformation and may sometimes lead to loss of activity. Exposure to high pressure may inactivate or activate enzymes. Most work related to the effect of HHP on enzyme activity has been performed with respect to pectin esterase (PE) and polygalacturonase (PG) in intact, cut and pureed vegetables and juices. It was reported that the pressure- temperature ranges that inactivate tomato PG were between 300 and 600 MPa and 5 and 50°C. However, PE activity in diced tomatoes markedly increased with application of 400 MPa pressure at 45 °C (Pandurangi and Balasubramaniam, 2005).

1.5.2 Effect of HHP on Lipids

The primary effects of pressure on phospholipids can be observed on the temperatures of the transitions. Pressure favors the crystalline state, as a result of the Le Chatelier principle (Heremans, 1995). As pressure increases at constant temperature, the lipid bilayer adapts by changing its conformation. A variety of pressure-induced phase transformations has been observed such as liquid-to-gel transition and gel-to-interdigitated gel transition. In contrast to Le Chatelier's principle, the volume of the lipid bilayer in liquid- to- gel transition increases with an increase in the fatty acyl chains (R-groups) length of the phospholipids. Pressures of 50-200 MPa cause the transition from the liquid-crystalline to gel. At higher pressures (above 200 MPa), a second pressure-induced phase transition, called interdigitated phase, is observed, and the bilayer volume decreases by 5%, accompanied by a decrease in its thickness (Kato and Hayashi, 1999; Winter, 2001).

A more complex situation is encountered in biomembranes. It has been found that the physical state of the lipids that surround the membrane proteins plays a crucial role in the activity of membrane-bound enzymes (Heremans, 1995). The lipid bilayer exists as a liquid state as a requirement for “optimum” biological function of membranes (Chong and Weber, 1983). Phase transition is from the natural liquid crystalline phase to an initially reversible gel phase, and finally to an irreversible integrated phase, together with a reduction in the thickness of the bilayers (Kalchayanand et al., 2002).

1.5.3 Effect of HHP on Starch

The stability and functionality of starch is determined by highly ordered structural components: crystalline and amorphous lamellae that form the crystalline growth ring and amorphous growth rings. The crystallinity is classified as A-type or B-type dependent on the configuration of the unit cell of the double helix of the polysaccharides. Cereal starches (rice, corn, waxy corn, wheat etc.), in most of the cases, show the A-pattern. Potato is an example for the B-polymorph (Knorr et al., 2006).

The disruption of this structure by heat is usually referred to as gelatinization. This process is essential in all kinds of industrial and culinary utilization of starch and is characterized by a loss in crystallinity by a solubilization of amylose and by irreversible swelling of the granules. There has been considerable interest in the use of high hydrostatic pressure (HHP) treatment for physical modification of starch, because HHP-treated starch shows unique gelatinization and retrogradation properties. For example, pressure-gelatinized starch maintains its granular structure, and shows a lower quantity of released amylase and lower initial rate of enzymatic reactivity than heat gelatinized one. In addition, it is

reported that retrogradation can be observed immediately after HHP treatment. Although retrogradation is understood to be a typical quality loss of starchy foods, it is of interest to use HHP-treated starch as resistant starch in recent years. Physical modification of starch–water mixtures with HHP treatment has often been investigated in terms of treatment pressure, treatment temperature, and holding time. At a constant temperature and time, degree of gelatinization of starch–water mixtures increases with increase in treatment pressure and decrease in starch content (Kawai et al., 2007). The application of pressures up to 400 MPa revealed that pressure has an impact on the gelatinization temperature in the case of wheat and potato starch. More recent studies confirmed these findings for wheat and rice also presenting elaborated pressure–temperature phase transition diagrams for those starches (Knorr et al., 2006).

Under HHP, the side by side dissociation and helix unwinding might be suppressed because van der Waals and hydrogen bonds are stabilized which should favor the helix structure. Consequently, starch gelatinization is interrupted because the disintegration of the crystalline regions remains incomplete. For a 690 MPa treatment at ambient temperature, it has been found that large parts of the crystalline regions are retained. Interestingly, A-starches underwent changes in the crystallinity pattern from A to the B- isomorph which obviously is favored by pressure because of the higher number of associated water molecules stabilizing the helix structure by van der Waals forces (Knorr et al., 2006).

1.5.4 Effect of HHP on Water

Several properties of water are modified under HHP. Water has low compressibility; however, at 100 MPa, 400 MPa, and 600 MPa water is compressed approximately 4, 12, and 15% respectively. Therefore, food that has

relatively high water and low gas content should have compressibility similar to that of water. The ionic dissociation of water is increased under pressure because of the electrorestriction phenomenon. Electrorestriction occurs as pressure causes the separation of electrical charges because the charged entities organize water molecules around them (due to dipole- dipole interactions and hydrogen bonding), resulting in a decrease in total volume. The increase in the ionization of water and other weak acids causes a drop in the pH of 0.2 to 0.5 pH units per 100 MPa. Depending on initial temperature and rate of compression, pressurization of water also leads to temperature increases of 2 to 3° C per 100 MPa. A similar temperature decrease is caused upon pressure release (Larsen, 2000).

This adiabatic temperature change is very predictable. All compressible substances change temperature during physical compression, an unavoidable thermodynamic effect. The magnitude of this change depends mainly on the compressibility of the substance and its specific heat. Liquids such as water are far less compressible. As a result, the change in temperature due to compression, even at very high pressures, is relatively low. Since water is a main ingredient in most foods, the compression of most foods exhibits adiabatic temperature changes (Table 1.2) very similar to that of water (Ting et al., 2002).

Table 1.2 Temperature change due to adiabatic compression for selected substances (Adapted from Buzrul et al., 2008; Ting et al., 2002)

Substance at 25°C	Temperature change per 100 MPa (°C)
Water	~ 3.0
Mashed Potato	~ 3.0
Orange Juice	~ 3.0
Tomato Salsa	~ 3.0
Whole milk	~ 3.0
Skim milk	~ 3.0
2%- Fat Milk	~ 3.0
Salmon	~ 3.2
Chicken Fat	~ 4.5
Water Glycol (50/50)	From 4.8 to <3.7 ^a
Ethanol	~ 12.8
Ethylene Glycol	~ 4.5
Beef Fat	~ 6.3
Olive Oil	From 8.7 to <6.3 ^a
Soy Oil	From 9.1 to <6.2 ^a

^a Substances exhibited decreasing T as pressure increased

1.6 Effect of HHP on Microorganisms

Effectiveness of HHP for the destruction and growth inhibition of yeasts and molds and their spores, bacterial cells and spores, parasites and protozoa and

viruses in low pH as well as high pH foods are being studied to produce high quality foods and to enhance their shelf- life and safety (Ray et al., 2001).

1.6.1 Bacterial Cells

One of the primary considerations in evaluating the effectiveness of any preservation treatment is its ability to eradicate pathogenic microorganisms and thus ensure product safety (Ritz et al., 2000). As high- pressure targets, microorganisms may be usefully categorized, first into those that cause food poisoning and those that cause food spoilage, and secondly into those that are relatively pressure sensitive and those that are pressure resistant (Gould, 1995). Infectious pathogens such as *Listeria*, *Salmonella* and verotoxigenic *E. coli* should be absent in foods. Consequently, inactivation of these organisms is a prerequisite to microbiological safety. Toxigenic pathogens such as *Staphylococcus aureus* and *Clostridium botulinum* are not infectious themselves and, if they are prevented from growing, they do not form a toxin in food (Smelt et al., 1998).

Food processors who wish to use HHP to preserve foods would benefit from a specified limited number of pressure-time combinations. These combinations would be proven to inactivate the "pertinent microorganism" (most resistant microorganism of public health significance that is likely to occur in the juice and is the pathogen that one must target for) by 5-log₁₀. By choosing the most resistant pathogen as target, it is also possible to treat the product for all other pathogens that are less resistant to the extent of the treatment (Anonymous, 2004). According to Juice HACCP Hazards and Controls Guidance, low acid juices, such as carrot juice, are not subjected to the Low Acid Canned Foods regulation and they need to be distributed under refrigeration. Therefore, selection of pressure

resistant strains of foodborne pathogens, such as *E. coli* O157:H7, *Listeria* spp., *Salmonella* spp., or *Staphylococcus* spp., will also apply for carrot juice.

Bactericidal efficiency of several combinations of hydrostatic pressure (107 MPa to 483 MPa), pressurization temperature (25° to 60°C), and pressurization time (5 to 30 min) was studied against eight bacterial species. The bacterial species used include both spoilage and pathogenic bacteria from Gram-positive as well as Gram-negative groups (*Listeria monocytogenes*, *Staphylococcus aureus*, *Salmonella typhimurium*, *Escherichia coli*, *Leuconostoc mesenteroides*, *Lactobacillus sake*, *Pseudomonas fluorescens* and *Serratia liquifaciens*). Increasing pressure keeping other conditions unchanged increased the viability loss of eight strains. Viability loss also increased by increasing the pressurization temperature, whereas increasing pressurization time did not increase the viability loss in all eight species. The results of this study showed that instead of using higher pressure (>600 MPa at 25°C), moderate pressure and temperature (345 MPa at 50°C) could be used to obtain high levels of inactivation against bacterial cells (Ray et al., 2001)

The influences of several other variables were also studied. In general, (i) Gram-negative bacterial cells are more sensitive to pressure than Gram-positive bacterial cells, (ii) rods are more sensitive than cocci, and (iii) cells from early stationary phase are more resistant than cells from exponential phase of growth (Alpas et al., 2000; Ray et al., 2001).

The species and strains in a species also differ in sensitivity to pressure. It was demonstrated that the pressure resistance of certain natural isolates of *E. coli* O157:H7 varied greatly. It is of concern that certain *E. coli* O157:H7 strains are among the most pressure-resistant vegetative bacteria known. It is therefore

critically important to characterize the innate HHP resistance in these strains (Robey et al., 2001). Among the pathogenic non-spore forming gram-positive bacteria, *L. monocytogenes* and *S. aureus* are the two well-studied pathogens regarding the use of HHP processing. *S. aureus* appears to have a high resistance to pressure (Anonymous, 2000). Patterson and Kilpatrick (1998) applied HHP for *E. coli* O157:H7 NCTC 12079 and *S. aureus* NCTC 10652 in milk and poultry. Their findings showed a practical necessity for combined use of pressure and elevated temperatures (400 MPa, 50°C, 15 min for *E. coli* O157:H7, 500 MPa, 50°C, 15 min for *S. aureus*), resulting in 5- to 6- \log_{10} (cfu g⁻¹) reduction in poultry meat and milk. Alone, neither treatment displayed effective inactivation (< one \log_{10}) of the pathogens. Investigations with *E. coli* O157:H7 NCTC 12709 in milk showed that pressure treatment of 600 MPa and 30 min at 20°C revealed only two- \log_{10} reduction (Rademacher et al., 1998).

1.6.2 Bacterial Spores

Spores of foodborne spoilage and pathogenic bacteria are not a major problem in low pH or high acid (pH < 4.6) foods as most fail to germinate. This has helped the commercialization of several hydrostatic pressure processed low acid foods. In high pH or low acid foods (pH \geq 4.6), efficient destruction of bacterial spores (e.g., *Clostridium botulinum*, *Bacillus cereus*) is necessary to obtain commercial sterility by HHP (Ray et al., 2001). However, the major barrier for the effective use of HHP for sterilization of products is the strong resistance of bacterial endospores to pressurization (Herdegen and Vogel, 1998). Vegetative cells of bacteria and yeast are inactivated around pressures of 300 to 400 MPa at ambient temperatures. Bacterial spores, however, can survive higher pressures and they are unlikely to be killed by HHP treatment at room temperature (Oh and Moon, 2003). Therefore, the sterilizing effects of hydrostatic pressure on bacterial spores

in combination with heat, irradiation, low pH and bacteriocins such as nisin have been studied (Furukawa et al., 2003).

The inactivation of bacterial spores through HHP, unlike the inactivation of vegetative bacteria, occurs in two steps: (i) high pressures cause spore germination, and (ii) high temperatures inactivate the germinated spores. The synergistic effect of high pressure and high temperature inactivates spores (Oh and Moon, 2003). In general, low pressures up to 200 MPa can enhance the germination of endospores whereas higher pressures lead to an inactivation. An ideal germination of *Bacillus subtilis* spores was achieved between 60 and 150 MPa. Only an alternating pressure between 60 and 500 MPa in 30 min intervals for an overall treatment of 180 min at 50°C led to a complete inactivation of spores. Regarding commercial aspects of the high pressure technology these parameters would need overall processing times that are much too long to be cost effective. Therefore, it was necessary to find a treatment of HHP to inactivate endospore forming bacteria with very short processing times and also with very low use of energy and without additives (Herdegen and Vogel, 1998). It was considered that the reciprocal compression decompression (reciprocal pressurization, RP) could increase the inactivation and injury of bacterial spores compared with continuous pressurization (CP), and, as a result, RP treatment was more effective for inactivating bacterial spores than CP treatment. Sporicidal mechanism in RP treatment was considered as follows: hydrostatic pressure treatment initiated the germination of bacterial spores, and reciprocal rapid decompression caused the disruption, injury and inactivation of germinated spores (Furukawa et al., 2003).

1.6.3 Fungi

Fungi can be divided into two groups based on their vegetative structures: unicellular fungi (yeasts) and those producing hyphae (moulds, mushrooms, etc.). Yeasts are an important group of spoilage microorganisms, but are generally not food pathogens, although toxic mould growth may be a safety concern in foods. Treatment at pressures less than 400 MPa for a few minutes is sufficient to inactivate most yeast. It was reported that, at about 100 MPa, the nuclear membranes of yeasts was affected and that at more than 400- 600 MPa further alteration occurred in the mitochondria and the cytoplasm. Moulds are mycelial fungi and many of these organisms are important industrially, e.g. in food spoilage, food fermentations and biodegradation processes. Pressures between 300 and 600 MPa can inactivate moulds. It was demonstrated that HHP was effective for inactivation of *Penicillium roqueforti* spores in cheese systems (Hogan et al., 2005).

1.6.4 Viruses

Viruses have a high degree of structural diversity, which results in a wide range of pressure resistances. There are two potential applications of pressure inactivation of viruses: vaccine development and virus sterilization. Pressurization inactivates viruses but preserves their immunogenic properties, because usually it does not markedly change viral structure (Mor-Mur and Yuste, 2005). The most common human enteric viruses are Norwalk- like viruses, hepatitis A, rotavirus and human astrovirus. Complete inactivation of suspensions of feline calicivirus (a Norwalk- like virus surrogate), adenovirus and hepatitis A can be achieved by treatment at 275 MPa for 5 minutes, 400 MPa for 15 minutes and at 450 MPa for 5 minutes, respectively (Hogan et al., 2005).

1.7 Mechanisms of Microbial Inactivation by HHP

HHP induced inactivation of microorganisms has been investigated intensively during the last decade. It is known that microorganisms are affected by increasing pressure, leading to sublethal injury of the membrane at low levels of 200 MPa, and to lethal effects at 800 MPa. The pathways for inactivation depend on the organisms and their environment, and are subject to ongoing research (Hartmann et al., 2006).

1.7.1 HHP Effects on Cell Morphology

Electron microscopy has been employed to characterize pressure-induced morphological changes in microorganisms in order to understand the events leading to cell inactivation. Using scanning electron microscopy (SEM), morphological changes in *Leuconostoc mesenteroides* cells after pressure treatment at 345 MPa were evaluated. It was reported that while the cell size, shape, and surface structure of inactivated cells were not different from those of living cells immediately after pressure treatment, cell lysis was observed after 2 h storage at 4° C (Kaletunç et al., 2004).

SEM examinations of *Listeria monocytogenes* cells before and after pressure treatment (400 MPa in citrate buffer, pH 5.6, for 10 min at 20 °C) revealed that pressure treatment induced the occurrence of bud scars as pimples and swellings on the surface of cells. These observations suggest that the cellular wall or membrane could be the target of high-pressure treatment. In addition, SEM examination showed that the 400 MPa treatments could induce some cell disruptions. Similar results were observed with *Salmonella typhimurium* cells in

different suspension buffers (Tholozan et al., 2000). This study demonstrated a progressive increase in cell invaginations regardless of the suspension buffer. These results show that even if the pressure treatment leads to total inactivation of the microbial population, individual cells may retain their morphological characteristics (Ritz et al., 2002; Tholozan et al., 2000).

Cell compression, with partial irreversibility upon return to atmospheric pressure, was also reported as one of the morphological changes under HHP (Mor-Mur and Yuste, 2005). Perrier-Cornet et al. (1995) developed a new optical device to observe *Saccharomyces cerevisiae* cells under high pressure treatment, and an image analysis system was connected with the light microscope to measure cell volume variation during the high pressure application. An average decrease of 35% of the initial cell volume was observed for a pressure treatment of 250 MPa- 15 min. Tholozan et al. (2000) measured the intracellular volume of *L. monocytogenes* and *S. typhimurium* cells with radioactive- labeled probes. Intracellular volume values of *L. monocytogenes* in phosphate buffer (pH= 7.0) were $2.48 \pm 0.08 \mu\text{l mg protein}^{-1}$ for reference and $10.99 \pm 0.25 \mu\text{l mg protein}^{-1}$ for 600 MPa- 10 min- 20°C. Reference volume of *S. typhimurium* was $1.24 \pm 0.17 \mu\text{l mg protein}^{-1}$ and its volume was $1.41 \pm 0.06 \mu\text{l mg protein}^{-1}$ at 400 MPa- 10 min- 20°C in phosphate buffer (pH= 7.0).

1.7.2 HHP Effects on Cellular Components

A large number of studies were reported on the destruction mechanism of foodborne bacterial cells by HHP (Ray et al., 2001). Pressure induced changes in several structural and functional components of vegetative microbial cells include loss of functions of the cell wall and cell membrane, dissociation of protein and

ribosomal subunit structures, and loss of activity of some enzymes (Kalchayanand et al., 2002).

Modification of membrane properties can be explained by, disruption or increase in permeability, lack of membrane integrity, denaturation of membrane-bound proteins and pressure-induced phase transition of membrane lipid bilayer (Perrier-Cornet et al., 1995; Hartmann et al., 2006). The major HHP-induced change has been firstly suspected to be associated with the phase transition of membrane lipid bilayers above 35°C (Chong and Weber 1983). This change, in turn, impairs many functions of the membrane, namely loss of permeability and transport of nutrients, and transmembrane proton gradient and proton motive force, leading to loss of ATP synthesis. HHP-induced cell death as well as sublethal injury, as a result of the structural and functional changes, but at different levels (Kalchayanand et al., 2002). Alpas et al., (2003) used differential scanning calorimetry (DSC) to evaluate the relative HHP resistances of bacterial strains from *S. aureus* and *E. coli* O157:H7 in vivo. The total apparent enthalpy change and thermal stability were two DSC parameters used to compare bacterial strains of untreated control and pressure-treated bacteria. DSC thermograms indicated that ribosomal denaturation appears to be a major factor in cell death by both thermal and high pressure treatments.

Pressure also induces mechanical stresses on the cell wall and functional proteins attached or embedded in the membrane, which, in turn is attached to the wall, and associated with the bilayer of phospholipid might be affected by these mechanical stresses (Hartmann et al., 2006; Kato and Hayashi, 1999). This effect occurs as an inhibition of protein synthesis and reversible protein denaturation within the pressure range of 20-180 MPa; loss of cell viability begins after 180 MPa with an

exponentially increasing inactivation rate with pressure. It is followed by the irreversible protein denaturation above 300 MPa (Lado and Yousef, 2002).

1.8 Injury due to HHP

HHP treatment not only kills bacterial cells, some survivors also become sublethally injured (Ray et al., 2001). Bacterial cells exposed to different physical and chemical treatments suffer injury that could be reversible in food materials during storage. Injury has been observed for many bacterial cells. The injured cells repair in a medium containing the necessary nutrients under the conditions of optimum pH and temperature leading to outbreaks of foodborne disease and food spoilage. Specific studies have shown that, the metabolic processes during injury repair vary with the nature of stress and involve the synthesis of ATP, RNA, DNA and mycopeptides. The structural and functional components known to be damaged by sublethal stresses are the cell wall, cytoplasmic membrane, ribosomal RNA and DNA, as well as some enzymes.

Injured bacteria may be repaired during storage, which could affect the microbiological quality of foodstuffs with an important safety consideration especially in low acid food products. On the other hand, HHP induced injury can be advantageous in high acid foods, where lower pressure can be used to produce injured cells that could not repair in acidic medium. If cells are injured, they time for adaptation (lag time) before they resume growth. Extension of lag time will result in a considerable delay in time to spoilage and hence the shelf-life will be extended (Smelt et al., 1998).

A recent study (Bozoğlu et al., 2004) in milk (HHP-T-t conditions) indicated two types of injury, (I1) and (I2), for all the pathogens (*Listeria monocytogenes* CA, *Staphylococcus aureus* 485, *Escherichia coli* O157:H7 933 and *Salmonella enteritidis* FDA) studied. i) primary injury (I1): can form visible colonies on non-selective agar but not on selective agar and; ii) secondary injury (I2): can not form visible colonies either on non-selective or selective agar. It was reported that I2 type injury is a major injury and after its repair (I2 to I1), the cells can form colonies on non-selective but not on selective agar. The formation of colonies on both selective and non-selective agar occurs only after full recovery of injury (I1 to AC). The results presented in this study show that even if injured cells are not detected immediately after HHP treatment, I2 type injury could be potentially present in food system. Therefore, it is imperative that shelf life studies must be conducted over a period of time for potential repair of I2 type injury either to detectible injury (I1) or to active cells (AC) to ascertain microbiological safety of especially low acid food products like milk, carrot juice etc.

1.9 The Hurdle Concept

In general, the magnitude of death was directly proportional to pressure and time of pressurization, but for the destruction of more than eight log cycles of some pathogens, namely *E. coli* O157:H7 and *S. aureus* in phosphate buffer, pressurization at 20°C at 700 MPa for 15 min was necessary. Such a high pressure to obtain a desirable inactivation of pathogens cannot be used to preserve foods without altering their texture and color. It will thus be necessary in a commercially successful pressure pasteurization to employ lower pressure yet to obtain high levels of destruction of foodborne pathogens. A 'Hurdle Concept' could be useful to obtain this objective (Alpas and Bozoglu, 2000).

The hurdle concept is a minimal processing technique that exploits synergistic interactions between traditional preservation treatments. According to the hurdle concept, preservation treatments combined at lower individual intensities have additive or even synergistic antimicrobial effects, while their impact on sensory and nutritive properties of the food is minimized. In a similar fashion, it is possible that combining two or more nonthermal technologies and conventional preservative techniques will produce synergistic antimicrobial effects while reducing the energy input and treatment intensities required (Ross et al., 2003).

1.9.1 HHP and Low pH

When combined with certain nonthermal processes, acidic conditions may result in greater inactivation of vegetative bacteria than at neutral pH. The greater inactivation of vegetative cells is presumably due to stressful changes in the cytoplasmic pH combined with loss of membrane functionality and other cell damage caused by the nonthermal processing hurdles.

1.9.2 HHP and Antimicrobial Agents

In low acid products, vegetative bacteria are much more pressure resistant, and pasteurization requires much higher pressures that are less economically feasible. An approach to increase bacterial inactivation at moderate pressures (<600 MPa) at room temperature is to add antimicrobial peptides (Masschalck et al., 2001). Combination of high hydrostatic pressure and antimicrobials would increase the death rate because cells surviving pressurization also become sublethally injured and may be killed by bacteriocins (Garriga et al., 2002). Interesting examples of synergistic inactivation between HHP and natural antimicrobial peptides, such as nisin, lysozyme and pediocin have been documented (Masschalck et al., 2001).

1.9.3 HHP and Mild Heat

Nonthermal processing technologies were designed to eliminate the use of elevated temperatures during processing and to avoid the adverse effects of heat on the flavor, appearance and nutritive value of foods. Heat remains as a powerful and reliable hurdle whenever microbial inactivation is desired. Temperatures of 40 to 70°C applied during HHP, PEF, manosonication and irradiation have been shown to cause significantly greater inactivation of vegetative microorganisms in foods, compared with treatments at ambient temperatures (Ross et al., 2003). Pressurizations is more effective at inactivating microorganisms when it is combined with mild heat treatment, since membrane repair of pressure-induced pores would be harder to accomplish if intermolecular forces are weakened by warming (Russell, 2002).

1.9.4 HHP and Water Activity (a_w)

The magnitude and direction of the shift of water activity, if any, as a function of pressure have not been reported. However, it was showed that a reduction of water activity (measured at one atmosphere) from 0.98-1.0 to 0.94-0.96 resulted in a marked reduction in inactivation rates for microbes suspended in a food. Reducing the water activity appears to protect microbes against inactivation by HPP; however, it is to be expected that microbes may be sublethally injured by pressure, and recovery of sublethally injured cells can be inhibited by low water activity. Consequently, the net effect of water activity may be difficult to predict (Anonymous, 2000).

1.10 Effect of HHP on Microorganisms in Food Systems

Different food constituents and ingredients can play a protective role against pressure. Carbohydrates are generally more baroprotective than salts. The effect of fat content was not clear: in some cases, either there was no baroprotection or increasing fat content did not result in increasing baroprotection (Mor-Mur and Yuste, 2005). In general, under similar pressurization conditions, microbial destruction is lower in a food system than in a buffer or bacteriological medium (Ray et al., 2001). Pressure treatment of 375 MPa for 20 min at 20°C induced a decrease of 6-7 log cfu/ml in phosphate buffer. In buffer with an added source of protein, carbohydrates or fat, counts were reduced by 3.5-5.5, 4.5-6 and 5-6 log cfu/ml, respectively. From that point of view, two facts greatly determine the microbiological safety and stability of food: the effect of the food during treatment and after treatment and during recovery of microorganisms. Therefore, the results of studies in suspensions or model food systems cannot be directly extrapolated to real foods (Mor-Mur and Yuste, 2005). In this respect, several authors reported that bacteria are more resilient in a complex matrix as milk or meat compared to a buffer at the same pH. A strong baroprotective effect of whole UHT milk on *Yersinia enterocolitica* was demonstrated. Inactivation levels were 3.5–4.5 logs lower than in phosphate buffer when treated at 350–450 MPa/ 22°C for 10 min. Authors reported 1.12–3.46 log units less inactivation of *Carnobacterium piscicola* LMG2739, *Enterococcus faecium* CTC492, *Lactobacillus sakei* CTC494 and CTC746, *Leuconostoc carnosum* CTC747, *Listeria innocua* CTC1014, *Pediococcus acidilactici* F, *Staphylococcus carnosus* LTH2102, and *E. coli* CTC1007 and CTC1023 in cooked ham homogenized with water (3:1) than in phosphate buffer after 500 MPa/ 40°C/ 10 min treatment (Van Opstal et al., 2005).

The efficiency of HHP treatment for destruction of *L. monocytogenes* in goat cheese from raw milk was also studied. The findings of this study showed that 450 MPa/ 10 min or 500 MPa/ 5 min treatments achieved more than 5.6 log units of reduction of this microorganism without significantly affecting sensory characteristics of cheese (Trujillo et al., 2002).

1.11 HHP Inactivation Kinetics of Microorganisms

Although the inactivation kinetics of microorganisms using heat has been extensively studied, information on the inactivation kinetics of microorganisms under HHP is limited. Predicting the effectiveness of HHP processing against foodborne pathogens based on accurate inactivation kinetics is essential to permit establishment of safe processing conditions and critical for its effective application in food preservation.

1.11.1 First-order Model

The inactivation of microorganisms by heat and other processing methods has been traditionally assumed to follow first-order kinetics. It assumes that all the cells or spores in a population have equal resistance to lethal treatments, which results in a linear relationship between the logarithm of the number of survivors and treatment time (Chen and Hoover, 2003):

$$\text{Log}_e[N/N_0] = -kt \quad (1.1)$$

where; N = number of surviving microorganisms after pressure treatment time (t) in min, N_0 number of microorganisms at time $t = 0$ min and k = reaction rate constant (min^{-1}). k values can be obtained from the regression of $\text{Log}_e[N/N_0]$

vs. time as negative slope. Decimal reduction time, or D -value, defined as the pressure treatment time required for 90% destruction of initial population at a specific pressure-level can be computed from the following equation:

$$D = [2.303 / k] \quad (1.2)$$

The pressure sensitivity parameter, z -value, is the pressure range between which the D value changes 10-fold. Mathematically:

$$\text{Log}[D_1 / D_2] = [P_2 - P_1] / z_p \quad (1.3)$$

where; P_2 and P_1 were pressures corresponding to decimal reduction times D_2 and D_1 respectively. The z_p value can be obtained as the negative reciprocal slope of the regression line representing $\log_{10} D$ vs. P relationship. To analyze the pressure sensitivity of D values, z_p (pressure z -values) must be estimated using a pressure death time (PDT) concept, which is analogous to the thermal death time (TDT) concept in thermal processing applications (Basak et al., 2002; Dogan and Erkmen, 2004).

The influence of pressure on the reaction rate may be described by the transition state theory; the rate constant of a reaction in a liquid phase is proportional to the equilibrium constant for the formation of the active reactants. Based on this assumption, it is reported that at constant temperature, the pressure dependence of the reaction velocity constant (k) is due to the volume change (ΔV^*):

$$(\delta \ln k / \delta P)_T = -\Delta V^* / RT \quad (1.4)$$

where; P is the pressure (MPa), R is the gas constant (8.314 cm³/ MPa/ K/ mol), and T is temperature (K). The positive slope obtained from the plots of pressure

inactivation rates ($\ln k$) vs. pressure and therefore a $-\Delta V^*$; indicates that a decrease in volume is related to the microbial inactivation process. The ΔV^* indicates the volume variation between the activated complex and initial states of the bacterial pressure inactivation reaction.

A negative ΔV^* represents a reaction favored by increased pressure, so a reaction with a greater absolute ΔV^* value indicates that increments in pressure can accelerate the response on microbial inactivation rate. It is very difficult to give a precise physical meaning to the ΔV^* found. The calculated ΔV^* may be considered as the sum of several changes such as chemical, conformational, intra-molecular and inter-molecular interactions and solvation. The changes can also occur at different levels and places in the microbial cell and account for the bacterial inactivation (Erkmen and Doğan, 2004). To account for these changes, recently it was reported that pressure treatment at 250 and 500 MPa produced morphological changes on the surface and internal structure of the *Leuconostoc mesenteroides* cells with these changes being observed by SEM and TEM. Dechaining of cells and blister formation on the surface of cells increased with pressure as observed in SEM micrographs. TEM studies showed that cytoplasmic components of the cells were also affected by HHP treatment (Kaletunç et al., 2004). The calculation of an apparent ΔV^* can be useful to describe the pressure and medium dependence of microbial inactivation rates.

Calculation of k and D values are based on the exponential death phase and maintain an inverse relationship. Therefore, ΔV^* and pressure z value, which are calculated from the logarithmic relation of k or D with pressure, also maintain an inverse relation. A greater ΔV^* value corresponds to a lower pressure z value. As traditionally used in thermal kinetic analysis, a combination of D and z can be used to determine pressure processing conditions but it does not fully define the

microbial pressure resistance due to the dependence of kinetic parameters on the pressure interval evaluated. The fact that pressure inactivation evaluation took place at different pressures is an indication of difference in the response of bacterial cells to pressure treatments. A thermodynamic approach may help to explain the pressure resistance of microorganisms; the ΔV^* describes the overall pressure and medium dependence of the inactivation process (Erkmen and Dogan, 2004).

Smelt and Rijke (1992) reported first-order kinetics for HHP inactivation of *E. coli* in a physiological saline solution, with D values of 25.9, 8.0, 2.5 and 0.8 min for treatments at 200, 250, 300 and 350 MPa, respectively. Doğan and Erkmen (2004) reported that the z values were 465, 440, and 556 MPa for aerobic bacteria in milk, peach juice and orange juice, respectively. They were 578, 480, 506 and 576 MPa for *Listeria monocytogenes* in broth, milk, peach juice and orange juice, respectively.

1.11.2 Non- linear Models

The inactivation of microorganisms by heat and other processing methods has been traditionally assumed to follow first-order kinetics. However, significant deviations from linearity have frequently been reported and different kinds of deviations have been observed as curves with a shoulder, tailing and sigmoid shape for HHP applications as shown in Figure 1.5. In order to describe the non-linear kinetics of HHP-induced microbial inactivation, appropriate functions such as log-logistic, modified Gompertz, Weibull, Fermi or Baranyi have been applied to the inactivation curves (Buzrul and Alpas, 2004; Chen, 2007; Koseki and Yamamoto; 2007).

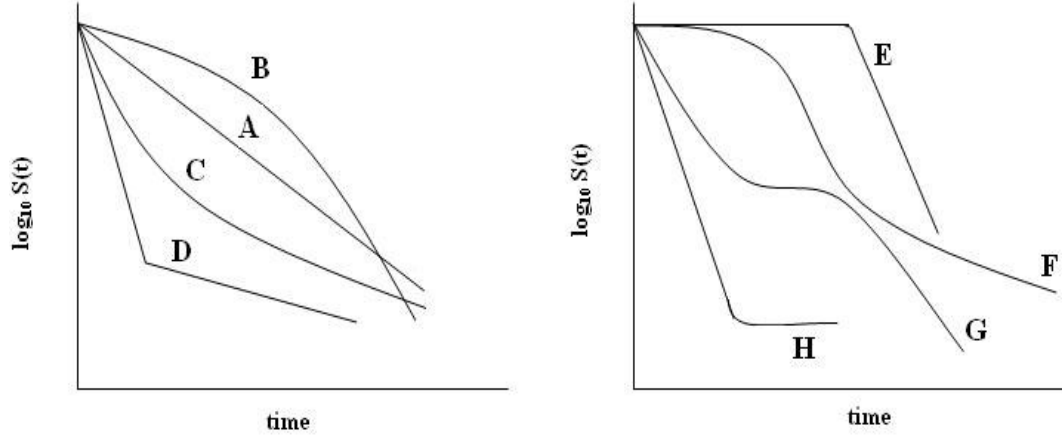


Figure 1.5 Commonly observed types of survival curves. Left plot: Linear [A], Downward concave [B], Upward concave [C] and biphasic [D]. Right plot: Linear with a preceding shoulder [E], Sigmoidal I – starting with a downward concavity and ending up with an upward concavity [F], Sigmoidal II – starting with a upward concavity and ending up with an downward concavity [G], Linear with tailing [H] (Adapted from Xiong et al., 1999; Peleg, 2003; Geeraerd et al., 2005)

Among these Weibull model has been successfully used in describing the non-linear inactivation of different microorganisms under various experimental conditions. The Weibull model assumes that cells and spores in a population have different resistances, and a survival curve is just the cumulative form of a distribution of lethal agents. The cumulative form of the Weibull distribution is as follows:

$$\text{Log}_{10}S(t) = -\left(\frac{t}{\alpha}\right)^\beta \quad (1.5)$$

where; $S(t)$ is the survival ratio, $S(t) = N(t)/N_0$, $N(t)$ = number of surviving microorganisms after pressure treatment time t in min, N_0 number of microorganisms at time $t = 0$ min, α and β are the scale and shape factors, respectively (Van Boekel, 2002).

Different forms of the Weibull model were presented in literature. However, decimal logarithm form, Eq. (1.5), seems suitable since its parameters have physical significance (Buzrul, 2007). Parameter α , which has the simple dimension of time, can be called time of first decimal reduction (D_1). This is distinguished from the conventional D value, which is derived from the first-order kinetics and represents the time of decimal reduction, regardless of the time of heating, the significance of the α value is restricted to first decimal reduction of surviving spores or cells from N_0 to $N_0/10$ (Mafart et al., 2002). Such a model presents the main advantage of remaining very simple and being sufficiently robust to describe both downward concave ($\beta > 1$) and upward concave survival curves ($\beta < 1$). The model also includes the traditional case where the survival curve is linear ($\beta = 1$) (Peleg and Cole, 1998).

This model, without further modifications, presents two major drawbacks: first, assessment of parameters requires a nonlinear regression. Secondly, β , which is a shape parameter, is structurally strongly correlated with α value. That is to say, both parameters are dependent: an error on α will be balanced by an error on β in the same way. Such an autocorrelation causes a certain instability of parameter estimates (Mafart et al., 2002). In addition, the Weibull model, Eq. 1.5, with one more parameter, is intrinsically more complex than the traditional first-order model, Eq. 1.1. The concept of D and z values is no longer valid in these non-linear cases. Thus, it seems worthwhile to fix β value characteristic to a strain for

the overall data (whole set of kinetic for each microorganism), so that D_I values can be estimated from a linear regression. Therefore, Eq. 1.6 was proposed for non-linear survival curves of microorganisms. The simplified Weibull Model is shown as:

$$\text{Log}_{10}S(t) = -\left(\frac{t}{\alpha}\right)^{\beta_{fixed}} \quad (1.6)$$

where β_{fixed} is a constant (Buzrul, 2007; Chen and Hoover, 2004).

Analogous to the traditional z value used in the linear model, z_p value was defined as the increase in pressure that results in one unit increase of α values. It provides information on the pressure sensitivity of α values. The α values were pressure dependent, and as pressure increased, α values increased. Assuming that α values had a linear relationship with pressure, the negative slope of the pressure (MPa) vs. α regression line will provide z_p value for simplified Weibull Model (Chen and Hoover, 2004).

The survival curves of *Yersinia enterocolitica* ATCC 35669 inactivated by high hydrostatic pressure were obtained at different pressure levels in sodium phosphate buffer and UHT whole milk. A linear model and three nonlinear models (log-logistic equation, modified Gompertz equation and Weibull model) were fitted to these data and the performances of these models were compared. Among the studied models, log-logistic equation and Weibull model allowed more accurate predictions of the inactivation kinetics of *Y. enterocolitica* 35669 at different pressure levels and substrates (Chen and Hoover, 2003).

Van Opstal et al. (2005) studied the inactivation of *Escherichia coli* MG1655 at different pressure and temperature combinations in Hepes–KOH buffer and fresh

carrot juice. In carrot juice, all inactivation curves were accurately described by a first order relationship. Opposed to what has been observed in carrot juice, in Hepes–KOH buffer, the Weibull model more accurately described the entire set of inactivation curves of *E. coli* MG1655 compared to the log-linear or the biphasic model.

Chen and Hoover (2004), obtained the survival curves of *Listeria monocytogenes* Scott A inactivated by high hydrostatic pressure at seven pressure levels in UHT whole milk. Weibull model produced a reasonably good fit to all the survival curves than the linear model.

1.12 Aim of the Study

The first part of the study aims to discuss the effect of HHP on foodborne pathogens in a low acid food and the inactivation patterns, while the second part examines the morphological changes and pressure induced inactivation mechanism of microorganisms by using scanning electron microscopy (SEM) and fluorescent microscopy.

The efficacy of HHP treatments for inactivation of vegetative bacteria in acidic foods (fruit juices, yoghurt) has been demonstrated and commercialized. However HHP-sterilized (i.e., shelf-stable) low-acid foods (milk, carrot juice, vegetable purees esp. infant food) are not yet available (Sizer et al., 2002). According to Juice HACCP Hazards and Controls Guidance low acid juices, such as carrot juice, are not subjected to the Low Acid Canned Foods regulation and they need to be distributed under refrigeration (Anonymous, 2004). Therefore, carrot juice was selected as the low- acid food system for our study. Since carrot juice is not

subjected to Low Acid Canned Foods, selection of pressure resistant strains of foodborne pathogens, such as *E. coli* O157:H7, *Listeria* spp., *Salmonella* spp., or *Staphylococcus* spp., will also be applicable for the production of shelf- stable and safe products.

In the first part of the study, experiments were performed to obtain the inactivation curves of two relatively pressure resistant foodborne pathogens (*E. coli* O157:H7 933 and *S. aureus* 485) in both carrot juice (pH= 6.22) and peptone water (pH = 6.95). The effect of HHP on inactivation was determined by comparison of the results.

The pressure treatment must ensure a satisfactory reduction in the initial microbial counts to increase microbial safety and stability of foods processed by HHP, thus kinetic analysis and the pressure dependence of microbial rates are necessary (Doğan and Erkmen, 2004). Although the number of kinetic studies on high-pressure inactivation of microorganisms is steadily increasing, information on the inactivation kinetics of foodborne pathogens especially in low acid foods under high pressure is still limited. Predicting the effectiveness of high-pressure processing against foodborne pathogens based on accurate inactivation kinetics is essential to permit the establishment of safe processing conditions, critical for its effective application in food preservation (Chen and Hoover, 2003).

In this study the followings were also among the aims; (i) To model the survival curves of these pathogens under HHP in carrot juice using the traditional linear and Weibull distribution models, (ii) To compare the parameters of both models to demonstrate over- and under-processing of carrot juice during HHP treatments, (iii) To determine the effects of pressure level and substrate on the shape of the survival curves and (iv) To determine the effect of pressure on the values of

model parameters and fit equations defining the model parameters, α (scale factor) as a function of pressure and shape factor, β .

Electron microscopy has been employed to characterize pressure-induced morphological changes in microorganisms in order to understand the events leading to cell inactivation. Among these, there was no previous study on calculation of cell volume and view area change induced by HHP using SEM micrographs.

In the second part of the study, scanning electron microscopy (SEM) was used for the determination of changes on cellular morphology induced by HHP. The view area was also calculated and a method was developed to calculate the volume of *S. aureus* 485 and *E. coli* O157:H7 933 before and after HHP application by image analysis.

The membrane integrity of the pressurized cells as a supplemental means to characterize the physiological status of the inactivated cells with fluorescence microscopy was also studied.

CHAPTER 2

MATERIALS AND METHODS

2.1 Materials

2.1.1 High Hydrostatic Pressure (HHP) Equipment

Preliminary HHP treatments were performed in the HHP laboratory (Middle East Technical University, Food Engineering Department) with a laboratory scale pressure system with 10 ml sampling capacity. The main parts of the HHP equipment were a cylindrically designed pressure vessel, a pressure pump, temperature control device and other system controls. Temperature inside the vessel was controlled at the intervals of 10-90°C by the temperature control device. The liquid inside the vessel was warmed prior to pressurization to the desired temperature. A pressure up to 250-300 MPa was created in the pressure vessel. The rate of pressure increase was approximately 30 MPa/sec, and pressure come-down time is 15 sec. An automatic device controls the pressure level and the temperature of pressurization.

HHP treatments for larger samples were performed in a high-pressure food processor with a 2 L sample capacity (Quintus QFP6; Flow Pressure Systems, WA, USA). For ideal applications, pressures should not be greater than 350 MPa, to reduce the capital investment costs of HHP processes (Jordan et al., 2001).

Accordingly the maximum pressure was selected as 400 MPa at a constant moderate temperature (40 °C) in this study.

A water/propylene glycol (Houghton-Safe 620-TY, Houghton Int., Inc., Valley Forge, PA) mixture (1:1, vol/vol) was used as the pressure transmitting fluid. The initial temperature of the pressure transmitting fluid was controlled to account for compression heating (3 to 4°C/100 MPa). The water jacket temperature was also maintained at the treatment temperature to reach the final temperature during pressurization. The rate of pressure increase was approximately 400 MPa min⁻¹ and pressure release time was less than 20 sec. Initial temperature of the medium, temperature changes during compression and decompression, and the final temperature were monitored with a thermocouple inserted in the pressure chamber. The pressure level, time and temperature of pressurization were set manually and controlled during the treatment by a remote controller.

2.1.2 Cultures and Media

The pathogens used were *Escherichia coli* O157:H7 933 (from M. Doyle, University of Georgia, Griffin, GA, USA) and *Staphylococcus aureus* 485 (from FDA Food Microbiology Laboratory, Washington, D.C., USA). Selected bacteria were all involved in foodborne diseases and toxications. Previous work had shown these strains to be relatively more pressure resistant (Alpas et al., 1999). The strains were cultivated in tryptic soy broth supplemented with 0.6% yeast extract (TSBYE, Merck, Darmstadt, Germany) at 37°C for 16-18 h and transferred to fresh broth every 48 h.

2.1.3 Raw Material

Carrots were purchased from a local market, washed with tap water and peeled. They were sliced and strained in a juice extractor (Moulinex, Spain) prior to experiments in order to obtain fresh carrot juice. Purchased carrots were stored at 4°C before sample preparation.

2.2 Methods

2.2.1 Determination of Early Stationary Growth Phase

E. coli O157:H7 933 and *S. aureus* 485 were grown in TSBYE at 37°C overnight and 100 µl of both culture broth was inoculated into 250 ml TSBYE in triplicate. Triplicate samples of each culture broth were taken from the incubator every hour to measure the Optical Density at 600 nm (OD_{600 nm}) using a UV- VIS spectrophotometer (UV1201, Shimadzu, Japan). This procedure was repeated until a constant OD_{600 nm} reading is observed. Plate counts were also performed every two hour, parallel with OD_{600 nm} measurements, on Tryptic Soy Agar supplemented with 0.6% Yeast Extract, (TSAYE; Merck, Darmstadt, Germany) as a non-selective agar medium. 0.1 mL portions of the selected dilutions were surface plated in duplicate on pre-poured non-selective agar media plates. The plates were incubated at 37°C for 48 h and plates containing 25-250 cfu mL⁻¹ were selected for enumeration. Each experiment was performed twice on separate days, and the average results are presented.

Growth curves were plotted for each strain as average OD_{600 nm} measurements versus time of incubation, and log number of survivals (cfu mL⁻¹) versus time of incubation (Appendix A). The time of early stationary phase of growth was determined for each strain by using the respective growth curve. This information was used in the subsequent studies to obtain cells at their early stationary phase of growth before HHP treatments.

2.2.2 Preparation and Inoculation of Carrot Juice and Model System

Fresh carrot juice was heat treated at 80°C for 12 min to minimize the initial load. 0.1% peptone water (Merck, Darmstadt, Germany) and carrot juice were inoculated with pure cultures at their early stationary phases to obtain about 10⁷ colony forming units (cfu mL⁻¹) per sample. Each sample was then aseptically transferred to a sterile stomacher bag (Fisher Scientific, Pittsburgh, Pa.) in 2 mL portions, vacuum packaged and heat-sealed. The bags were placed inside a second sterile stomacher bag and heat-sealed under vacuum to prevent contamination of the high-pressure unit if the primary package were to fail. After packaging, the samples were kept in ice-water until pressurization.

2.2.3 Determination of pH

After sterilization, pH values of peptone water and carrot juice were measured by a pH- meter (MP 220, Mettler Toledo International Inc.). pH measurements were performed triplicate on separate days and average results are presented.

2.2.4 HHP Treatment

E. coli O157:H7 933 cells inoculated in peptone water and carrot juice were subjected to HHP at 200, 250 MPa for 0- 40 min in peptone water and carrot juice, at 275, 300 and 325 MPa for 0- 10 min in peptone water, and 0- 15 min in carrot juice at 40°C. For *S. aureus* 485, HHP conditions were 200, 250 MPa for 0- 40 min in peptone water, 300, 350, and 400 MPa for 0- 15 min 40°C in peptone water and carrot juice. Pressurization times did not include the pressure increase and release times. Duplicate bags were used for each treatment. Immediately after pressurization the bags were removed, cooled in an ice bath for enumeration of viable cells (cfu mL⁻¹). A control was held in ice bath at atmospheric pressure.

2.2.5 Enumeration of Viable Cells

Pressurized and control cell suspensions were serially diluted in 0.1% sterile peptone water. The non-selective agar medium for both pathogens was Tryptic Soy Agar supplemented with 0.6% Yeast Extract (TSAYE; Merck, Darmstadt, Germany). From the selected dilutions, 0.1 mL portions were surface plated in duplicate on prepoired non-selective agar media plates. The total of four plates (two bags x two plates) was incubated at 37°C for 48 h and plates containing 25- 250 cfu mL⁻¹ were selected for enumeration. Each experiment, with duplicate bags for each strain, was performed twice on separate days, and the average results are presented (n=8).

2.2.6 Modeling of the Inactivation Curves

2.2.6.1 First-order Kinetics

Integrated form of the first-order model that was used to describe the microbial inactivation as a function of time was:

$$\text{Log}_{10}S(t) = -\frac{t}{D} \quad (2.1)$$

where; $S(t)$ is the survival ratio, $S(t) = N(t)/N_0$, N = number of surviving microorganisms after pressure treatment time t in min, N_0 number of microorganisms at time $t = 0$ min, D is the decimal reduction time (Basak et al., 2002). $\text{Log}_{10} S(t)$ versus time t was a straight line on a semi-log plot, so Eq. (2.1) was used to fit linear survival curves and related D values for each pressure level was calculated from the negative reciprocal slope of the regression line.

2.2.6.2 Weibull Model

The cumulative form of the Weibull distribution that was used to describe the inactivation curves was:

$$\text{Log}_{10}S(t) = -\left(\frac{t}{\alpha}\right)^{\beta} \quad (2.2)$$

where α and β are the scale and shape factors, respectively (Van Boekel, 2002).

$\log_{10} S(t)$ versus time t was plotted and the inactivation curves were obtained for each pathogen studied. Model parameters were calculated from the obtained curves. Such a model presents the main advantage of remaining very simple and being sufficiently robust to describe both downward concave ($\beta > 1$) and upward concave survival curves ($\beta < 1$). The model also includes the traditional case where the survival curve is linear ($\beta = 1$) (Mafart et al., 2002; Peleg and Cole, 1998).

2.2.7 SEM Analysis

SEM analyses were performed right after pressurization of *E. coli* O157:H7 933 and *S. aureus* 485 to prevent the autolysis of injured and dead cells. *E. coli* O157:H7 933 cells were subjected to HHP at 200, 250, 275, 300, and 325 MPa for 1 min at 40°C in peptone water. For *S. aureus* 485, HHP conditions were 200, 250, 300, 350, and 400 MPa for 5 min at 40°C in peptone water. These pressure-time parameters were chosen specifically for each bacterium based on their inactivation level. Time remained constant for each pressure treatment to observe the changes in cell morphology and to compare the area and volume changes of the cells with increasing pressure.

Cell pellets of *E. coli* O157:H7 933 and *S. aureus* 485 were prepared from untreated and pressure-treated cell suspensions by centrifugation at 10 000 g for 10 min and washed twice with 0.1 M phosphate buffer at pH 7.4. Cell pellets were then re-suspended in 1 ml of 0.1 M phosphate buffer. Suspended bacteria were filtered (0.22 μm Millipore, GSWP) and fixed on the membrane with 10 ml 3% glutaraldehyde in 0.1 M phosphate buffer (pH 7.4). Fixatives were left in contact with the cells overnight at 4°C. Membranes were then taken to glass vials, washed 3 times with buffer, after 10 min for each treatment, and post-fixed for 1h in 1% osmium tetroxide. Membranes were rinsed with buffer twice with 10 min

intervals. They were dehydrated through a series of ethanol (EtOH) solutions (with increasing concentrations 50%, 70%, 80%, 95% and 100%), rinsing with 10 ml ethanol at each concentration, and waiting for 10 min for each. Instead of critical point drier hexamethyldisilazane (HMDS), drying was used as a chemical drying method. Membranes were washed with a series of HMDS solutions (3:1 EtOH: HMDS 15 min, 1:1 EtOH: HMDS 15 min, 1:3 EtOH: HMDS 15 min, 100% HMDS 2x15 min) and dried in the hood overnight. After mounting the dried specimens on stubs, they were sputter-coated with a heavy metal (platinum, gold or gold-palladium) for electrical conductivity, and observed in SEM (FEI Nova Nanosem 400, FEI Company, OR, USA).

2.2.8 Fluorescent Microscopy

Live/DEAD Backlight Bacterial Viability Kit (Invitrogen, Molecular Probes, Eugene, Oregon, USA) was used for fluorescent microscopy. 3.34 mM SYTO 9 Nucleic acid stain solution in DMSO is combining with live cells. 20 mM propidium iodide (PI) solution in DMSO is used as the membrane permeable dye and combines with only dead cells.

Cell pellets of selected pathogens were prepared from untreated and pressure-treated cell suspensions with the same pressure time combinations as in SEM analysis by centrifugation at 10 000 g for 10 min, washed twice with 0.1 M phosphate buffer and resuspended in 1 ml buffer. PI and SYTO 9 dyes were added to the cell suspension and incubated for 20 min in dark. Cell suspension loaded with probes was transferred to microscope slide with cover slip and examined with fluorescent microscopy (Olympus DP70, Olympus America Inc., NY, USA) equipped with a computer for image analysis.

2.2.9 Machine Vision Analysis

SEM images were used for calculation of the view area and volume. The SEM image (Figure 2.1) was “cleaned” using Corel PhotoPaint 11 image editing software. This involves erasing everything manually but the organisms that were visible in full form (not partially blocked by other organisms), not dividing, and not touching the image edges. The scale line of the SEM image was used as a size reference square using the rectangle tool in Corel PhotoPaint 11 (assuming square pixels, Figure 2.2). LenseEye version 7.5.1 software was used to calculate the view area of the organisms, taking the square shape as a size reference.

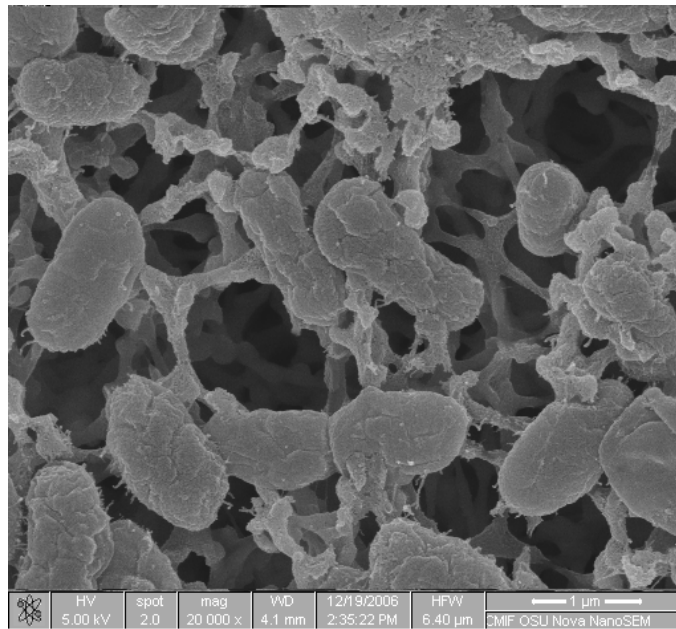


Figure 2.1 SEM micrograph of pressurized (325 MPa- 1 min- 40°C) *E. coli* O157:H7 933

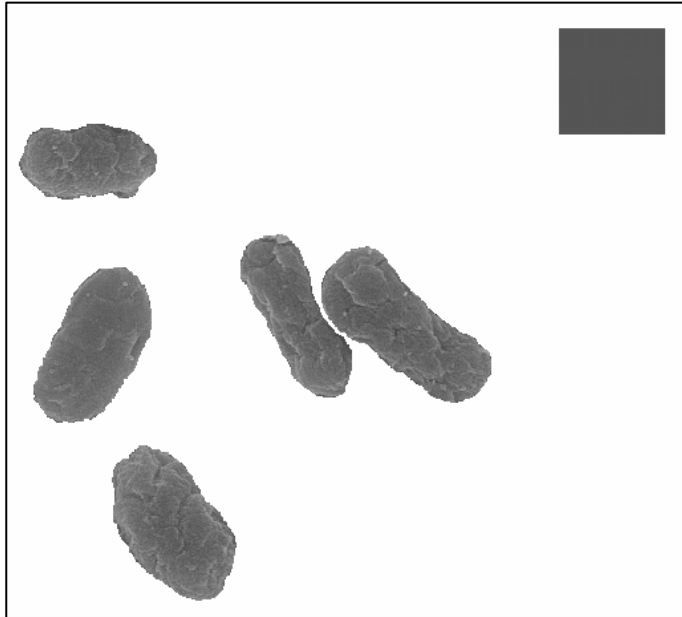


Figure 2.2 Isolated organisms from Figure 1, with size reference square

Volume calculation was based on the assumption that there exists a “curve of symmetry” (CS) of the two-dimensional image (Figure 2.3). It was assumed that the organism has a volume of revolution around the CS. The curve of symmetry was found from the “distance transform (DT)” function. First, the perimeter points of the image was identified, then the distances of each and every point within the image to all the perimeter points are calculated, and finally the minimum distance was taken for each point so that DT will result in a CS (Figure 2.3).

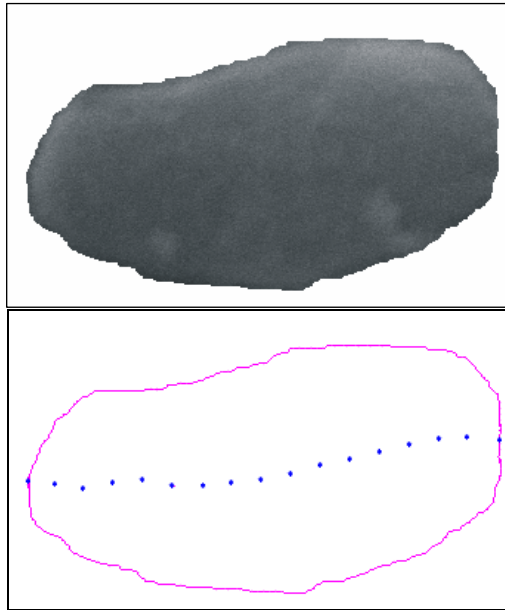


Figure 2.3 An isolated organism, its perimeter and its curve of symmetry obtained by image analysis

Once the CS is defined, then perpendiculars to the perimeter were drawn at regular intervals (Figure 2.4). Each slice was assumed a circular section. If the slices are not perpendicular to the CS, then the cross-sections of the slices will not necessarily be circles, but ellipses. This will make the calculations much more complex. The perpendicular sections are shown in Figure 2.4. Circular portions of this image were rotated around the symmetry axis to result in a three-dimensional solid of rotation. The volume of each slice can then be calculated by assuming cylindrical cuts. In addition, the ends were considered as spherical cuts and their volume were added to the total. In Figure 2.4, the centers of the left and right spherical caps are shown, as well as the CS, the perpendicular lines, and the

circular approximations. The first line on the left (denoted by 1) represents the spherical cut on the left, and the rightmost line (represented by 19) shows the spherical cut on the right.

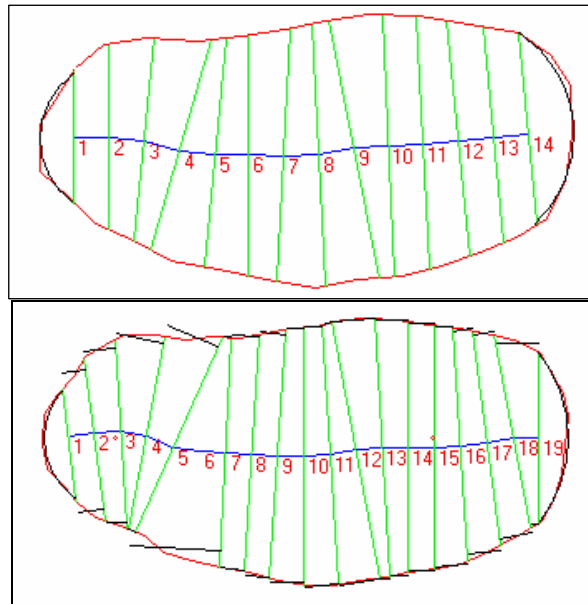


Figure 2.4 Volume calculation details for the organism in Figure 3, with different number of volume slices

The accuracy of the volume calculations depends on the number of perimeter points, the number of slices, and the angle of the object relative to the CS. The effect of the variables on the calculated volume was investigated by using a test image developed with a known geometry and therefore known volume of rotation (Figure 2.5). The typical error in calculating the volume was on the average less

than 1% (Appendix B.1). This method of calculating volume seems quite stable, independent of the angle of CS from the horizontal, number of perimeters taken, and number of slices allowed. This suggests a robust method of volume estimation. Figure 2.6 shows details of volume calculation of the cells using the LensEye Software.

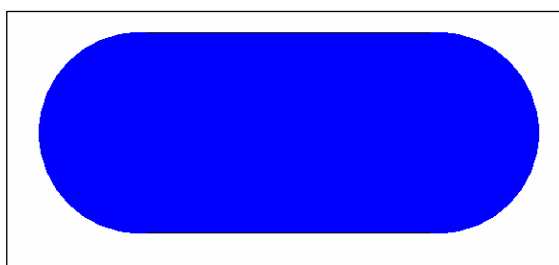


Figure 2.5 Test image to confirm volume calculation accuracy

The effect of SEM magnification on the view area of cells was also studied. Average error was less than 2.5 % for four different magnification levels on the same microorganism (Appendix B.2).

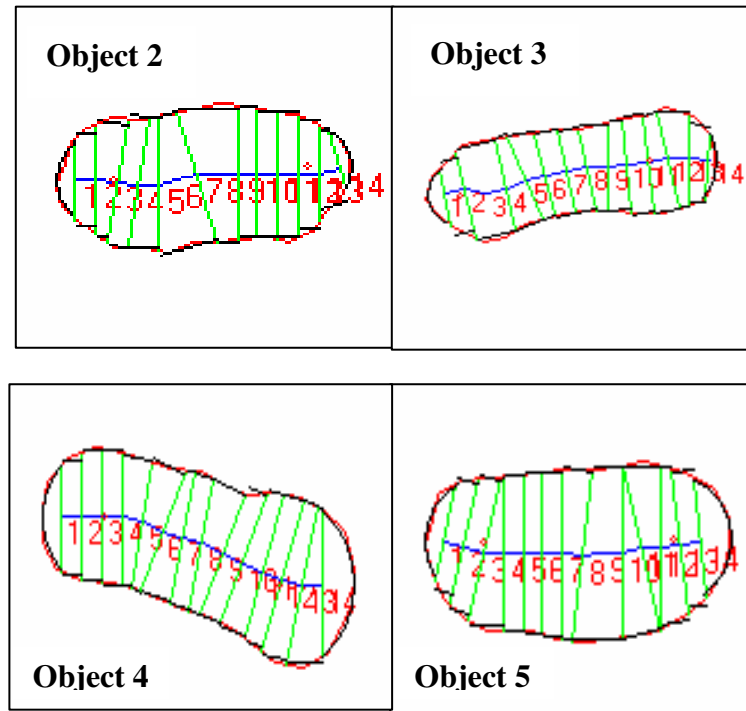


Figure 2.6 Volume calculation details for different organisms

2.2.10 Data Analysis

2.2.10.1 Model Evaluation

SigmaPlot 2000 Version 6.00 (Chicago, IL, USA) was used for linear and nonlinear regression analysis and for determination of the first- order and Weibull model parameters. The goodness-of-fit of the model was assessed using adjusted regression coefficient (R^2_{adj}) and root mean square error (RMSE) values. Table

Curve 3D (Version 4.0 Systat Software Inc., CA, USA) was used to fit equations and plot 3D graphs for the Weibull model parameters.

2.2.10.2 Statistical Analysis

One-way ANOVA and Tukey's pairwise comparisons tests were performed to determine the effect of pressure levels on volume and the view area of microorganisms. MINITAB 13 for Windows was used for this purpose. Calculated view area and volume values were presented as \pm standard deviation (SD). Comparison tests were performed within the confidence interval of 95% ($p < 0.05$).

CHAPTER 3

RESULTS AND DISCUSSION

3.1 Inactivation of *Escherichia coli* O157:H7 933 and *Staphylococcus aureus* 485 by High Hydrostatic Pressure (HHP) in Carrot Juice

3.1.1 Pressure Inactivation Curves of Foodborne Pathogens

Inactivation curves of *E. coli* O157:H7 933 and *S. aureus* 485 determined at different pressure levels (200 to 400 MPa) at a constant temperature (40°C) in peptone water (pH= 6.95) and carrot juice (pH= 6.22) are given in Figures 3.1 to 3.7. The rate of microbial inactivation increased with increasing pressure in both carrot juice and peptone water. However, the effect of treatment media varied: more reduction was obtained in peptone water (5.7-log_{10} cfu mL⁻¹) than in carrot juice (4.6-log_{10} cfu mL⁻¹) for *E. coli* O157:H7 933. In case of *S. aureus* 485 higher reduction was obtained in carrot juice (5.6-log_{10} cfu mL⁻¹) than in peptone water (4.5-log_{10} cfu mL⁻¹).

In general, Gram-negative bacterial cells are more sensitive to pressure than Gram-positive bacterial cells (Alpas et al., 2000). The same phenomenon was observed in peptone water but not in carrot juice in this study. Furthermore, a

classification scheme was suggested correlating pressure sensitivity and morphology of the bacteria. Corresponding to this scheme, a correlation with the gram-type could not be observed. Most pressure sensitive bacteria are rod- or spiral-shaped, whereas the most resistant ones are spherical in shape. Concerning the gram-type, it was concluded that the cell wall itself does not protect the bacteria against high pressure (Hartmann et al., 2006).

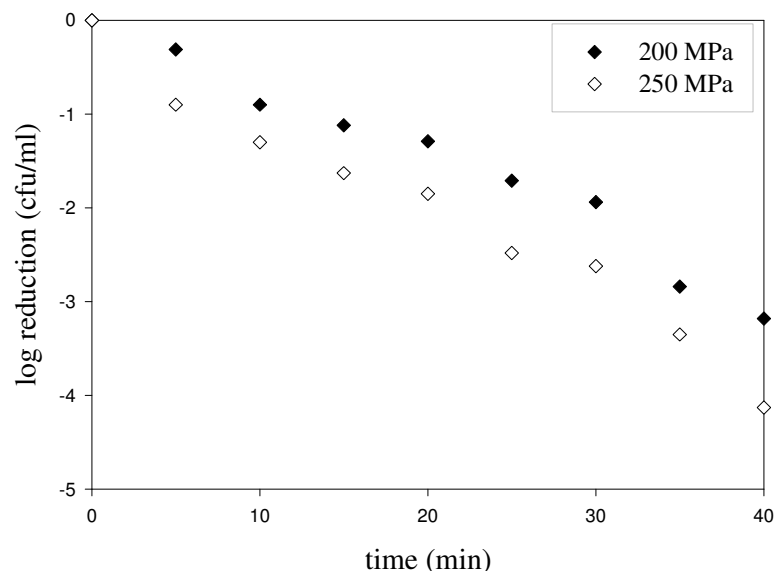


Figure 3.1 Inactivation curves of *E. coli* O157:H7 933 for 200 MPa and 250 MPa in peptone water (pH= 6.95) at 40 °C

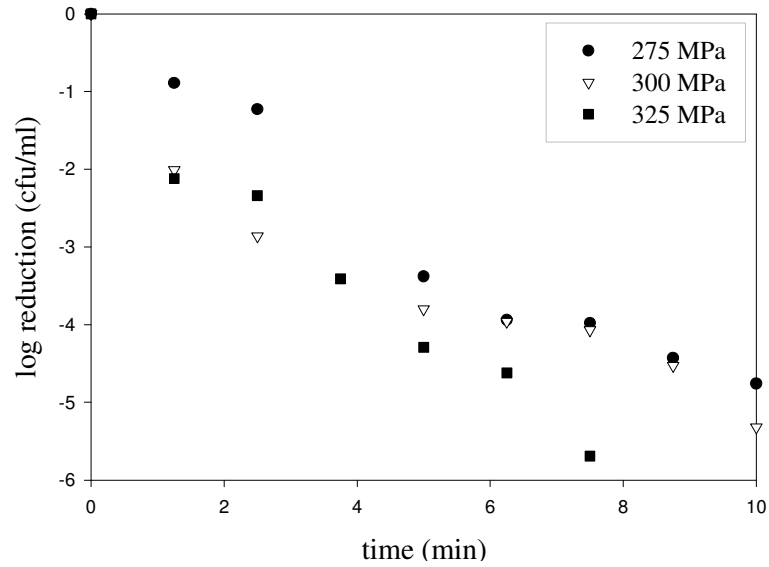


Figure 3.2 Inactivation curves of *E. coli* O157:H7 933 for 275 MPa, 300 MPa and 325 MPa in peptone water (pH= 6.95) at 40 °C

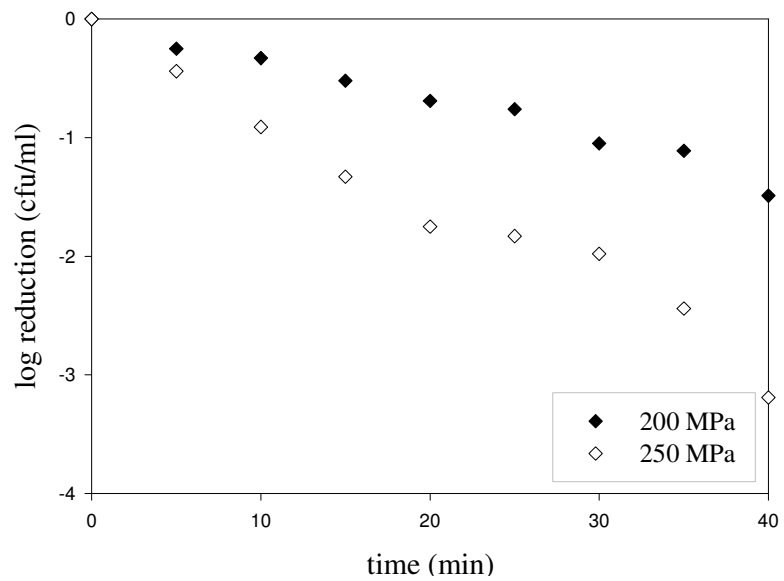


Figure 3.3 Inactivation curves of *E. coli* O157:H7 933 for 200 MPa and 250 MPa in carrot juice (pH= 6.22) at 40 °C

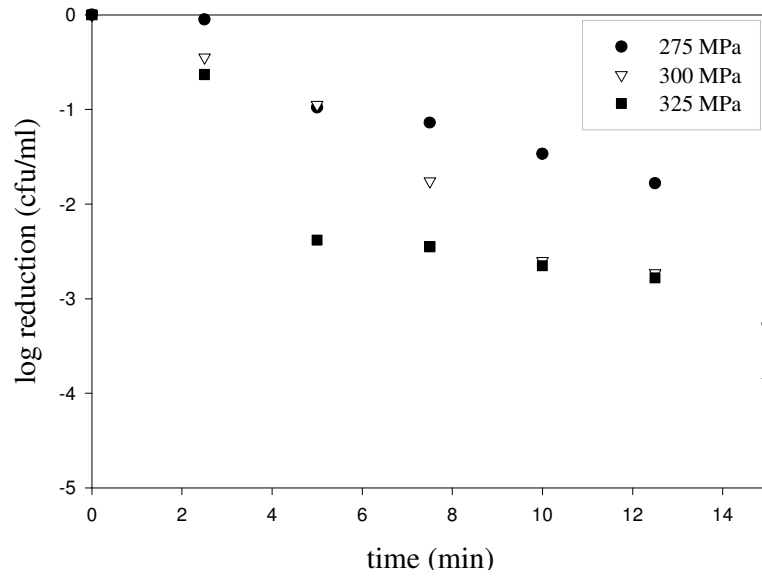


Figure 3.4 Inactivation curves of *E. coli* O157:H7 933 for 275 MPa, 300 MPa and 325 MPa in carrot juice (pH= 6.22) at 40 °C

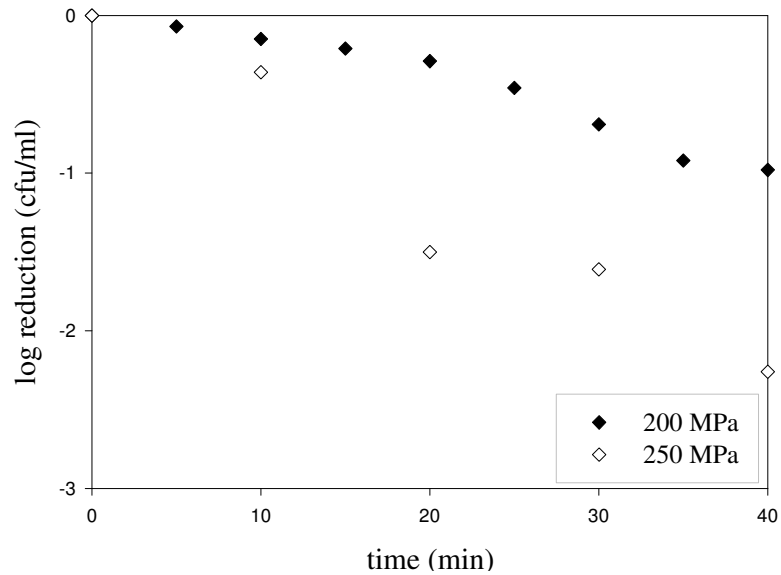


Figure 3.5 Inactivation curves of *S. aureus* 485 for 200 MPa and 250 MPa in peptone water (pH= 6.95) at 40 °C

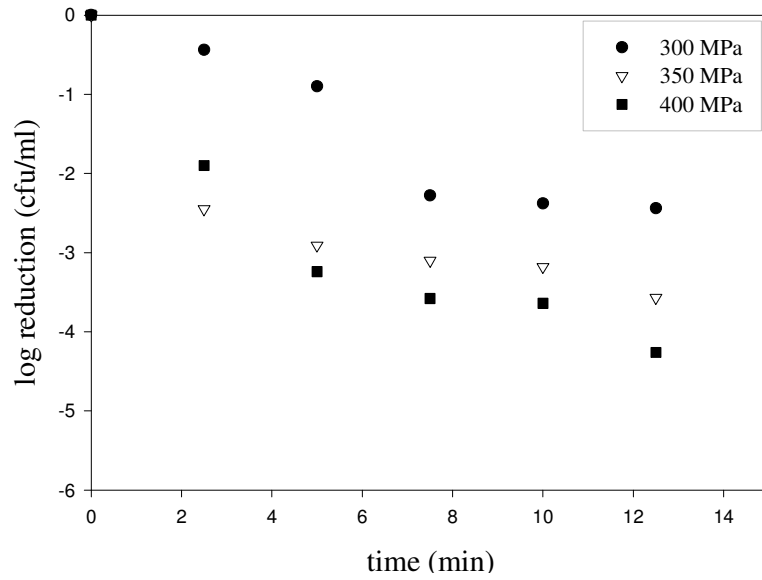


Figure 3.6 Inactivation curves of *S. aureus* 485 for 300 MPa, 350 MPa and 400 MPa in peptone water (pH= 6.95) at 40 °C

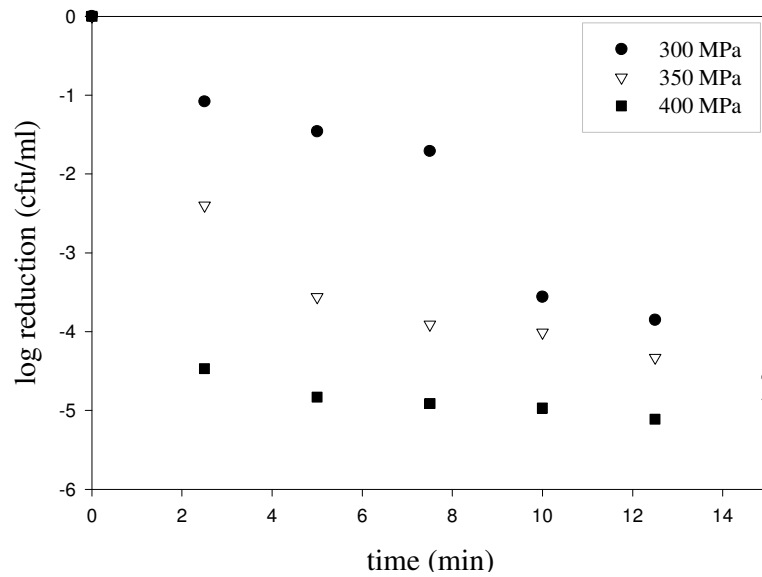


Figure 3.7 Inactivation curves of *S. aureus* 485 for 300 MPa, 350 MPa and 400 MPa in carrot juice (pH= 6.22) at 40 °C

3.1.2 Modeling of Inactivation Kinetics

The fits of the Weibull model for *E. coli* O157:H7 933 and *S. aureus* 485 are shown in Figures 3.8 to 3.11. The fits of the first-order model and the regression result sheets of both models are detailed in Appendix C. The goodness-of-fit of the Weibull and first-order models was compared by computing R^2_{adj} and RMSE values (Table 3.1). R^2_{adj} measures how well a model fit to the data and higher the R^2_{adj} value, the better is the adequacy of the model to describe the data. RMSE measures the average deviation between the observed and fitted values. Small RMSE value of a model indicates a better fit of the data for that model (Buzrul and Alpas, 2004). Higher R^2_{adj} and smaller RMSE mean values were obtained for almost all treatment conditions for the Weibull model, which indicates better fit. As the pressure increased (300 to 400 MPa) the linear model had lower R^2_{adj} and higher RMSE values than Weibull model since the shapes of the inactivation curves changed their pattern by a rapid initial drop in bacterial counts followed by tailing. However, the Weibull model produced almost linear fittings at low pressure levels (200 and 250 MPa).

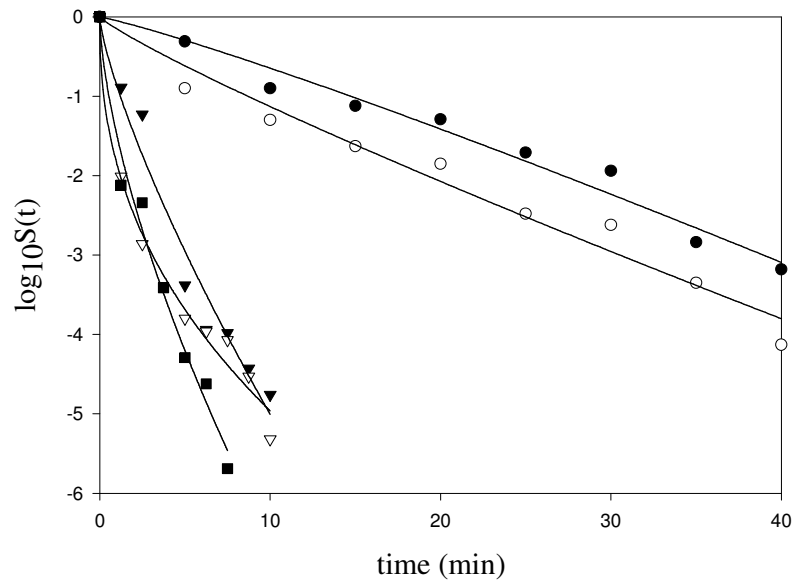


Figure 3.8 Inactivation curves of *E. coli* O157:H7 933 at different pressure levels (●, 200 MPa; ○, 250 MPa; ▼, 275 MPa; ▽, 300 MPa; ■, 325 MPa) in peptone water (pH= 6.95) at 40°C modeled with Weibull distribution

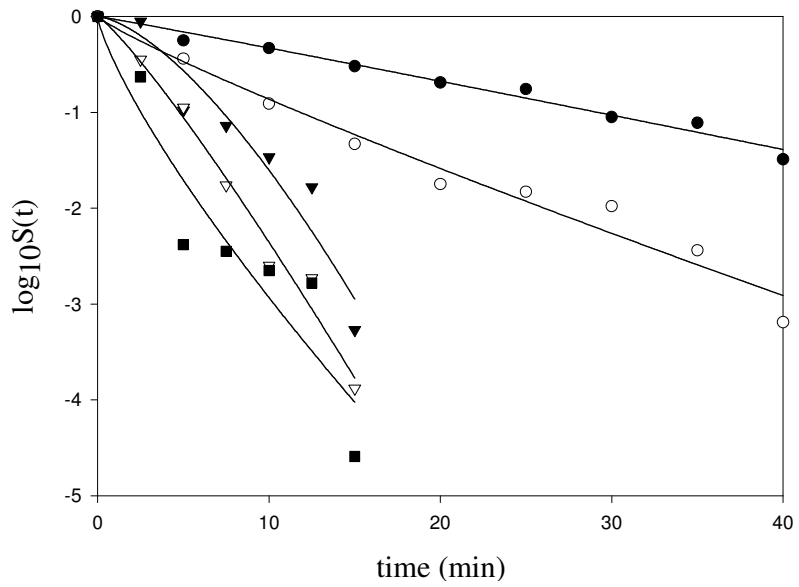


Figure 3.9 Inactivation curves of *E. coli* O157:H7 933 at different pressure levels (●, 200 MPa; ○, 250 MPa; ▼, 275 MPa; ▽, 300 MPa) in carrot juice (pH= 6.22) at 40°C modeled with Weibull distribution

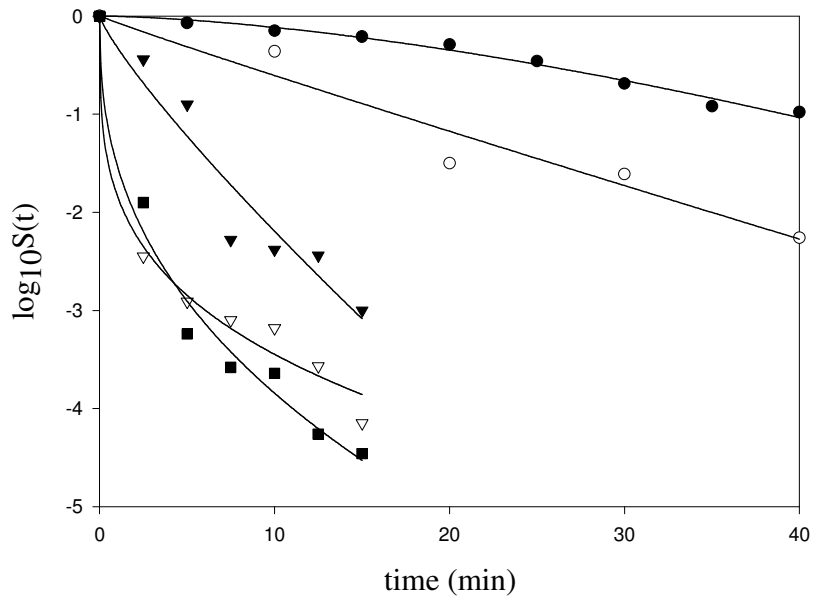


Figure 3.10 Inactivation curves of *S. aureus* 485 at different pressure levels (●, 200 MPa; ○, 250 MPa; ▼, 275 MPa; ▽, 300 MPa; ■, 325 MPa) in peptone water (pH= 6.95) at 40°C modeled with Weibull distribution

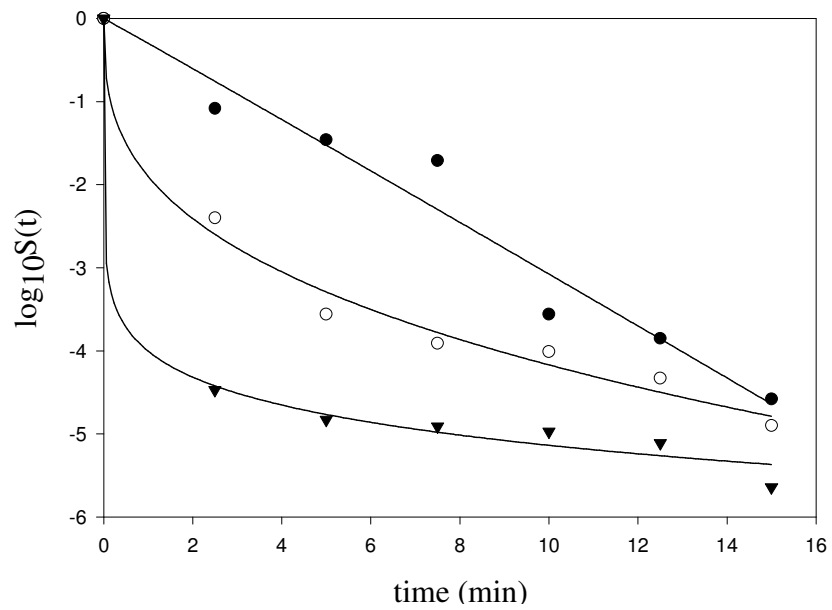


Figure 3.11 Inactivation curves of *S. aureus* 485 at different pressure levels (●, 300 MPa; ○, 350 MPa; ▼, 400 MPa) in carrot juice (pH= 6.22) at 40°C modeled with Weibull distribution

Table 3.1 Comparison of the first-order and Weibull models for the inactivation curves of foodborne pathogens in peptone water (PW) and carrot juice (CJ) at 40°C

Bacterial Strain	Medium	Pressure (MPa)	Weibull Distribution		First-order kinetics	
			R^2_{adj} ^(a)	RMSE ^(b)	R^2_{adj}	RMSE
<i>E. coli</i> O157:H7 933	PW	200	0.97	0.18	0.97	0.18
		250	0.97	0.23	0.96	0.24
		275	0.96	0.35	0.94	0.43
		300	0.98	0.22	0.74	0.86
		325	0.98	0.28	0.91	0.56
		Mean	0.97	0.25	0.91	0.45
<i>E. coli</i> O157:H7 933	CJ	200	0.98	0.07	0.98	0.07
		250	0.97	0.18	0.96	0.19
		275	0.91	0.33	0.89	0.38
		300	0.98	0.20	0.98	0.21
		325	0.87	0.55	0.87	0.54
		Mean	0.94	0.26	0.94	0.28
<i>S. aureus</i> 485	PW	200	0.98	0.05	0.92	0.10
		250	0.93	0.25	0.95	0.21
		300	0.92	0.33	0.92	0.33
		350	0.98	0.19	0.48	0.96
		400	0.98	0.23	0.67	0.89
		Mean	0.96	0.21	0.79	0.50
<i>S. aureus</i> 485	CJ	300	0.95	0.37	0.96	0.34
		350	0.99	0.20	0.58	1.06
		400	0.99	0.17	0.02	1.89
		Mean	0.98	0.24	0.59	0.95

^(a) Adjusted regression coefficient, ^(b) Root mean square error

3.1.3 Parameters of the Models

Parameters and the standard errors of the Weibull model, [scale factor (α) and shape factor (β)], and D-value of the first-order model are given in Table 3.2. The shape factors (β) of Weibull model indicated that survival curves of *E. coli* O157:H7 933 and *S. aureus* 485 in peptone water and carrot juice at 40°C were both concave downward ($\beta > 1$) and concave upward ($\beta < 1$). Among the studied parameters, shape factor (β) decreased with increasing pressure; however, there were some exceptional cases where it was greater at higher pressure levels. For example; at 275 and 300 MPa, shape factors of *E. coli* O157:H7 933 in carrot juice were greater ($\beta = 1.5 \pm 0.3$ and 1.2 ± 0.1 , respectively) than those at 200 MPa ($\beta = 1.0 \pm 0.1$). There was only one case where the Weibull model was inappropriate to fit the data of *E. coli* O157:H7 933 in carrot juice (at 325 MPa, see Table 3.1).

Although the Weibull model has an empirical nature, a link can be made with microbial inactivation as follows. Downward concavity ($\beta > 1$) indicates that remaining members become increasingly damaged; whereas upward concavity ($\beta < 1$) indicates that remaining members have the ability to adapt to the applied stress (van Boekel, 2002). Therefore, concave upward ($\beta < 1$) survival curves of the organisms fitted with this model can be interpreted as an evidence of weak or sensitive members of the population that are destroyed at a relatively fast rate leaving behind survivors of higher resistance (Buzrul et al., 2005; Peleg, 2000).

Table 3.2 Parameters of the Weibull and first-order models in peptone water (PW) and carrot juice (CJ) at 40°C

Bacterial Strain	Medium	Pressure (MPa)	Weibull Distribution		First-order kinetics
			α (D_1) ^(a) (min)	β ^(b)	D- value (min)
<i>E. coli</i> O157:H7 933	PW	200	14.73±1.17	1.13±0.11	13.40±0.47
		250	8.70±1.17	0.87±0.09	10.16±0.35
		275	1.21±0.30	0.76±0.10	1.88±0.09
		300	0.24±0.08	0.43±0.04	1.72±0.15
		325	0.54±0.14	0.65±0.07	1.24±0.07
<i>E. coli</i> O157:H7 933	CJ	200	29.17±0.85	1.04±0.09	29.15±0.85
		250	11.82±1.24	0.88±0.09	13.26±0.46
		275	7.30±0.92	1.50±0.32	5.71±0.52
		300	4.78±0.45	1.16±0.11	4.14±0.15
		325	2.52±1.04	0.78±0.21	3.51±0.28
<i>S. aureus</i> 485	PW	200	39.13±0.92	1.58±0.13	44.64±2.80
		250	16.91±2.98	0.95±0.24	17.42±1.19
		300	3.93±0.93	0.84±0.18	4.66±0.30
		350	0.11±0.08	0.28±0.05	3.11±0.40
		400	0.36±0.16	0.40±0.05	2.78±0.29
<i>S. aureus</i> 485	CJ	300	3.30±0.66	1.01±0.16	3.25±0.15
		350	0.15±0.07	0.34±0.04	2.57±0.30
		400	0.00±0.00	0.11±0.02	2.10±0.36

^(a) Scale factor (first decimal reduction time), ^(b) Shape factor

In the Weibull model, the scale parameter (α) represents the first reduction time (D_1) that leads to 10-fold reduction of the surviving population (analogous to the D-value) (Peleg, 1999; van Boekel, 2002). This parameter can be compared with the classical D-value of the first-order model, even though it has a different meaning. When α (D_1) and D-values in Table 3.2 were compared, it was observed that, except for some values (especially at pressure levels lower than 250 MPa), α values were smaller than the D-values for both microorganisms. This indicated over-processing if first-order model had been used instead of Weibull model. There is also a risk of under-processing when α value is greater than the D-value. However, one log reduction is rarely a target in food processing, therefore it is wise to compare the total process times for sterilization or pasteurization depending on the food product. According to Juice HACCP Hazards and Controls Guidance (Anonymous, 2004), 5- \log_{10} pathogen reduction must be accomplished for carrot juice; therefore it would be more useful and accurate to compare 5- \log_{10} reduction values of both models.

In order to calculate other log reductions, one can use;

$$t = D_d = d^{1/\beta} \cdot \alpha \quad (3.1)$$

where (d) represents decades reduction of a microbial population and α is the time of first decimal reduction (D_1) obtained from equation (2.2) (Buzrul, 2007; Peleg, 1999). As a consequence of non-linear behavior, time needed for 5- \log_{10} reduction for the Weibull model is not $5D_1$ but it is D_5 . For instance, for *E. coli* O157:H7 933 in peptone water at 250 MPa $D_5= 54.7$ min, but $5D= 50.8$ min. This indicates under-processing if first-order model is used instead of Weibull model when the target is 5- \log_{10} reduction.

When D_5 and $5D$ values in Table 3.3 were compared, one can say that for both pathogens under-processing occurred in peptone water for treatments higher than 200 MPa if first-order model was used. In case of carrot juice both under- and over-processing concepts were observed for both pathogens at the pressure levels studied.

Van Opstal et al. (2005) studied the inactivation of *E. coli* MG1655 in HEPES-KOH buffer and in fresh carrot juice. In contradiction to the results presented here, a linear relationship between \log_{10} inactivation and holding time for all pressure-temperature combinations were reported in carrot juice. However, the Weibull model described the entire set of inactivation curves of *E. coli* MG1655 in HEPES-KOH buffer more accurately when compared to the log-linear or the biphasic model.

Table 3.3 Process times calculated to accomplish 5- \log_{10} reduction in peptone water (PW) and carrot juice (CJ) at 40°C by using Weibull distribution and first-order kinetics

Bacterial Strain	Medium	Pressure (MPa)	Weibull Distribution	First-order kinetics
			$D_5^{(a)}$ (min)	$5D^{(b)}$ (min)
<i>E. coli</i> O157:H7 933	PW	200	61.21	67.02
		250	54.72	50.81
		275	9.98	9.41
		300	10.18	8.62
		325	6.54	6.22
<i>E. coli</i> O157:H7 933	CJ	200	137.38	145.77
		250	74.11	66.31
		275	21.31	28.56
		300	19.12	20.70
		325	19.80	17.56
<i>S. aureus</i> 485	PW	200	108.44	223.21
		250	91.43	87.11
		300	26.63	23.31
		350	38.30	15.57
		400	19.19	13.92
<i>S. aureus</i> 485	CJ	300	16.15	16.23
		350	17.03	12.88
		400	7.82	10.52

^{(a), (b)} Time needed for 5- \log_{10} reduction

3.1.4 Pressure Dependence of Model Parameters

Since Weibull model fitted well to all of the survival curves, the model was further analyzed to determine the effect of pressure on 'α' and 'β' values. It was obvious that the two parameters, α and β, were pressure dependent. Although the Weibull model describes non-linear survival curves better than the linear model, with one more parameter, it is intrinsically more complex. The model can be simplified by fixing 'β' at an average value, but in this study the difference between 'β' values were large. It is also known that 'β' is structurally strongly correlated with 'α' values (Mafart et al., 2002; Chen and Hoover, 2004). Since 'β' could not be fixed at an average value in this study, a set of equations to determine the pressure and 'β' dependency of the scale factor, α was defined.

The Weibull model parameters (see Table 3.2) for each treatment were further analyzed with Table Curve 3D. The software fitted equations and plotted 3D graphs. Since approximately 100 equations for each treatment (Appendix D) have been obtained, one equation was selected according to the R² and Fit Standard Error values. An effort was also made to select the simpler forms of the equations with high R² (>0.90) and low Fit Standard Error values to be able to explain the mathematical relation of scale factor (α) with pressure and shape factor (β). Related graphs are presented in Figures 3.12 to 3.14 with equations selected. The data for *S. aureus* 485 in carrot juice could not be analyzed as at least four data points are required to plot a 3D graph by Table Curve 3D.

3D Graph for *E. coli* O157:H7 933 PW
Rank 73 Eqn 16 $z=a+bx+cx^2+dy$
 $r^2=0.9387886$ DF Adj $r^2=-.1NF$ FitStdErr=3.1803154 Fstat=5.1122756
 $a=70.459223$ $b=-0.42752956$
 $c=0.000620824$ $d=4.7520339$

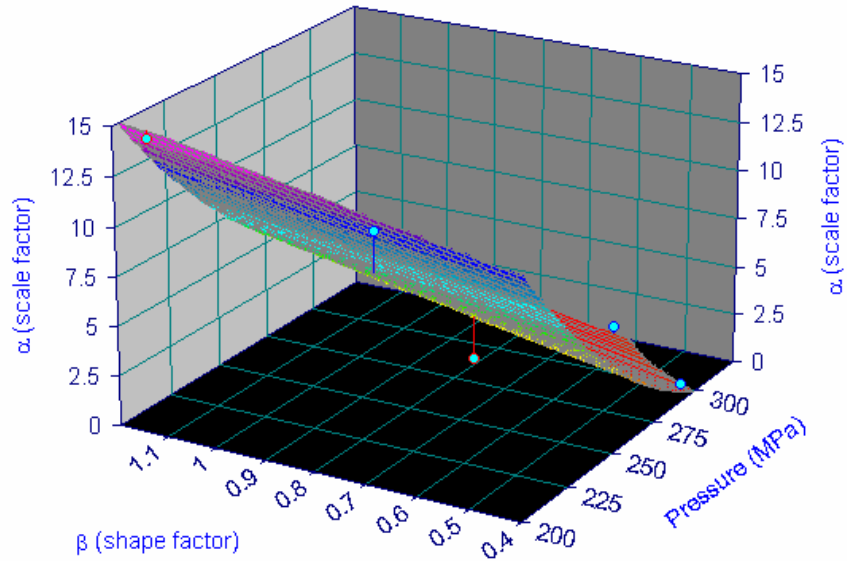


Figure 3.12 Dependence of scale factor (α) on pressure (MPa) and shape factor (β) for *E. coli* O157:H7 933 in peptone water

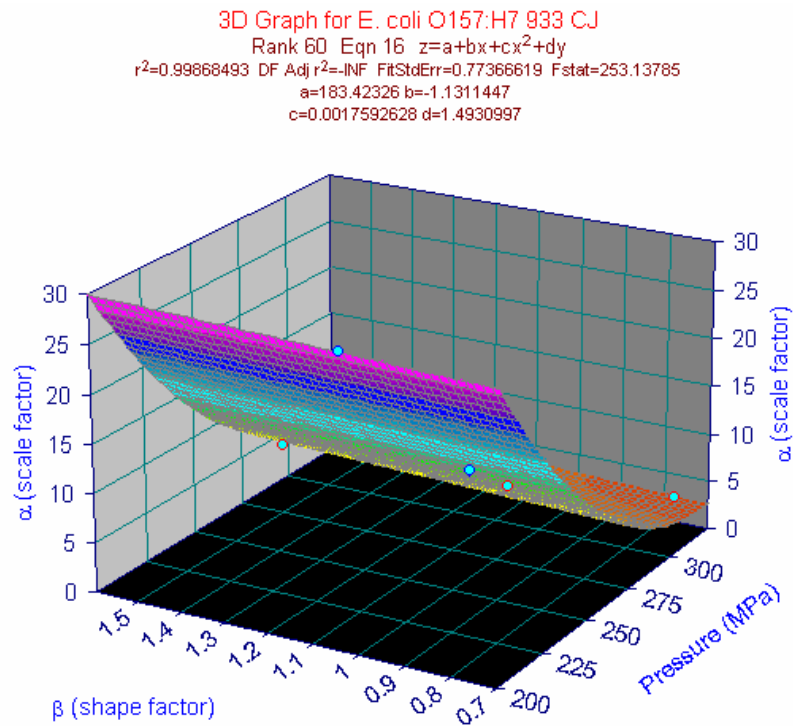


Figure 3.13 Dependence of scale factor (α) on pressure (MPa) and shape factor (β) for *E. coli* O157:H7 933 in carrot juice

E. coli O157:H7 933 in peptone water and carrot juice had the same equation for the 3D graph (Figures 3.12- 3.13). The equation for *S. aureus* 485 in peptone water is given in Figure 3.14. According to these equations the scale factor ‘ α ’ had both direct and polynomial relationship with pressure and a direct relationship with shape factor for *E. coli* O157:H7 933. Polynomial effect of pressure was very small relative to its direct effect. The negative sign for pressure also indicated that as pressure increased scale factor decreased as it was also the

observed fact during experiments. The shape factor was the only difference between the equations of *S. aureus* 485 and *E. coli* O157:H7 933. The effect of pressure remained the same where the scale factor had an inverse relationship with shape factor for *S. aureus* 485.

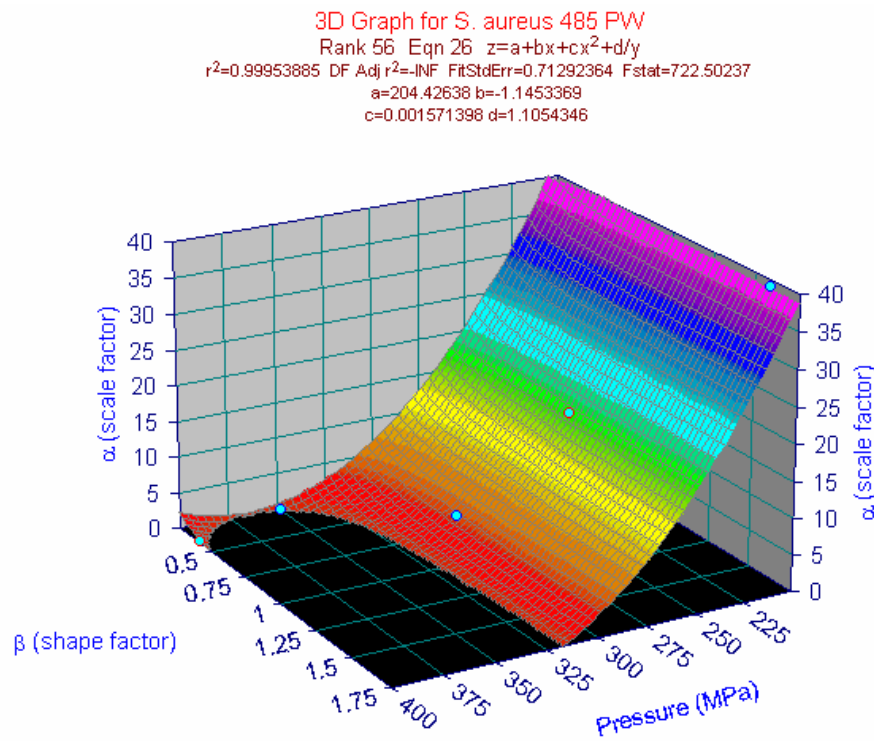


Figure 3.14 Dependence of scale factor (α) on pressure (MPa) and shape factor (β) for *S. aureus* 485 in peptone water

3.1.5 Effect of External Factors on Inactivation Curves

The shapes of the inactivation curves of both pathogens were very similar (See Figures 3.1- 3.7). A treatment of 400 MPa for 2.5 min at 40°C in carrot juice reduced the microbial load of *S. aureus* 485 around 4-5 log₁₀; however, extending the treatment time to 15 min increased the reduction by an additional one log₁₀. The results indicated that small populations of bacteria were much more pressure resistant than the rest of the population. Although the reason for this phenomenon is not clearly understood, one possible explanation may be the heterogeneous sensitivities of the bacterial populations caused by different physiological states. Consequently, it is not desirable to extend treatment time to increase pressure inactivation of these pathogens. A more effective way for the inactivation would be to increase pressure level and/or temperature so that treatment time can be substantially decreased (Chen, 2007; Bayındırlı et al., 2006).

The kinetic data indicated that the pressure resistance of *E. coli* O157:H7 933 and *S. aureus* 485 depended on the pressurization medium. *E. coli* O157:H7 933 was more pressure sensitive in peptone water than in carrot juice whereas *S. aureus* 485 suspended in peptone water was more pressure resistant than in carrot juice. Although, it was reported that the cells in food systems are more resistant to pressure than in buffer solutions (Alpas et al., 2003; Chen and Hoover, 2003; Van Opstal et al., 2005), the results of our study revealed that food systems can exhibit either protective or sensitizing effect on microorganisms. This may be due to the naturally occurring constituents or phytoalexins in cellular and vascular fluids released as a result of rupturing carrot cells that could have a bactericidal effect on *S. aureus* 485. Studies suggested that, the compound exerted its toxic effect by interacting with cell membranes and disturbing membrane associated functions (Beuchat and Brackett, 1990).

6- Methoxymellein was identified as a common phytoalexin produced by carrot roots and had a broad antimicrobial spectrum. Phytoalexins were defined as the low molecular weight antimicrobial compounds produced by plants in response to the infection by microorganisms. These compounds are accumulated at the site of infection and were considered to be involved in the defense mechanism of plant to potential plant pathogens. The ability of 6- methoxymellein to inhibit the growth of several fungi, yeasts and bacteria was reported. It was found effective in inhibiting the growth of several fungi. The antibacterial activities of 6-methoxymellein are summarized in Table 3.4. In general, Gram-positive bacteria were reported to be more sensitive to 6- methoxymellein than Gram-negative bacteria (Kurosaki and Nishi, 1983).

Table 3.4 Antibacterial activities of 6- methoxymellein (Adapted from Kurosaki and Nishi, 1983).

Bacteria	Incubation Time (hour)	Inhibition (%) Concentration 0.5 mM
Gram-positive		
<i>Staphylococcus aureus</i>	30	93
	48	31
<i>S. epidermis</i>	12	59
	24	33
<i>Bacillus subtilis</i>	12	73
	24	65
Gram-negative		
<i>Salmonella typhimurium</i>	12	20
	24	15
<i>Escherichia coli</i>	24	21
	12	18
<i>Serratia marcescens</i>	12	18
	24	21

3.2 Morphological Changes

The changes in cell morphology due to HHP treatments were examined by scanning electron microscopy (SEM). SEM analysis for *E. coli* O157:H7 933 and *S. aureus* 485 were performed only in peptone water as the constituents of carrot juice were blocking the cells on the membrane and visualization of the cells with SEM was not possible.

It is known that microorganisms are gradually affected by increasing pressure levels leading to sublethal injury of the membrane at rather low levels of pressure (200 MPa) up to lethal effects at 800 MPa. The individual pathways of the inactivation depend on the organism and the environment and are still subject of current research. Recent findings show that pressure primarily affects functions of the cell membrane through denaturation of membrane-bound proteins and pressure-induced phase transitions of the lipid bilayer (Hartmann et al., 2006).

In this study, unpressurized cells exhibited a smooth surface appearance (Figures 3.15 and 3.21). SEM micrographs revealed that surface appearance of *E. coli* O157:H7 933 cells were not as smooth as *S. aureus* 485 cells due to the cell wall structure of gram-negative bacteria. The additional outer membrane of gram-negative bacteria that contains protein, phospholipids and lipopolysaccharide gives the uneven surface structure. However, gram-positive bacteria have a more even surface structure having a rigid peptidoglycan outlayer (Ritz et al., 2000). *E. coli* O157:H7 933 cells exposed to 200 MPa (Figure 3.16) had smoother surface appearance and appeared larger than the untreated cells. The surface of *E. coli* O157:H7 933 cells after 250 MPa treatment (Figures 3.17 to 3.20) was distorted with dimples and pinches.

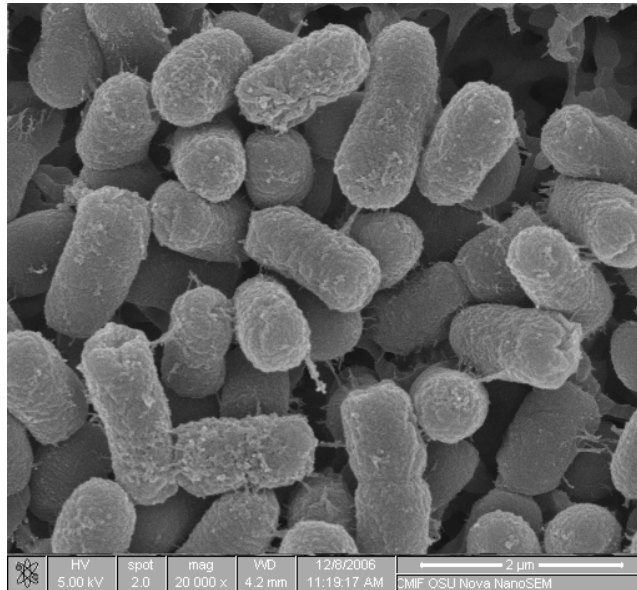


Figure 3.15 SEM micrograph of unpressurized *E. coli* O157:H7 933

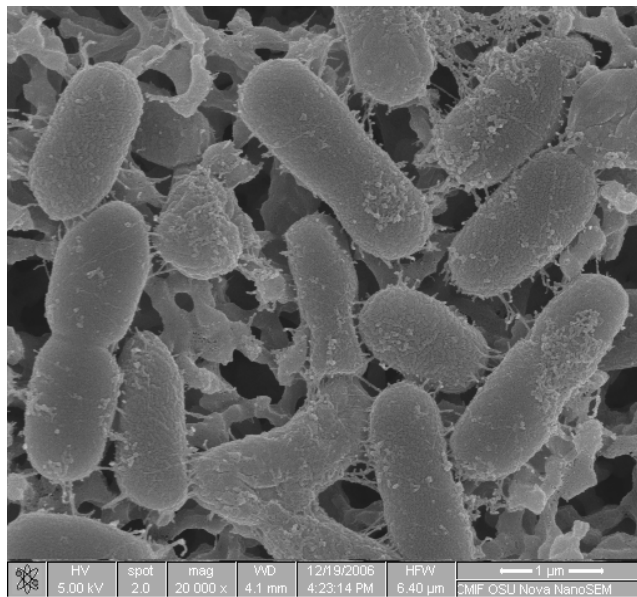


Figure 3.16 SEM micrograph of pressurized (200 MPa- 1 min- 40°C) *E. coli* O157:H7 933

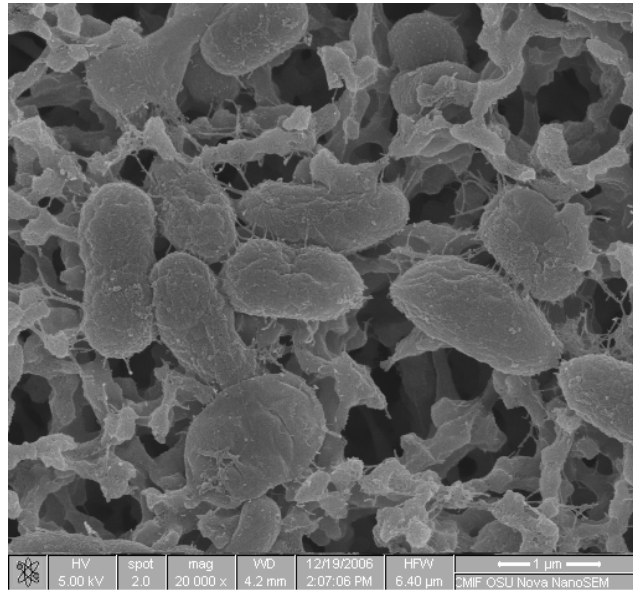


Figure 3.17 SEM micrograph of pressurized (250 MPa- 1 min- 40°C) *E. coli* O157:H7 933

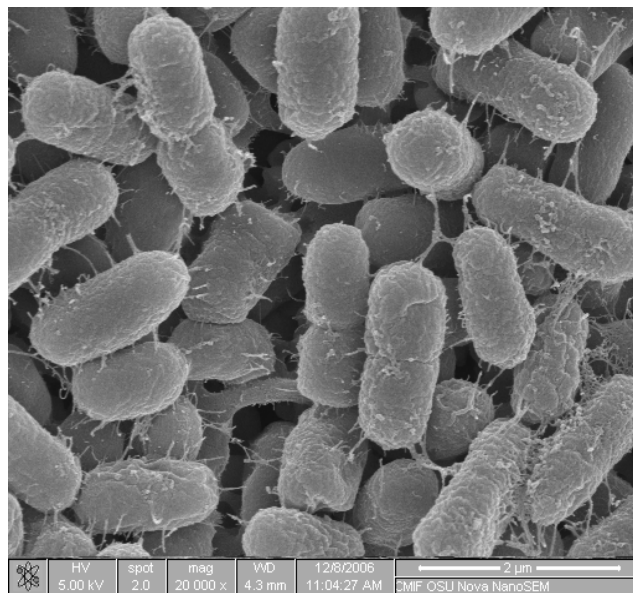


Figure 3.18 SEM micrograph of pressurized (275 MPa- 1 min- 40°C) *E. coli* O157:H7 933

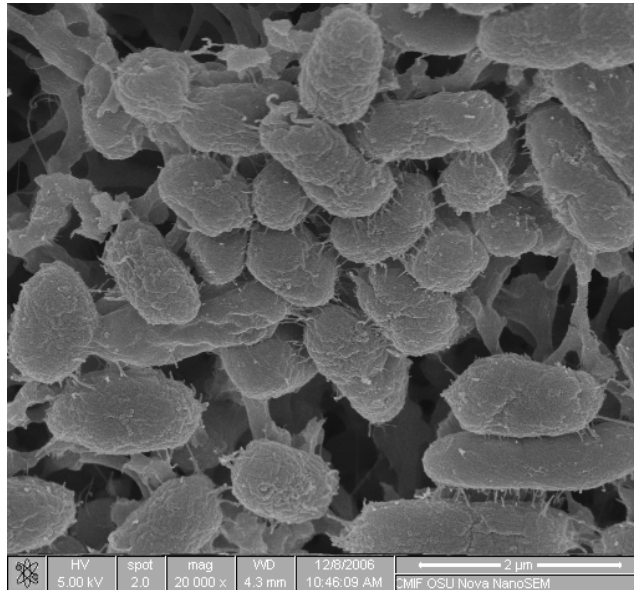


Figure 3.19 SEM micrograph of pressurized (300 MPa- 1 min- 40°C) *E. coli* O157:H7 933

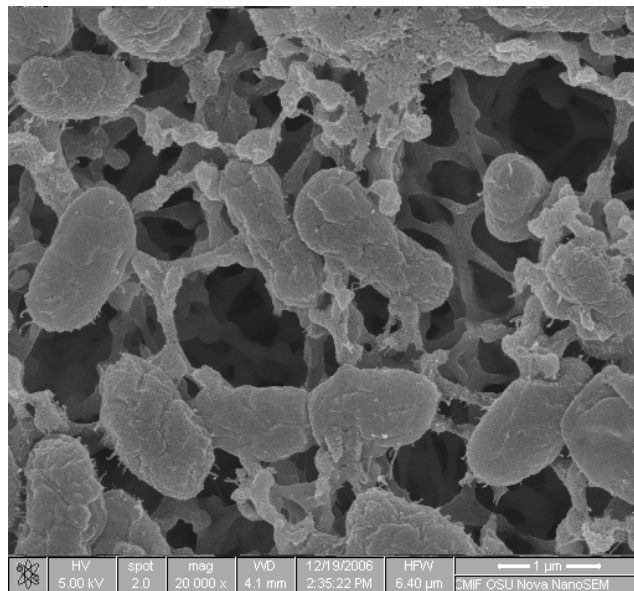


Figure 3.20 SEM micrograph of pressurized (325 MPa- 1 min- 40°C) *E. coli* O157:H7 933

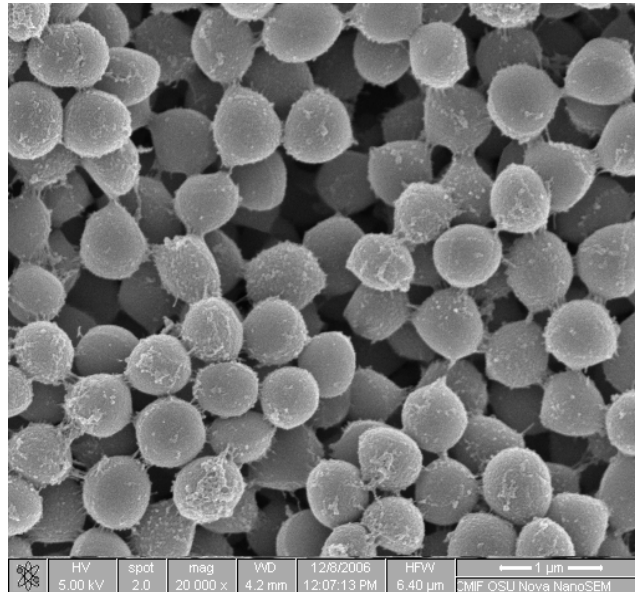


Figure 3.21 SEM micrograph of unpressurized *S. aureus* 485

In case of *S. aureus* 485, the cells pressurized at 200 MPa and 250 MPa did not show any significant change in the original smooth surface and cocci shape (Figures 3.22 and 3.23). The surface appearance became rough and cracked (Figures 3.24 to 3.26) when the cells were exposed to higher pressure levels (300 MPa, 350 MPa and 400 MPa). It was apparent that *S. aureus* 485 cells were less affected by higher pressure - time combinations. SEM micrograph also showed that even if the pressure treatment leads to total inactivation of the population, individual cells retained their morphological characteristics.

These results are in agreement with the report of Ludwig and Schreck (1997). A stronger pressure sensitivity of slender rod- and rod-shaped bacteria compared to spherically shaped bacteria was also implied. For example, *P. aeruginosa* (slender

rod-shaped) is more pressure sensitive than *E. coli* (rod-shaped), whereas *S. aureus* (cocci) is the most resistant species amongst all studied in this contribution. Corresponding to this scheme, most pressure sensitive bacteria are rod- or spiral-shaped, whereas the most resistant ones are spheres. Medium sensitive bacteria exhibit a mixed assortment of forms between short rods and cocci (pleomorphic shape). Concerning the gram-type, it was concluded that the cell wall itself does not protect the bacteria against high pressure.

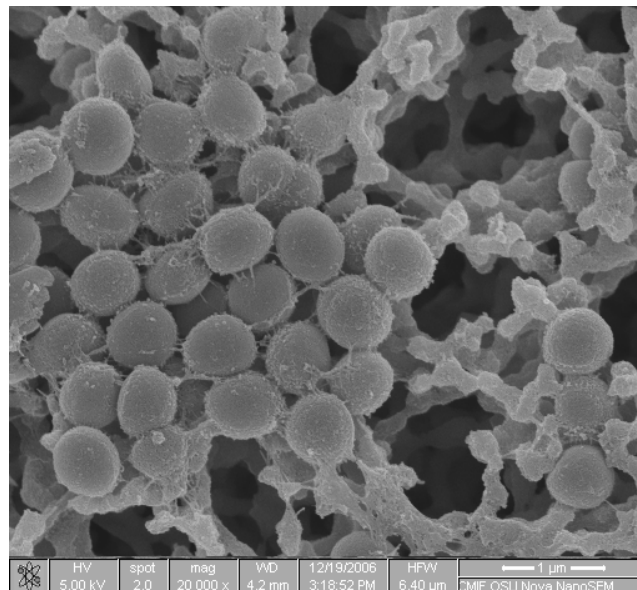


Figure 3.22 SEM micrograph of pressurized (200 MPa- 5 min- 40 °C) *S. aureus*
485

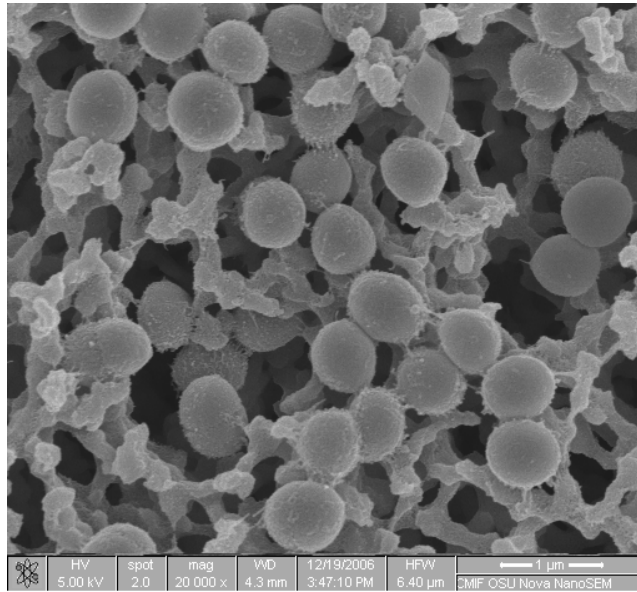


Figure 3.23 SEM micrograph of pressurized (250 MPa- 5 min- 40 °C) *S. aureus*
485

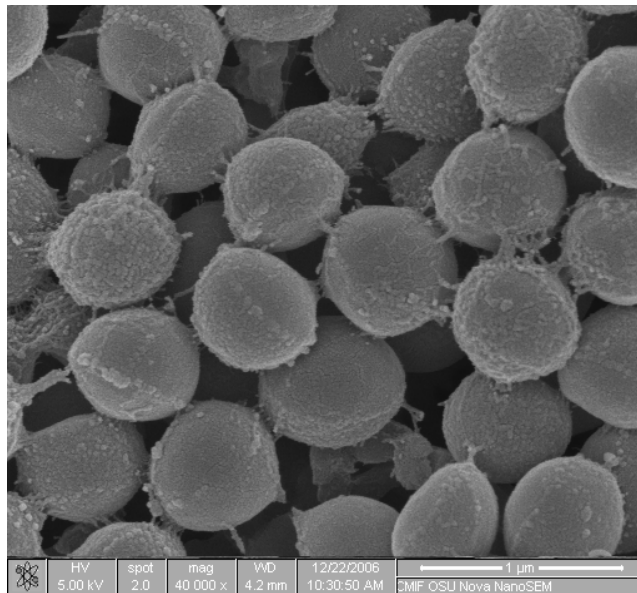


Figure 3.24 SEM micrograph of pressurized (300 MPa- 5 min- 40 °C) *S. aureus*
485

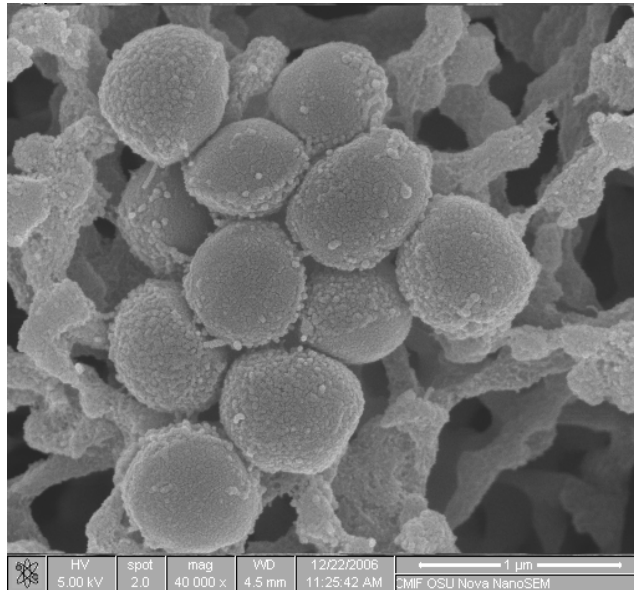


Figure 3.25 SEM micrograph of pressurized (350 MPa- 5 min- 40 °C) *S. aureus*
485

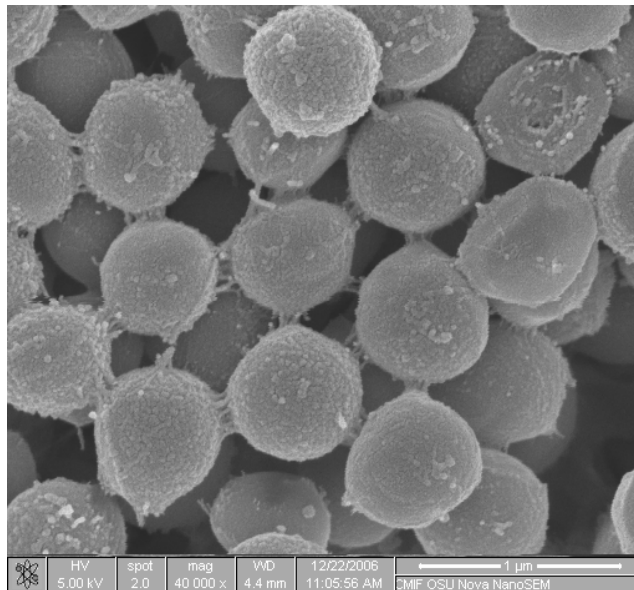


Figure 3.26 SEM micrograph of pressurized (400 MPa- 5 min- 40 °C) *S. aureus*
485

3.3 Membrane Integrity

Fluorescent micrographs were taken for the same pressure– time combinations as in SEM experiments to compare the results of both analyses and are shown in Figures 3.27 and 3.28. Green fluorescent illustrates live cells and red fluorescent illustrates dead cells.

Membrane integrity examination is a supplemental means to characterize the physiological status of inactivated cells. It has been suggested previously that the cell membrane could be a target for high pressure by disorganization of membrane phospholipids (Ritz et al., 2002). Our experiments with Live/DEAD Backlight Bacterial Viability Kit showed that all untreated (control) cells revealed the green fluorescence of the SYTO9 stain, which represented live or intact cells. After 200 MPa pressure treatment, *E. coli* O157:H7 933 cells were not observed like dead or live cells. The cells had a yellowish color due to the absorption of both dyes. This revealed the injury of the outer membrane. *E. coli* O157:H7 933 cells were divided into two different populations with regard to membrane integrity after 250 MPa treatment. A small proportion of *E. coli* O157:H7 933 cells were not stained by PI (green fluorescent cells) at lower pressure levels, suggesting that their membranes were not seriously damaged. The other part of the cell population was stained by PI (red fluorescent cells) like dead cells and the number of PI stained cells increased with increasing pressure. Almost all *E. coli* O157:H7 933 cells were red fluorescent at 325 MPa.

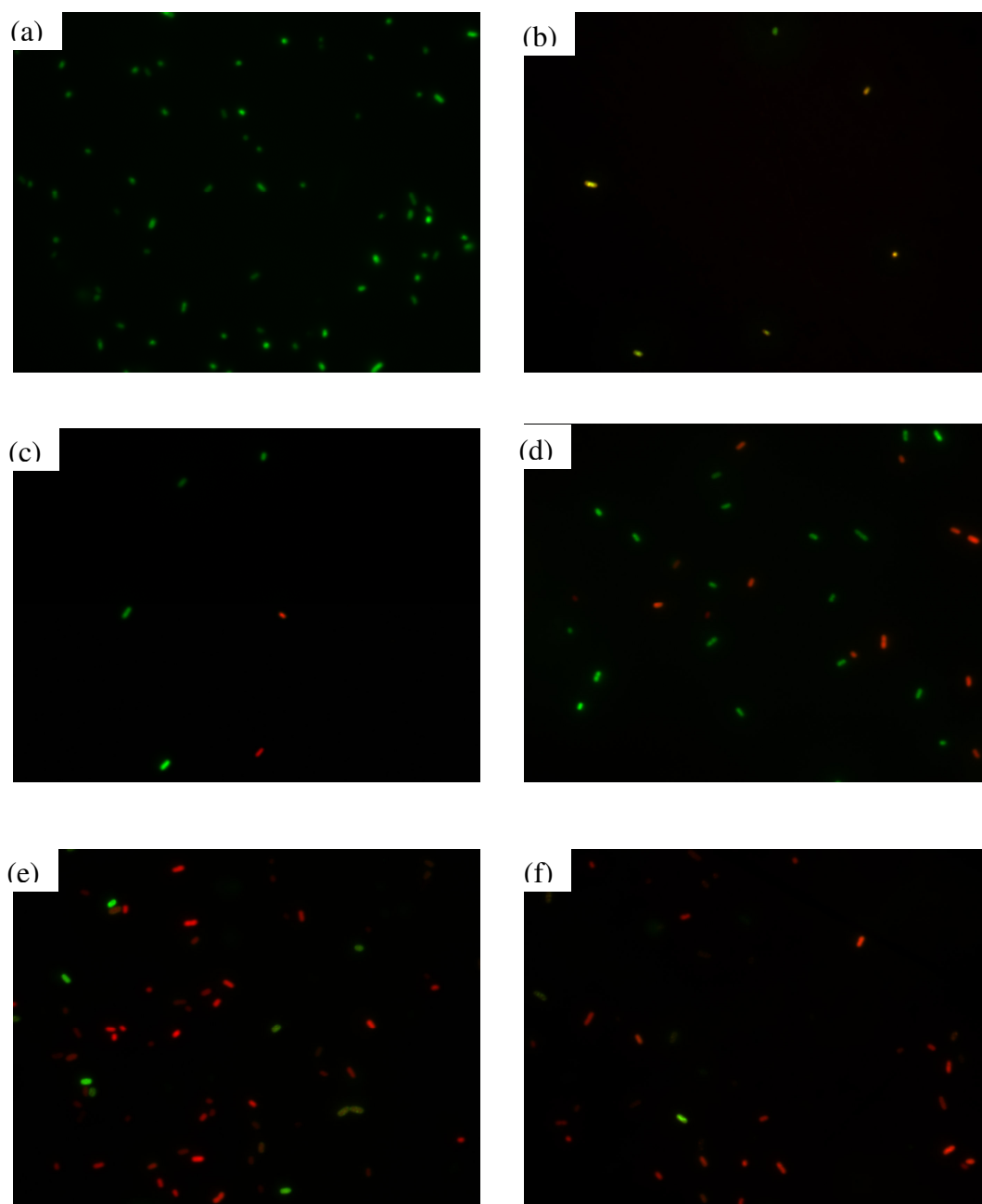


Figure 3.27 Fluorecent microscopy image of (a) unpressurized, pressurized at (b) 200 MPa- 1 min- 40°C, (c) 250 MPa- 1 min- 40°C, (d) 275 MPa- 1 min- 40°C, (e) 300 MPa- 5 min- 40°C, (f) 325 MPa- 5 min- 40°C, *E. coli* O157:H7 933

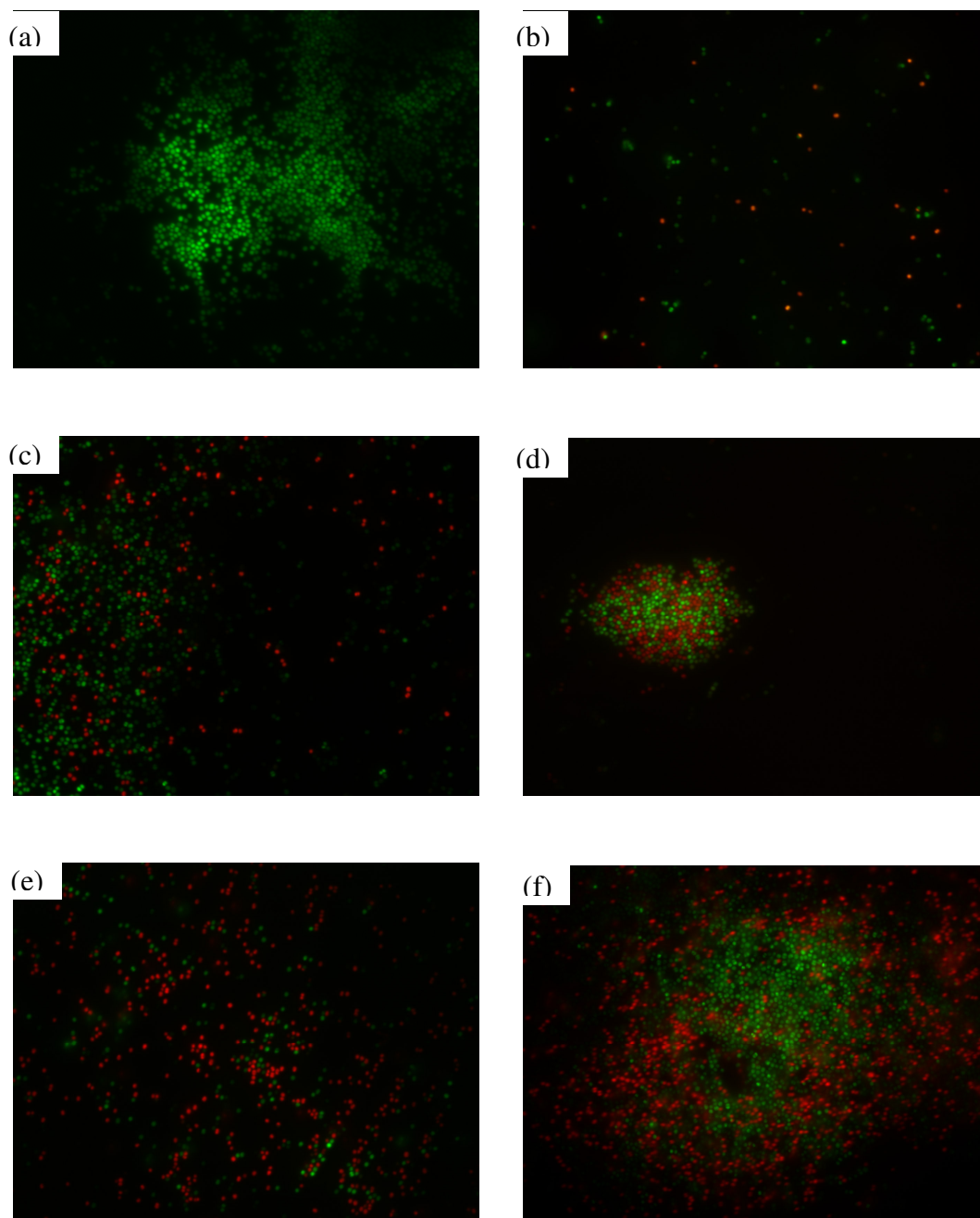


Figure 3.28 Fluorecent microscopy image of (a) unpressurized, pressurized at (b) 200 MPa- 5 min- 40°C, (c) 250 MPa- 5 min- 40°C, (d) 300 MPa- 5 min- 40°C, (e) 350 MPa- 5 min- 40°C, (f) 400 MPa- 5 min- 40°C, *S. aureus* 485

S. aureus 485 cells were also divided into two different populations with regard to membrane integrity after pressure treatments and the number of red fluorescent cells increased with increasing pressure. The number of red and green fluorescent cells was still close to each other even at high pressure levels (400 MPa- 5 min).

This indicated the pressure resistance of *S. aureus* 485 cells. For all conditions, red fluorescent indicated that there was an alteration of outer membrane as an increase in permeability of the pressure treated cells. Thongbai et al. (2006) observed similar changes in outer membrane of temperature- and pH- stressed *Salmonella typhimurium* cells exposed to cetylpyridinium chloride and nisin. Overall, the results of the Backlight nucleic acid stain correlate with morphological changes from SEM. Generally, cell membrane appears to be one of the main targets of high pressure treatments, and results in increased cell permeabilization (Tholozan et al., 2000). Although high hydrostatic pressure treatments are considered to be isostatic (i.e., equal pressure at every point of the treatment vessel), this study showed that cellular damage was not equally withstood by all the cells, suggesting that more resistant or less damaged cells are present in the pressurized cell population (Ritz et al., 2002).

3.4 Machine Vision Based Quantification of Bacterial Volume Change with HHP

3.4.1 View Area and Volume Distributions with Pressure

Calculated view area and volume distributions of *E. coli* O157:H7 933 and *S. aureus* 485 that were analyzed from representative SEM images are given in Figures 3.29 to 3.32 as histograms. Average values of the view area and volume

of *E. coli* O157:H7 933 and *S. aureus* 485 cells calculated for each pressure levels are also presented in Table 3.5. The calculation's details are given in Appendix E.

Average values of the view area and volume of *S. aureus* 485 cells did not change up to 350 MPa compared to control cells, whereas the increase in average values of the view area and volume was significant at 400 MPa ($p < 0.05$). Average values of volume for *E. coli* O157:H7 933 cells did not change for pressure levels of 250, 275, 300, and 325 MPa compared to control cells ($p < 0.05$). However, the increase in average values of the view area was significant at 325 MPa for *E. coli* O157:H7 933 cells ($p < 0.05$). In contrast to *S. aureus* 485 cells, the increase in average values of the view area and volume were significant at 200 MPa for *E. coli* O157:H7 933 cells. Statistical analysis of significant differences for the view area and volume changes with pressure levels are given in Appendix F.

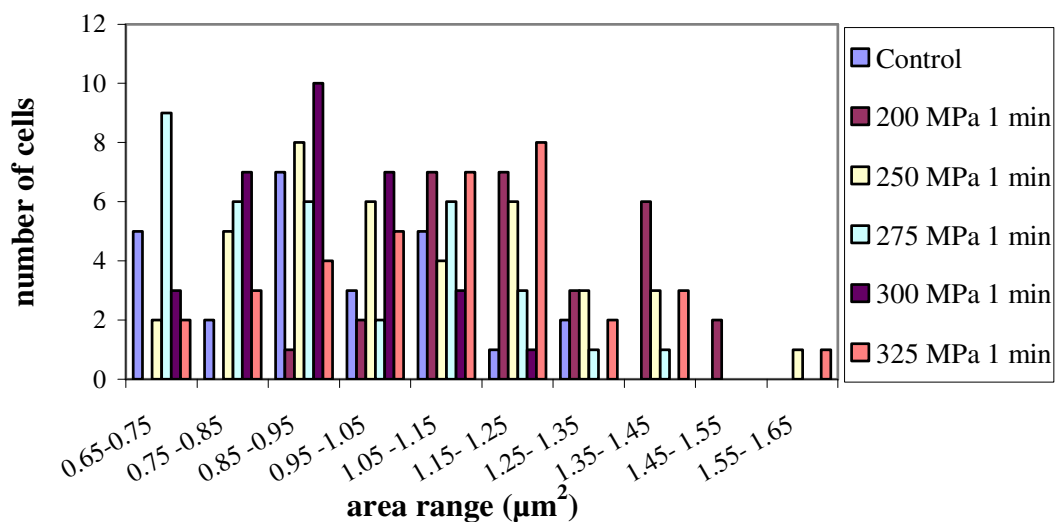


Figure 3.29 Area distributions of *E. coli* O157:H7 933 cells under different pressure treatments at 40°C

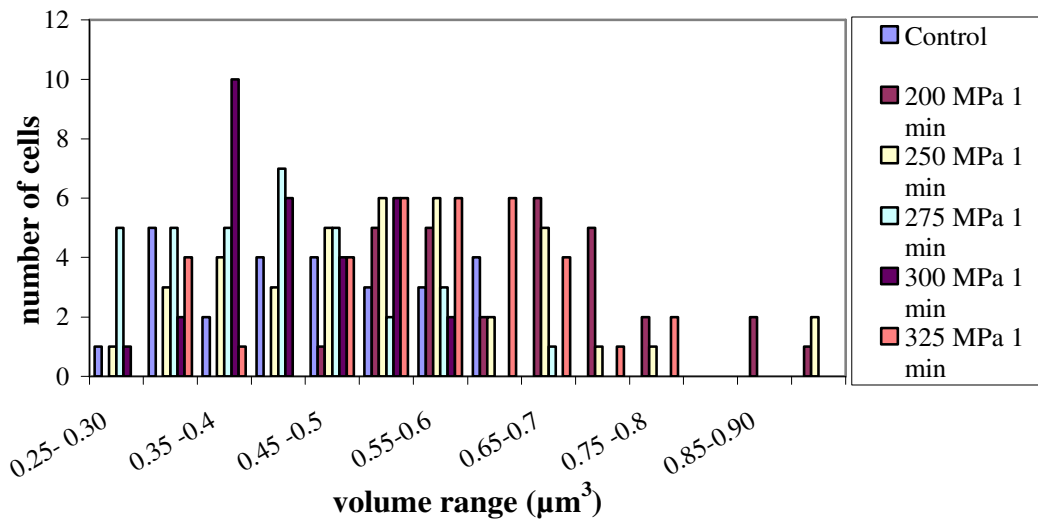


Figure 3.30 Volume distributions of *E. coli* O157:H7 933 cells under different pressure treatments at 40°C

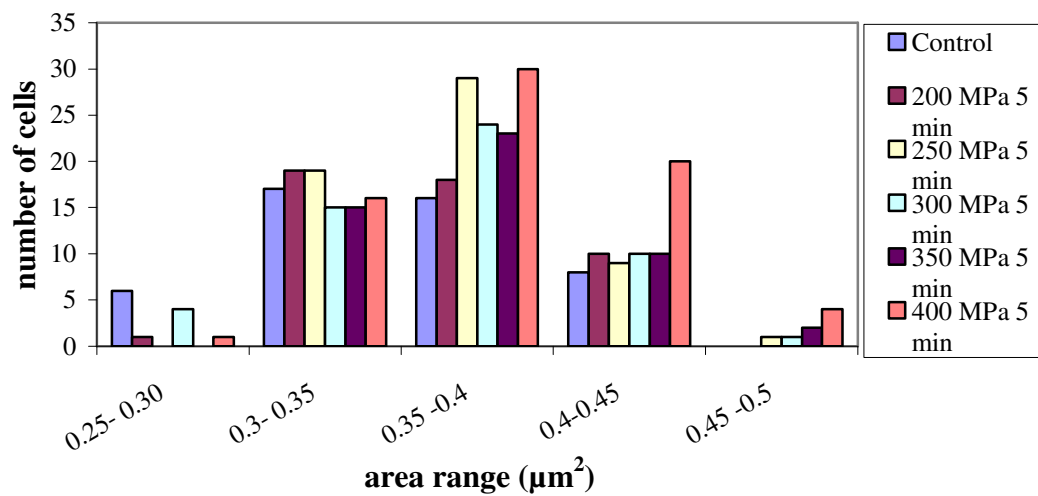


Figure 3.31 Area distributions of *S. aureus* 485 cells under different pressure treatments at 40°C

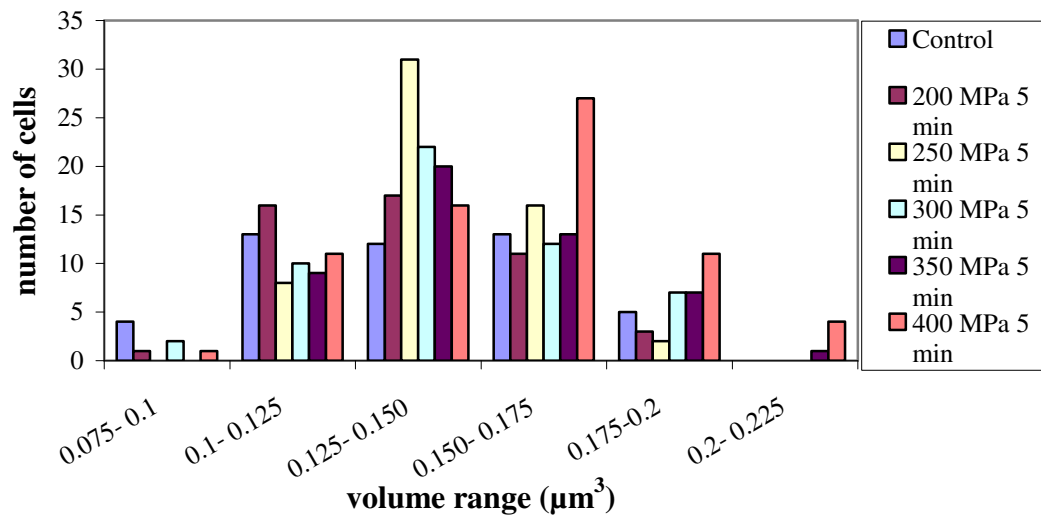


Figure 3.32 Volume distributions of *S. aureus* 485 cells under different pressure treatments at 40°C

Table 3.5 Average values of the view area and volume of *E. coli* O157:H7 933 and *S. aureus* 485 for each pressure treatment at 40°C

Microorganism	Pressure-time combination	Number of cells (n)	Average volume (μm^3)	Average view area (μm^2)
<i>E. coli</i> O157:H7 933	Control	25	0.469± 0.110	0.938± 0.177
	200 MPa- 1 min	30	0.676± 0.136	1.267± 0.202
	250 MPa- 1 min	39	0.544± 0.152	1.052± 0.214
	275 MPa- 1 min	33	0.416± 0.105	0.913± 0.186
	300 MPa- 1 min	31	0.430±0.075	0.904±0.123
	325 MPa- 1 min	34	0.557± 0.125	1.097± 0.202
<i>S. aureus</i> 485	Control	47	0.138± 0.028	0.356± 0.044
	200 MPa- 5 min	48	0.138± 0.022	0.364± 0.038
	250 MPa- 5 min	57	0.142±0.018	0.366± 0.034
	300 MPa- 5 min	53	0.144± 0.024	0.368± 0.043
	350 MPa- 5 min	50	0.148± 0.025	0.374± 0.041
	400 MPa- 5 min	70	0.154± 0.028	0.383± 0.042

± Standard Deviation (SD)

Tholozan et al. (2000) measured the intracellular volume of *Listeria monocytogenes* and *Salmonella* Typhimurium cells with radioactively- labeled probes. Cell volume of *L. monocytogenes* was unchanged up to a pressure treatment of 325 MPa in citrate buffer (pH= 5.6), and up to 425 MPa in phosphate buffer (pH= 7.0). Higher pressure treatments causing more than 3 log₁₀ reduction in the cell populations in both buffers led to an increase in the calculated cell volume up to fourfold. Cell volume of *S. Typhimurium* suspensions was unchanged whatever the pressure treatment or buffer of cell suspension is used.

Perrier-Cornet et al. (1995) reported an in situ observation of yeast cells under high hydrostatic pressure. Cell volume variations were measured for *Saccharomyces fibuligera* on fixed cells and on a population sample and shrinkage in average cell volume was reported after a pressure treatment of 250 MPa. The observed compression rate (25%) under pressure and the partial irreversibility of cell compression (10%) after return to atmospheric pressure led to the conclusion that mass transfer between cell and cultivation medium occurred. This could be explained by a modification of membrane properties, i.e., disruption or increase in permeability. The histogram of the initial yeast cell volume had a normal distribution. During the pressure application, the distribution of cell volume kept the same form but clearly moved to the left. This displacement corresponded to an average decrease of 35% in volume. When yeasts were observed after pressurization, population histogram did not really differ from that of under high pressure. It was concluded that yeast cells did not recover their initial volume after a treatment of 250 MPa for 15 min. This observation has confirmed the hypothesis of an irreversible mass transfer that occurred during pressure holding time.

In this study, as pressure increased, the view area and volume of the organisms also increased for the highest pressure levels applied, except for *E. coli* O157:H7 933 cells at 200 MPa. On the histograms, area and volume distributions of pressurized cells shifted to the right (increase in size) compared to the control distribution. The results are similar to those reported by Tholazan et al. (2000). For *S. aureus* 485 the results are similar with the study of Perrier-Cornet et al. (1995) on yeast cells. This may be due to the similarity between the morphology of cells (both are spherical in shape).

3.4.2 Volume Change Related Inactivation Mechanism

The increase in volume at high pressure levels could be explained by mass transfer between cell and culture medium. The cause of this transfer could be; modification of membrane properties, i.e., disruption or increase in permeability, lack of membrane integrity, denaturation of membrane-bound proteins and pressure-induced phase transition of membrane lipid bilayer (Perrier- Cornet et al., 1995; Hartmann et al., 2006). The major HHP-induced change has been suspected to be associated with the phase transition of membrane lipid bilayer. The lipid bilayer exists in liquid state as a requirement for “optimum” biological functions of membranes (Chong and Weber, 1983). Phase transition is from the natural liquid crystalline phase to an initially reversible gel phase, and finally to an irreversible integrated phase, together with a reduction in the thickness of the bilayers (Kalchayanand et al., 2002). Pressure also induces mechanical stresses on the cell wall and functional proteins attached or embedded in the membrane, which, in turn is attached to the wall, and associated with the bilayer of phospholipid (Hartmann et al., 2006; Kato and Hayashi, 1999). This effect results as an inhibition of protein synthesis and reversible protein denaturation within the pressure range of 20-180 MPa; loss of cell viability begins after 180 MPa with an

exponentially increasing inactivation rate with pressure. It is finally followed by the irreversible protein denaturation above 300 MPa (Lado and Yousef, 2002).

Le Chatelier's principle favors reduction of the system volume with an increase in pressure (Monzhaev et al., 1996). As pressure increases at constant temperature, the lipid bilayer adapts by changing its conformation. A variety of pressure-induced phase transformations has been observed such as liquid-to-gel transition and gel-to-interdigitated gel transition. In contrast to Le Chatelier's principle, the volume of the lipid bilayer in liquid-to-gel transition increases with an increase in the fatty acyl chains (R-groups) of the phospholipids. Pressures of 50-200 MPa cause the transition from the liquid-crystalline to gel. At higher pressures (above 200 MPa), a second pressure-induced phase transition, called interdigitated phase, is observed, and the bilayer volume decreases by 5%, accompanied by a decrease in its thickness (Kato and Hayashi, 1999; Winter, 2001).

When hydrostatic pressure is applied, the protein- solvent system evolves toward the global configuration that occupies the least volume. Since in the unfolded state, the excluded volume of packing defects is eliminated and charges and hydrophobic residues are exposed to solvation, it is this form of the protein that is favored by pressure. Based on the criteria of intrinsic packing and hydration, denatured protein species can be conceptually divided into three classes: compact intermediate states (such as molten globules), partially unfolded states, and the fully unfolded state. The volume of the protein- solvent system in the transition state (molten globule- like) is significantly larger than the one in the unfolded state and somewhat larger than in the folded state. Thus, it is reasonable to interpret the large increase in volume between unfolded and transition states as a result of the collapse of the unfolded polypeptide chain to a loosely packed globule from which solvent is excluded. The observed decrease in volume

between the transition state and the folded state most likely arises from more efficient packing in the final folded structure (Vidugiris et al., 1995; Chalikian, 2003).

Based on studies of the transfer of small hydrophobic compounds to water, the volume change of unfolding proteins is predicted to be negative and very large. The volume change for this transfer will become positive with increasing pressure. This contradiction is called as the protein volume paradox: “the liquid hydrocarbon model fails almost completely when one attempts to extend it to the effects of pressure on protein denaturation” (Meersman et al., 2006).

The cell envelope of gram- negative bacteria has a more complex structure than gram-positive bacteria with an additional membrane structure, the outer membrane or L-layer at the surface of the cell. This outer membrane contains substantial amounts of protein and phospholipids and in addition most or all of the lipopolysaccharide of the cell envelope. It is demonstrated that this outer membrane is more damaged under HHP than the cytoplasmic membrane for *Salmonella typhimurium* (Ritz et al., 2000).

The increase in volume of *E. coli* O157:H7 933 cells at 200 MPa can be explained by the increase in volume of liquid-to-gel transition of lipid bilayer, and the denatured proteins in the transition state (molten- like globules). A similar increase for *S. aureus* 485 cells at moderate pressures (<400 MPa) is not observed since the additional outer membrane does not exist as in gram- negative cells.

At high pressure levels (400 MPa- 5 min for *S. aureus* 485 and 325 MPa- 1 min for *E. coli* O157:H7 933) volume increase is observed. Lethality begins above 200 MPa and irreversible protein denaturation occurs above 300 MPa. Both

inactivation level and the damage to the cell membrane increase with increasing pressure, membrane permeability begins to disrupt, followed by the loss of membrane integrity and swelling. It is also predicted that the volume change upon unfolding of proteins will become positive with increasing pressure.

CHAPTER 4

CONCLUSIONS AND RECOMMENDATIONS

The results presented in this study indicated that high hydrostatic pressure combined with mild heat (40 °C) has the potential to improve the safety of carrot juice. However, there are considerable variations within the species studied. *E. coli* O157:H7 933 was more pressure sensitive than *S. aureus* 485 in peptone water, whereas *S. aureus* 485 was more pressure sensitive than *E. coli* O157:H7 933 in carrot juice.

Most of the survival curves obtained in this study were concave upward. The tailing of the survival curves indicated that traditional first-order kinetics was not appropriate for describing pressure inactivation kinetics of the relatively pressure resistant foodborne pathogens in a low acid food. Weibull model allowed more accurate description of the inactivation kinetics of both pathogens. The development of accurate mathematical models to describe the pressure inactivation kinetics of microorganisms would be very beneficial to the food industry by developing safe processing conditions for HHP processing of foods.

This study also revealed that HHP and phytoalexins could be used as a potent bactericidal combination against *S. aureus* 485; however, further research is necessary to determine the effect of phytoalexins combined with HHP for other Gram-positive bacteria.

The change in volume and the view area of microorganisms added another dimension to the understanding of inactivation mechanisms of microbial cells by HHP. Examining membrane integrity was a supplemental means to characterize the physiological status of inactivated cells and the results supported the outcomes of SEM analysis. However, more studies should be carried out for different microorganisms and at different pressure levels to have more accurate understanding of pressure on cell size.

SEM analysis showed that spherical shapes (cocci) show no morphological changes, however rods do so in the form of dimples and swelling. A study on spherical structures and baker's yeast revealed a heterogeneous stress state in the yeast cell wall and a hydrostatic stress state in the interior part of the organism. As further research, effect of cell geometry on deformation of cellular structures could also be examined in terms of mechanical stresses (non-hydrostatic stresses in the shell and hydrostatic stress in the core).

REFERENCES

- Alpas, H., Kalchayanand, N., Bozoğlu, F., Sikes, A., Dunne, C.P. and Ray, B. 1999. Variation in resistance to hydrostatic pressure among strains of food-borne pathogens. *Applied and Environmental Microbiology*, Vol. 65, pp 4248-4251.
- Alpas, H. and Bozoğlu, F., 2000. The combined effect of high hydrostatic pressure, heat and bacteriocins on inactivation of foodborne pathogens in milk and orange juice. *World Journal of Microbiology and Biotechnology*, Vol. 16, pp 387- 392.
- Alpas, H., Kalchayanand, N., Bozoğlu, F. and Ray, B., 2000. Interactions of High Hydrostatic Pressure, Pressurization Temperature and pH on Death and Injury of Pressure-Resistant and Pressure-Sensitive Strains of Foodborne Pathogens. *International Journal of Food Microbiology*, Vol. 60, pp 33-42.
- Alpas, H., Lee, J., Bozoğlu, F. and Kaletunç, G. 2003. Evaluation of high hydrostatic pressure sensitivity of *Staphylococcus aureus* and *Escherichia coli* O157:H7 by differential scanning calorimetry. *International Journal of Food Microbiology*, Vol. 87, pp 229-237.
- Anonymous, 2000. Food and Drug Administration, U.S., Center for Food Safety and Applied Nutrition, June. Kinetics of microbial inactivation for alternative food processing technologies: High pressure processing.
- Anonymous, 2004. Food and Drug Administration, U.S., Center for Food Safety and Applied Nutrition, February. Juice HACCP Hazards and Controls Guidance, First Edition.

Basak, S., Ramaswamy, H. S. and Piette, J. P. G., 2002. High Pressure Destruction Kinetics of *Leuconostoc mesenteroides* and *Saccharomyces cerevisiae* in Single Strength and Concentrated Orange Juice. *Innovative Food Science & Emerging Technologies*, Vol. 3, pp 223-231.

Bayındırlı, A., Alpas, H., Bozoğlu, F. and Hızal, M. 2006. Efficiency of high pressure treatment on inactivation of pathogenic microorganisms and enzymes in apple, orange, apricot and sour cherry juices. *Food Control*, Vol.17, Issue 1, pp 52-58.

Bertucco, A. and Spilimbergo, S., 2001. Treating Micro-organisms with High Pressure. In: Bertucco, A. and Vetter, G. (Eds), *High Pressure Process Technology: Fundamentals and Applications*, Elsevier, Amsterdam, Netherlands, pp 626- 640.

Beuchat, L. R. and Brackett, R. E., 1990. Inhibitory effects of raw carrots on *Listeria monocytogenes*. *Applied and Environmental Microbiology*, Vol. 56, pp 1734-1742.

Bozoğlu, F., Alpas, H. and Kaletunç, G., 2004. Injury Recovery of Foodborne Pathogens in High Hydrostatic Pressure Treated Milk During Storage. *FEMS Immunology and Medical Microbiology*, Vol. 40, pp 243-247.

Butz, P. and Tauscher, B., 2002. Emerging Technologies: Chemical Aspects. *Food Research International*, Vol. 35, pp 279-284.

Buzrul, S. and Alpas, H., 2004. Modeling the synergistic effect of high pressure and heat on inactivation kinetics of *Listeria innocua*: a preliminary study. *FEMS Microbiology Letters*, Vol. 238, pp 29-36.

Buzrul, S., Alpas, H. and Bozoğlu, F., 2005. Use of Weibull frequency distribution model to describe the inactivation of *Alicyclobacillus acidoterrestris* by high pressure at different temperatures. Food Research International, Vol. 38, pp 151- 157.

Buzrul, S. 2007. A suitable model of microbial survival curves for beer pasteurization. LWT- Food Science and Technology, Vol. 40, pp 1330-1336.

Buzrul, S., Alpas, H., Largeteau, A., Bozoglu, F. and Demazeau, G., 2008. Compression heating of selected pressure transmitting fluids and liquid foods during high hydrostatic pressure treatment. Journal of Food Engineering, Vol. 85, pp 466- 472.

Chalikian, T. G., 2003. Volumetric Properties of Proteins. Annual Review of Biophysics and Biomolecular Structure, Vol. 32, pp 207- 235.

Chen, H. and Hoover, G. D., 2003. Pressure inactivation kinetics of *Yersinia enterocolitica* ATCC 35669. International Journal of Food Microbiology, Vol. 87, pp 161- 171.

Chen, H. and Hoover, G. D., 2004. Use of Weibull model to describe and predict pressure inactivation of *Listeria monocytogenes* Scott A in whole milk. Innovative Food Science and Emerging Technologies, Vol. 5, pp 269- 276.

Chen, H. 2007. Use of linear, Weibull, and log-logistic functions to model pressure inactivation of seven foodborne pathogens in milk. Food Microbiology, Vol. 24, pp 197- 204.

Chong, P. L. G. and Weber, G., 1983. Pressure Dependence of 1,6- Diphenyl- 1, 3, 5- hexatriene Fluorescence in Single- Component Phosphatidylcholine Liposomes. Biochemistry, Vol. 22, No. 24, pp 5544- 5550.

Deplace, G., 1995. Design of High Pressure Isostatic Units for Laboratory and Industrial Treatment of Food Products. In: Ledward, D.A., Johnston, D.E.,

Earnshaw, R.G. and Hasting, A.P.M. (Eds), *High Pressure Processing of Foods*, Nottingham University Press, Leicestershire, Nottingham, pp 137- 154.

Dogan, C. and Erkmen, O., 2004. High pressure inactivation kinetics of *Listeria monocytogenes* inactivation in broth, milk, and peach and orange juices. *Journal of Food Engineering*, Vol. 62, pp 47- 52.

Erkmen, O. and Dogan, C., 2004. Kinetic analysis of *Escherichia coli* inactivation by high hydrostatic pressure in broth and foods. *Food Microbiology*, Vol. 21, pp 181-185.

Furukawa, S., Shimoda, M. and Hayakawa, I., 2003. Mechanism of the inactivation of bacterial spores by reciprocal pressurization treatment. *Journal of Applied Microbiology*, Vol. 94, pp 836- 841.

Garriga, M., Aymerich, M. T., Costa, S., Monfort, J. M., and Hugas M., 2002. Bactericidal Synergism through Bacteriocins and High Pressure in a meat Modelsystem During Storage. *Food Microbiology*, Vol. 19, pp 509-518.

Geeraerd, A.H., Valdramidis, V.P. and Van Impe, J.F., 2005. GInaFiT, a freeware tool to assess non-log-linear microbial survivor curves. *International Journal of Food Microbiology*, Vol. 102, pp 95-105.

Gould, G. W., 1995. The Microbe as a High Pressure Target. In: Ledward, D.A., Johnston, D.E., Earnshaw, R.G. and Hasting, A.P.M. (Eds), *High Pressure Processing of Foods*, Nottingham University Press, Leicestershire, Nottingham, pp 81- 97.

Hartmann, C., Mathmann, K. and Delgado, A., 2006. Mechanical stresses in cellular structures under high hydrostatic pressure. *Innovative Food Science & Emerging Technologies*, Vol. 7, pp 1-12.

Herdegen, V. and Vogel, R. F., 1998. Strategies for High Pressure Inactivation of Endospore-forming Bacteria. In *High pressure Food Science, Bioscience and Chemistry*, (Isaacs, S. N., ed.), Royal Society of Chemistry, Cambridge, England., pp. 394- 402.

Heremans, K., 1995. High Pressure Effects on Biomolecules. In: Ledward, D.A., Johnston, D.E., Earnshaw, R.G. and Hasting, A.P.M. (Eds), *High Pressure Processing of Foods*, Nottingham University Press, Leicestershire, Nottingham, pp 81- 97.

Hogan, E., Kelly, A. L. and Sun, D., 2005. High Pressure processing of Foods: An Overview. In: Sun, Da-Wen (Edt.), *Emerging Technologies for Food Processing*, Elsevier Academic Press, pp 3-32.

Jordan, S. L., Pascual, C., Bracey, E. and Mackey, B. M., 2001. Inactivation and injury of pressure-resistant strains of *Escherichia coli* O157 and *Listeria monocytogenes* in fruit juices. *Journal of Applied Microbiology*, Vol. 91, pp 463-469.

Kalchayanand, N., Frethem, C., Dunne, P., Sikes, A. and Ray, B., 2002. Hydrostatic pressure and bacteriocin-triggered cell wall lysis of *Leuconostoc mesenteroides*. *Innovative Food Science & Emerging Technologies*, Vol. 3, pp 33- 40.

Kaletunç, G., Lee, J., Alpas, H. and Bozoğlu, F., 2004. Evaluation of Structural Changes Induced by High Hydrostatic Pressure in *Leuconostoc mesenteroides*. *Applied and Environmental Microbiology*, Vol. 70, No. 2, pp 1116- 1122.

Kato, M. and Hayashi, R., 1999. Effects of High Pressure on Lipids and Biomembranes for Understanding High- Pressure- Induced Biological Phenomena. *Bioscience Biotechnology and Biochemistry*, Vol. 63, Issue 8, pp 1321-1328.

Kawai, K., Fukami, K. and Yamamoto, K., 2007. Effects of treatment pressure, holding time, and starch content on gelatinization and retrogradation properties of potato starch–water mixtures treated with high hydrostatic pressure. *Carbohydrate Polymers*, Vol. 69, pp 590- 596.

Knorr, D., Heinz, V. and Buckow, R., 2006. High pressure application for food biopolymers. *Biochimica et Biophysica Acta*, Vol. 1764, pp 619– 631.

Koseki, S. and Yamamoto, K., 2007. A novel approach to predicting microbial inactivation kinetics during high pressure processing. *International Journal of Food Microbiology*, Vol. 116, pp 275- 282.

Kurosaki, F. and Nishi, A., 1983. Isolation and Antimicrobial Activity of the Phytoalexin 6-Methoxymellein from Cultured Carrot Cells. *Phytochemistry*, Vol. 22, No. 3, pp 669- 672.

Lado, B. H., Yousef, A. E., 2002. Alternative food-preservation technologies: efficacy and mechanisms. *Microbes and Infection*, Vol. 4, pp 433– 440.

Larsen, G. A., August 2000. Efficiency of High Hydrostatic Pressure and Bacteriocins on Death of Pathogens in Processed Meat Products. Master of Science, University of Wyoming, USA.

Ludwig, H. and Schreck, C., 1997. The inactivation of vegetative bacteria by pressure. In: Heremans, K. (Edt.), *High Pressure Research in Bioscience and Biotechnology*, Leuven: Leuven University Press, pp 221– 224.

Mafart, P., Couvert, O., Gaillard, S. and Leguerinel, I. 2002. On calculating sterility in thermal preservation methods: application of the Weibull frequency distribution model. *International Journal of Food Microbiology*, Vol. 72, pp 107-113.

Masschalk, B., Houdt R. V. and Michiels C.W. 2001. High Pressure Increases Bactericidal Activity and Spectrum of Lactoferrin, Lactoferricin and Nisin. *International Journal of Food Microbiology*, Vol. 64, pp 325-332.

Meersman, F., Dobson, C. M. and Heremans, K., 2006. Protein unfolding, amyloid fibril formation and configurational energy landscapes under high pressure conditions. *Chemical Society Reviews*, Vol. 35, pp 908-917.

Monzhaev, V. V., Heremans, K., Frank, J., Masson, P. and Balny, C., 1996. High Pressure Effects on Protein Structure and Function. *Proteins: Structure Function and Genetics*, Vol. 24, pp 81- 91.

Moreau, C., 1995. Semi-Continuous High Pressure Cell for Liquid Processing. In: Ledward, D.A., Johnston, D.E., Earnshaw, R.G. and Hasting, A.P.M. (Eds), *High Pressure Processing of Foods*, Nottingham University Press, Leicestershire, Nottingham, pp 181- 197.

Mor-Mur, M. and Yuste, J., 2005. Microbiological Aspects of High-pressure Processing. In: Sun, Da-Wen (Edt.), *Emerging Technologies for Food Processing*, Elsevier Academic Press, pp 47- 65.

Oh, S. and Moon, M-J., 2003. Inactivation of *Bacillus cereus* Spores by High Hydrostatic Pressure at Different Temperatures. *Journal of Food Protection*, Vol. 66, No. 4, pp 599- 603.

Ohlsson, T., 2002. Minimal Processing of Foods with Non-thermal Methods. In: Ohlsson, T. and Bengtsson, N. (Eds.), *Minimal Processing Technologies in the Food Industry*, 1st Ed., CRC Press, Boca Raton, pp 34-47.

Olsson, S., 1995. Production Equipment for Commercial Use. In: Ledward, D.A., Johnston, D.E., Earnshaw, R.G. and Hasting, A.P.M. (Eds), *High Pressure Processing of Foods*, Nottingham University Press, Leicestershire, Nottingham, pp 167- 180.

Pandurangi, S. and Balasubramaniam, V. M., 2005. High-pressure Processing of Salads and Ready Meals. In: Sun, Da-Wen (Edt.), *Emerging Technologies for Food Processing*, Elsevier Academic Press, pp 33- 45.

Patterson, M. F. and Kilpatrick, D. J., 1998. The combined effect of high hydrostatic pressure and mild heat on inactivation of pathogens in milk and poultry. *Journal of Food Protection*, Vol. 61, pp 432-436.

Peleg, M. and Cole, M. B., 1998. Reinterpretation of microbial survival curves. *Critical Reviews in Food Science and Nutrition*, Vol. 38, pp 353- 380.

Peleg, M., 1999. On calculating sterility in thermal and non-thermal preservation methods. *Food Research International*, Vol. 32, pp 271- 278.

Peleg, M., 2000. Microbial survival curves- the reality of flat “shoulders” and absolute thermal death times. *Food Research International*, Vol. 33, pp 531- 538.

Peleg, M., 2003. Calculation of the non-isothermal inactivation patterns of microbes having sigmoidal isothermal semi-logarithmic survival curves. *Critical Reviews in Food Science and Nutrition*, Vol. 43, pp 645-658.

Perrier-Cornet, J-M., Markchal, P-A. and Gervais, P., 1995. A new design intended to relate high pressure treatment to yeast cell mass transfer. *Journal of Biotechnology*, Vol. 41, pp 49- 58.

Radamacher, B., Pfeiffer, B. and Kessler, H. G., 1998. Inactivation of microorganisms and enzymes in pressure-treated raw milk. In *High pressure Food Science, Bioscience and Chemistry*, (Isaacs, S. N., ed.), Royal Society of Chemistry, Cambridge, England, pp 403-407.

Ray, B., Kalchayanand, N., Dunne, P. and Sikes, A., 2001. Microbial Destruction During Hydrostatic Pressure Processing of Food. In: Bozoğlu, F., Deak, T. and Ray, B.(Eds.), *Novel Processes and Control Technologies In The Food Industry*, IOS Press, Amsterdam, pp 95-122.

Ritz, M., Jugiau, F., Rama, F., Courcoux, P., Semenou, M. and Federighi, M., 2000. Inactivation of *Listeria monocytogenes* by High Hydrostatic Pressure: Effects and Interactions of Treatment Variables Studied By Analysis of Variance. *Food Microbiology*, Vol. 17, pp 375-382.

Ritz, M., Tholozan, J.L., Federighi, M. and Pilet, M.F., 2002. Physiological damages of *Listeria monocytogenes* treated by high hydrostatic pressure. *International Journal of Food Microbiology*, Vol. 79, pp 47– 53.

Robey, M., Benito, A., Hutson, R.H., Pascual, C., Park, S.F., and Mackey, B.M., 2001. Variation in resistance to high hydrostatic pressure and *rpoS* heterogeneity in natural isolates of *Escherichia coli* O157:H7. *Applied and Environmental Microbiology*, Vol. 67, No. 10, pp 4901-4907.

Rodriguez, J. J., August 2003. Processing Foods by High Hydrostatic Pressure. PhD Thesis, Washington State University.

Ross, I. V., Griffiths, M. W., Mittal, G. S. and Deeth, H. C., 2003. Combining Non-thermal Technologies to Control Foodborne Microorganisms. *International Journal of Food Microbiology*, Vol. 89, pp 125-138.

Russell, N. J., 2002. Bacterial membranes: the effects of chill storage and food processing. An overview. *International Journal of Food Microbiology*, Vol. 79, pp 27- 34.

Silva, J. L. and Weber, G., 1993. Pressure Stability of Proteins. *Annual Review of Physical Chemistry*, Vol. 44, pp 89- 113.

Sizer, C. E., Balasubramaniam (Bala), V. M., and Ting, E., 2002. Validating High-Pressure Processes for Low-Acid Foods. *Food Technology*, Vol. 56, No.2, pp 36-42.

Smelt, J. and Rijke, G., 1992. High pressure treatment as a tool for pasteurization of foods. In: Balny, C., Hayashi, R., Heremans, K., Masson, P. (Eds.), *High Pressure and Biotechnology*, Colloque Inserm/John Libbey Eurotex Ltd., pp 361-363.

Smelt, J. P. P. M., Dutreux, N. and Hellemons, J. C., 1998. Inactivation Kinetics of Microorganisms by High Pressure. In: Isaacs, S. N. (Editor), *High pressure Food Science, Bioscience and Chemistry*, Cambridge (England); Royal Society of Chemistry, pp 403-407.

Tauc, P., Mateo, C. R. and Brochon, J., 2002. Investigation of the effect of high hydrostatic pressure on proteins and lipidic membranes by dynamic fluorescence spectroscopy. *Biochimica et Biophysica Acta*, Vol. 1595, pp 103- 115.

Tholozan, J. L., Ritz, M., Jugiau, F., Federighi, M. and Tissier, J. P., 2000. Physiological effects of high hydrostatic pressure treatments on *Listeria monocytogenes* and *Salmonella typhimurium*. *Journal of Applied Microbiology*, Vol. 88, pp 202-212.

Thongbai, B., Gasaluck, P. and Waites, W., 2006. Morphological changes of temperature- and pH-stressed *Salmonella* following exposure to cetylpyridinium chloride and nisin. *LWT, Food Science and Technology*, Vol. 39, pp 1180- 1188.

Ting, E., Balasubramaniam (Bala), V. M. and Raghubeer, E., 2002. Determining Thermal Effects in High- Pressure Processing. *Food Technology*, Vol. 56, No. 2, pp 31-35.

Trujillo, A. J., Capellas, M., Saldo, J., Gervilla, R. and Guamis, B., 2002. Applications of High-hydrostatic Pressure on Milk and Dairy Products: A Review. *Innovative Food Science and Emerging Technologies*, Vol. 3, pp 295-307.

Van Boekel, M.A.J.S., 2002. On the use of the Weibull model to describe thermal inactivation of microbial vegetative cells. *International Journal of Food Microbiology*, Vol. 74, pp 139- 159.

Van Opstal, I., Vanmuysen, S. C. M., Wuytack, E. Y., Masschalck, B. and Michiels, C. W., 2005. Inactivation of *Escherichia coli* by high hydrostatic pressure at different temperatures in buffer and carrot juice. *International Journal of Food Microbiology*, Vol. 98, pp 179-191.

Venugopal, V., 2006. High Pressure Processing. In: *Seafood Processing: Adding Value Through Quick Freezing, Reportable Packaging, and Cook-Chilling*, CRC Press, Taylor and Francis Group, pp 319- 340.

Vidugiris, J. A., Markley, J. L. and Royer, C., 1995. Evidence for a Molten Globule- Like Transition State in Protein Folding from Determination of Activation Volumes. *Biochemistry*, Vol. 34, Issue 15, pp 4909-4912.

Winter, R., 2001. Effects of hydrostatic pressure on lipid and surfactant phases. *Current Opinion in Colloid and Interface Science*, Vol. 6, pp 303-312.

Xiong, R., Xie, G., Edmondson, A.E. and Sheard, M.A., 1999. A mathematical model for bacterial inactivation. *International Journal of Food Microbiology*, Vol. 46, pp 45-55.

APPENDIX A

GROWTH CURVES

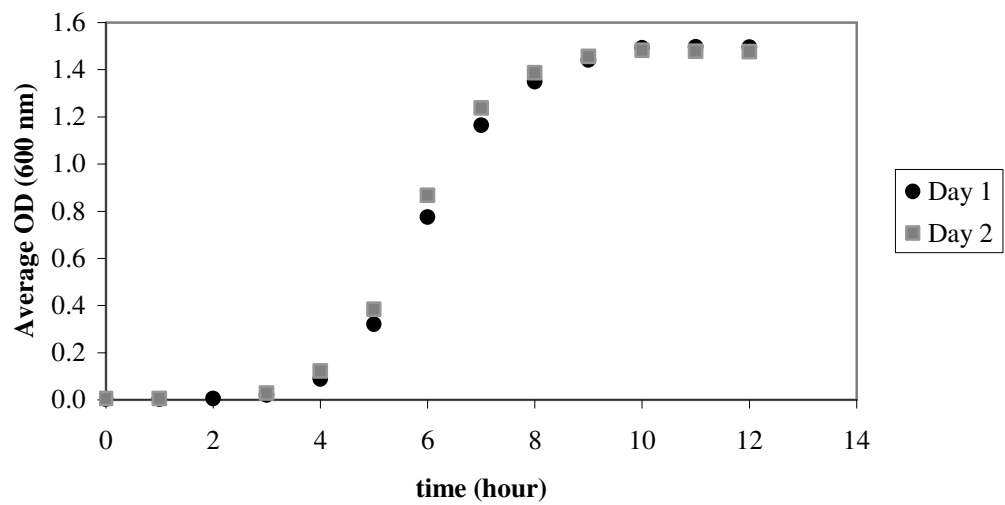


Figure A. 1 Growth curve of *E. coli* O157:H7 933

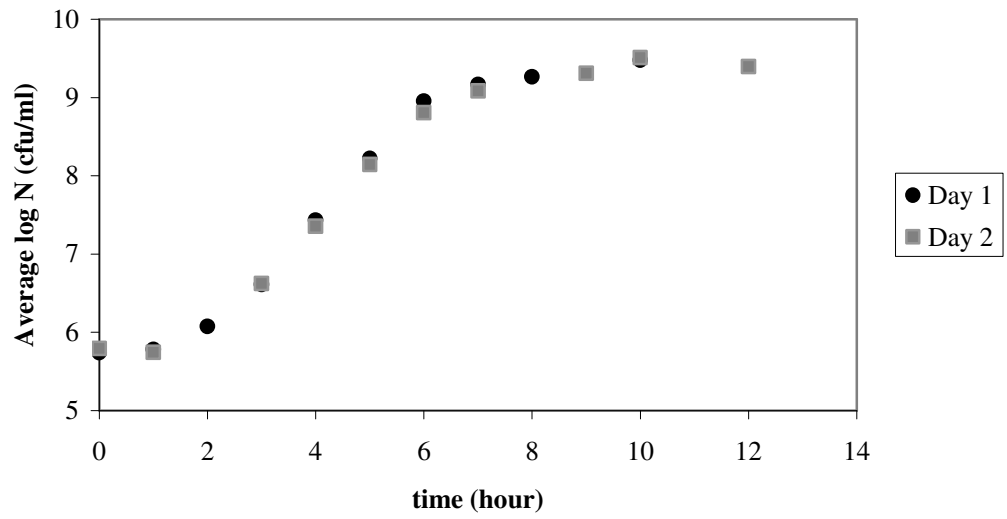


Figure A. 2 Growth curve of *E. coli* O157:H7 933

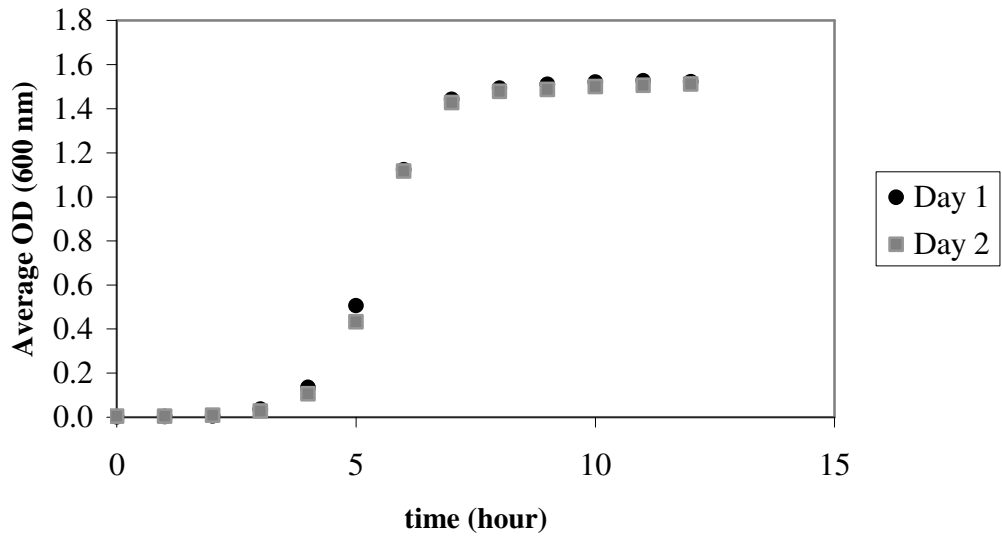


Figure A.3 Growth curve of *S. aureus* 485

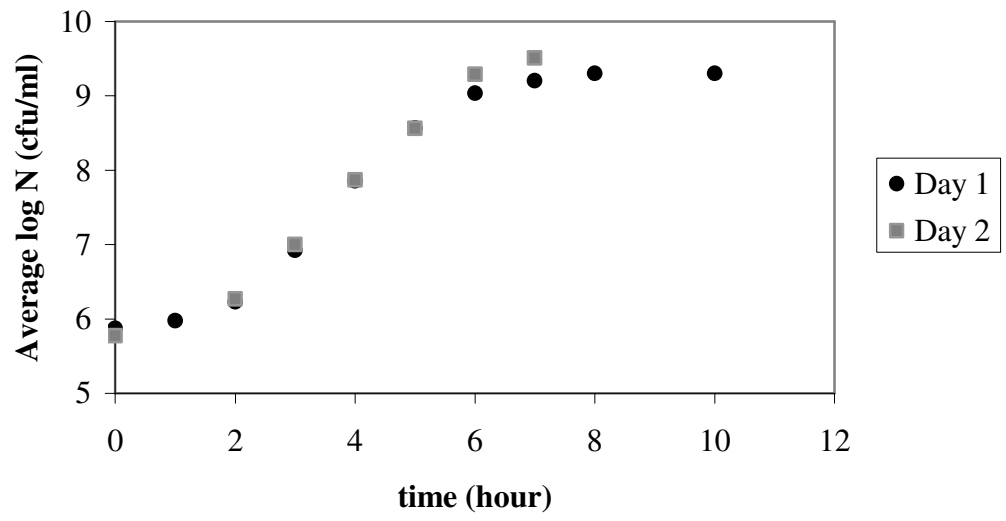


Figure A.4 Growth curve of *S. aureus* 485

APPENDIX B

EFFECT OF VARIABLES ON MACHINE VISION ANALYSIS

B.1 Effect of Software Variables on Volume Calculations

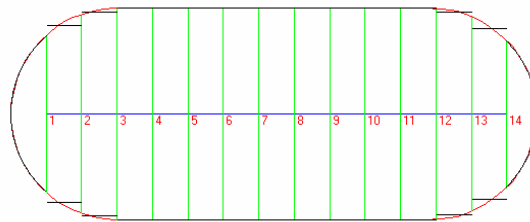


Figure B.1.1 Details of the volume calculation of test image. Zero degrees rotation, 80 points on the perimeter, and 15 slices

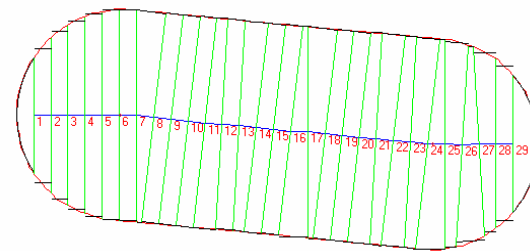


Figure B.1.2 Details of the volume calculation of the test image. Rotation angle -5, 200 points on the perimeter, and 30 slices

Table B.1. 1 Error analysis of the volume calculation of test image

Points on perimeter	50	80	200	200	200
	15	15	15	30	50
Angle	Divisions	Divisions	Divisions	Divisions	Divisions
Volume of the test image					
0	15.17	15.19	15.2	15.25	15.15
1	15.2	15.21	15.16	15.28	15.2
2	15.16	15.27	15.17	15.26	15.43
3	15.15	15.25	15.1	15.23	15.24
4	15.15	15.13	15.09	15.17	15.19
5	15.17	15.24	15.2	15.21	15.23
6	15.14	15.15	15.2	15.25	15.17
7	15.14	15.23	15.23	15.35	15.29
8	15.16	15.28	15.23	15.37	15.38
9	15.11	15.28	15.18	15.25	15.23
10	15.2	15.25	15.19	15.17	15.19
-1	15.14	15.19	15.27	15.2	15.26
-2	15.2	15.15	15.17	15.3	15.24
-3	15.22	15.11	15.1	15.23	15.21
-4	15.17	15.13	15.15	15.19	15.26
-5	15.24	15.19	15.27	15.23	15.25
-6	15.15	15.16	15.21	15.25	15.15
-7	15.28	15.21	15.18	15.28	15.2
-8	15.13	15.15	15.18	15.26	15.34
-9	15.27	15.16	15.22	15.25	15.21
-10	15.26	15.19	15.25	15.24	15.19
Average	15.18	15.20	15.19	15.25	15.24
St.Dev	0.05	0.05	0.05	0.05	0.07
% Error	0.77	0.68	0.73	0.34	0.40

B.2 Effect of SEM Magnification on Calculation of View Area

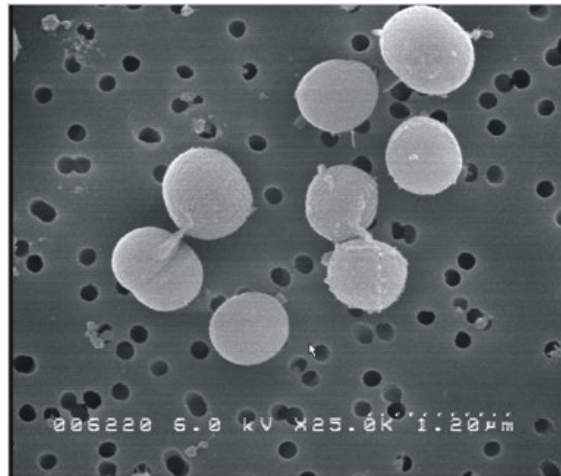


Figure B.2.1 SEM micrograph of unpressurized *S. aureus* 485 with a magnification of x 25 000

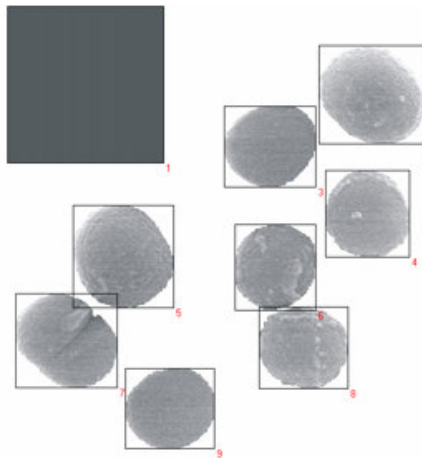


Figure B.2.2 Isolated organisms from Figure B.2.1, with size reference square

Table B.2.1 View area results of *S. aureus* 485 cells calculated by LenseEye Software from Fig. B.2.2

Object #	View Area (pixels)	View Area (user units)
1	35721	1.4400
2	11439	0.4611
3	8511	0.3431
4	8392	0.3383
5	11530	0.4648
6	8014	0.3231
7	10210	0.4116
8	8390	0.3382
9	8245	0.3324

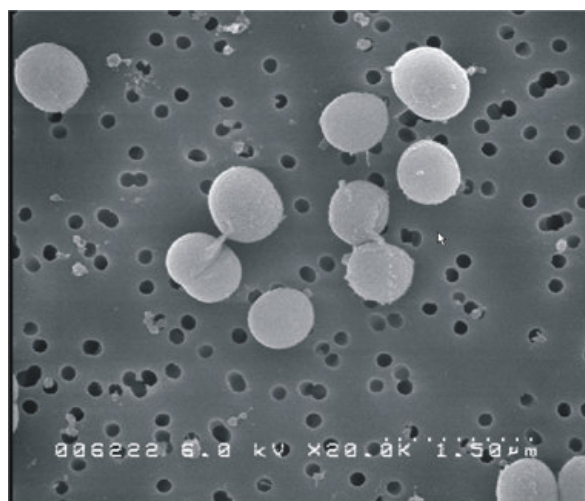


Figure B.2.3 SEM micrograph of unpressurized *S. aureus* 485 with a magnification of x 20 000

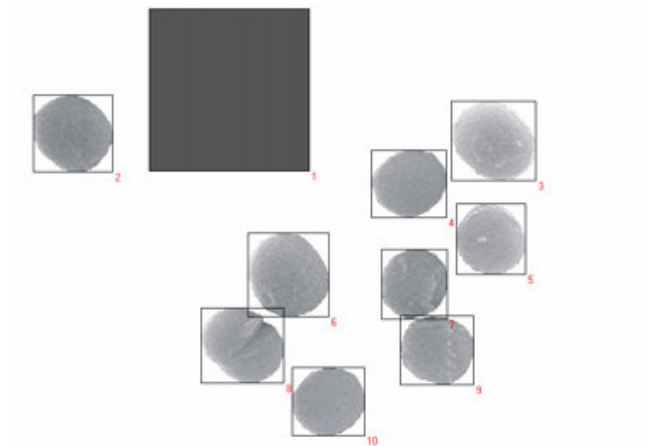


Figure B.2.4 Isolated organisms from Figure B.2.3, with size reference square

Table B.2.2 View area results of *S. aureus* 485 cells calculated by LenseEye Software from Fig. B.2.4

Object #	View Area (pixels)	View Area (user units)
1	35721	2.2500
2	6351	0.4000
3	6959	0.4383
4	5277	0.3324
5	5207	0.3280
6	7162	0.4511
7	5007	0.3154
8	6326	0.3985
9	5380	0.3389
10	5257	0.3311



Figure B.2.5 SEM micrograph of unpressurized *S. aureus* 485 with a magnification of x 15 000

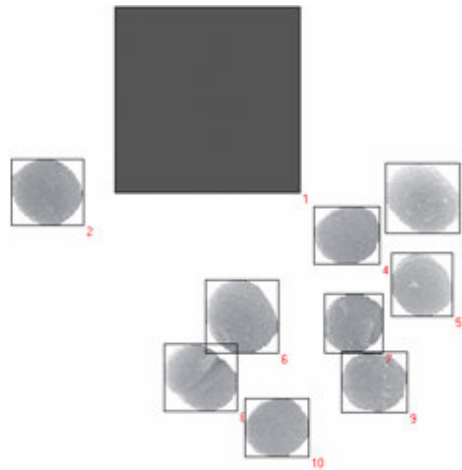


Figure B.2.6 Isolated organisms from Figure B.2.5, with size reference square

Table B.2.3 View area results of *S. aureus* 485 cells calculated by LenseEye Software from Fig. B.2.6

Object #	View Area (pixels)	View Area (user units)
1	35721	4.0000
2	3709	0.4153
3	4111	0.4603
4	3088	0.3456
5	3080	0.3449
6	4207	0.4711
7	2902	0.3250
8	3742	0.4190
9	3142	0.3518
10	3027	0.3390

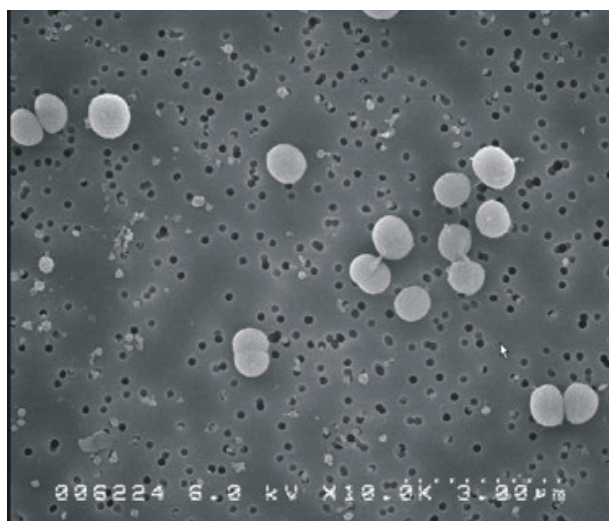


Figure B.2.7 SEM micrograph of unpressurized *S. aureus* 485 with a magnification of x 10 000

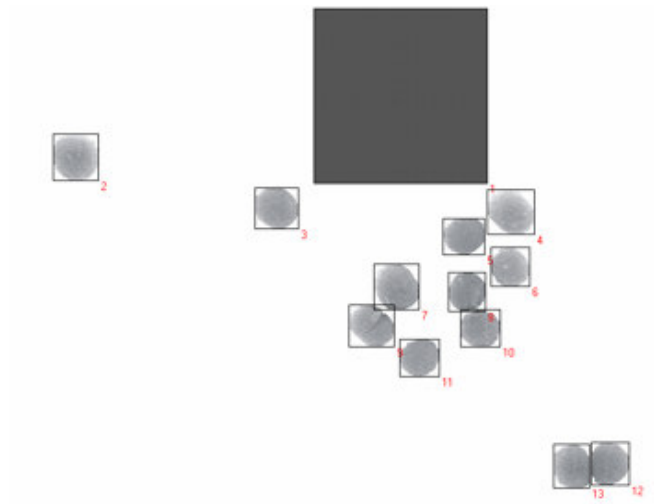


Figure B.2.8 Isolated organisms from Figure B.2.7, with size reference square

Table B.2.4 View area results of *S. aureus* 485 cells calculated by LenseEye Software from Fig. B.2.8

Object #	View Area (pixels)	View Area (user units)
1	35721	9.0000
2	2045	0.5152
3	1671	0.4210
4	1877	0.4729
5	1406	0.3542
6	1388	0.3497
7	1908	0.4807
8	1344	0.3386
9	1662	0.4187
10	1394	0.3512
11	1356	0.3416
12	1548	0.3900
13	1582	0.3986

Table B.2.5 Error analysis of magnification level for the view area calculations (common cells at different magnification levels are indicated as bold in Tables B.1.1-B.1.4)

Magnification Level						
x25000	x20000	x15000	x10000	Average View Area	Std. Dev.	%Error
0.4611	0.4383	0.4603	0.4729	0.4582	0.0144	3.15
0.3431	0.3324	0.3456	0.3542	0.3439	0.0090	2.62
0.3383	0.3280	0.3449	0.3497	0.3402	0.0094	2.76
0.4648	0.4511	0.4711	0.4807	0.4669	0.0124	2.66
0.3231	0.3154	0.3250	0.3386	0.3255	0.0097	2.97
0.4116	0.3985	0.4190	0.4187	0.4120	0.0096	2.34
0.3382	0.3389	0.3518	0.3512	0.3450	0.0075	2.17
0.3324	0.3311	0.3390	0.3416	0.3360	0.0051	1.51
				Averages		
				0.3785	0.0096	2.52

APPENDIX C

MODELING AND REGRESSION RESULTS

C.1 FIRST ORDER MODELING OF INACTIVATION CURVES

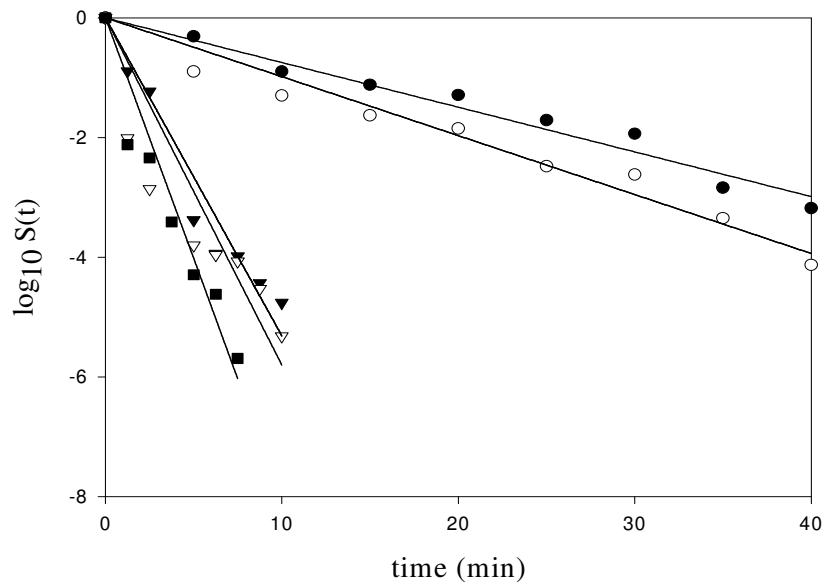


Figure C.1.1 Inactivation curves of *E. coli* O157:H7 933 in peptone water (0.1% peptone, pH 6.95) at different pressure levels (●, 200 MPa; ○, 250 MPa; ▼, 275 MPa; ▽, 300 MPa; ■, 325 MPa) at 40°C

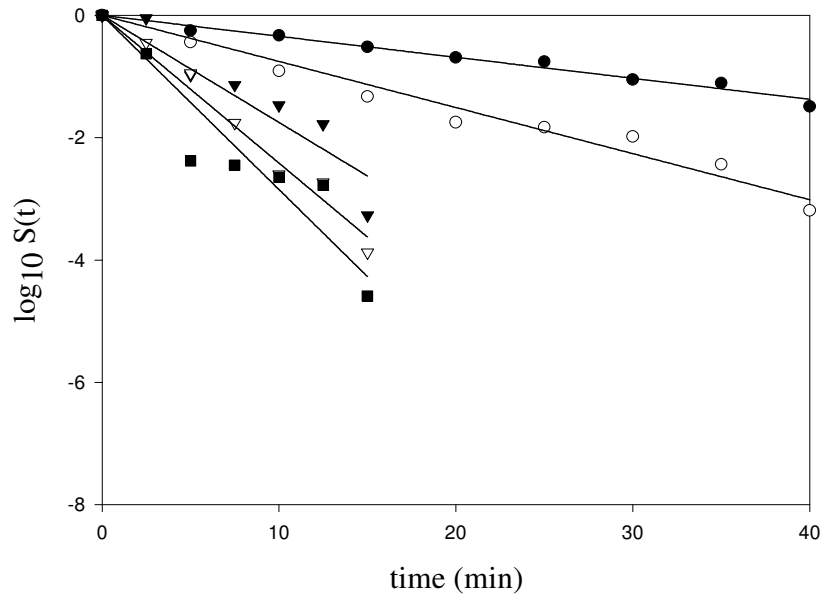


Figure C.1.2 Inactivation curves of *E. coli* O157:H7 933 in carrot juice (pH 6.22) at different pressure levels (●, 200 MPa; ○, 250 MPa; ▼, 275 MPa; ▽, 300 MPa; ■, 325 MPa) at 40°C

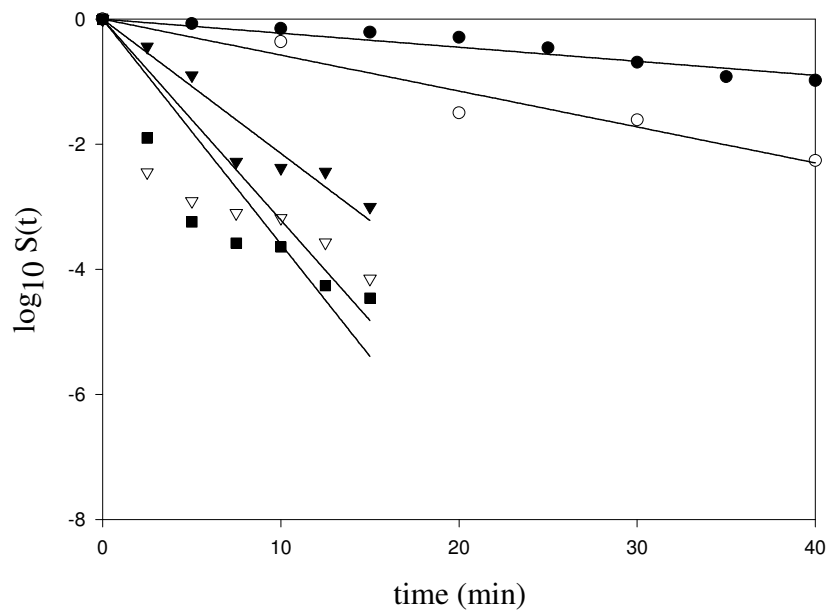


Figure C.1.3 Inactivation curves of *S. aureus* 485 in peptone water (0.1% peptone, pH 6.95) at different pressure levels (●, 200 MPa; ○, 250 MPa; ▼, 300 MPa; ▽, 350 MPa; ■, 400 MPa) at 40°C

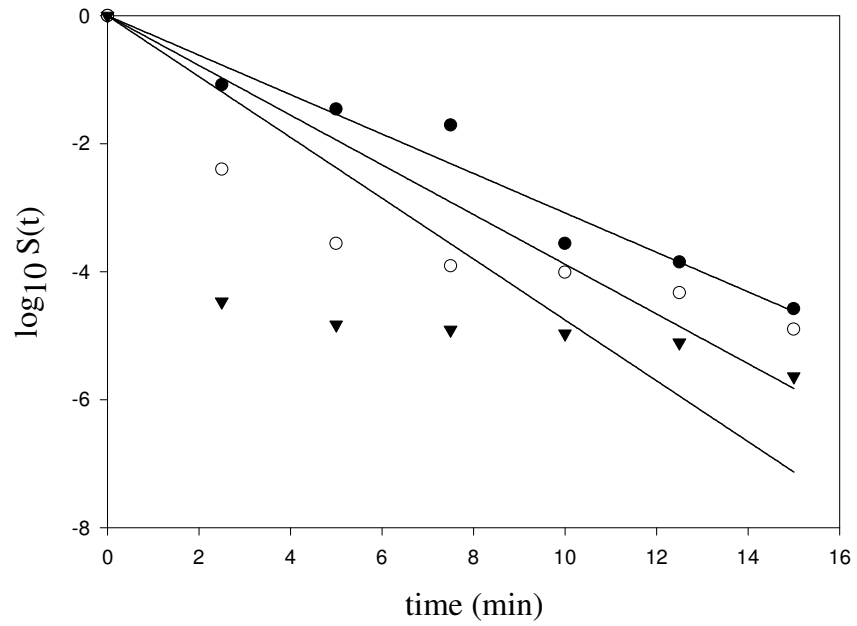


Figure C.1.4 Inactivation curves of *S. aureus* 485 in carrot juice (pH 6.22) at different pressure levels (●, 300 MPa; ○, 350 MPa; ▼, 400 MPa) at 40°C

C.2 REGRESSION RESULTS OF FIRST ORDER AND WEIBULL MODELS

Table C.2.1 Regression results from Sigma Plot for *E. coli* O157:H7 933 in peptone water for first-order model at 200 MPa

R = 0.98487443 Rsqr = 0.96997764 Adj Rsqr = 0.96997764

Standard Error of Estimate = 0.1844

	Coefficient	Std. Error	t	P
a	-0.0746	0.0026	-28.9019	<0.0001

Analysis of Variance:

	DF	SS	MS	F	P
Regression	0	8.7932	8.7932	258.4681	(NAN)
Residual	8	0.2722	0.0340		
Total	8	9.0654	1.1332		

Table C.2.2 Regression results from Sigma Plot for *E. coli* O157:H7 933 in peptone water for first-order model at 250 MPa

R = 0.98186234 Rsqr = 0.96405366 Adj Rsqr = 0.96405366

Standard Error of Estimate = 0.2401

	Coefficient	Std. Error	t	P
a	-0.0984	0.0034	-29.2812	<0.0001

Analysis of Variance:

	DF	SS	MS	F	P
Regression	0	12.3650	12.3650	214.5539	(NAN)
Residual	8	0.4611	0.0576		
Total	8	12.8261	1.6033		

Table C.2.3 Regression results from Sigma Plot for *E. coli* O157:H7 933 in peptone water for first-order model at 275 MPa

R = 0.97144500 Rsqr = 0.94370539 Adj Rsqr = 0.94370539

Standard Error of Estimate = 0.4345

	Coefficient	Std. Error	t	P
a	-0.5314	0.0249	-21.3503	<0.0001

Analysis of Variance:

	DF	SS	MS	F	P
Regression	0	22.1529	22.1529	117.3458	(NAN)
Residual	7	1.3215	0.1888		
Total	7	23.4744	3.3535		

Table C.2.4 Regression results from Sigma Plot for *E. coli* O157:H7 933 in peptone water for first-order model at 300 MPa

R = 0.85824427 Rsqr = 0.73658322 Adj Rsqr = 0.73658322

Standard Error of Estimate = 0.8592

	Coefficient	Std. Error	t	P
a	-0.5802	0.0492	-11.7871	<0.0001

Analysis of Variance:

	DF	SS	MS	F	P
Regression	0	14.4493	14.4493	19.5739	(NAN)
Residual	7	5.1674	0.7382		
Total	7	19.6167	2.8024		

Table C.2.5 Regression results from Sigma Plot for *E. coli* O157:H7 933 in peptone water for first-order model at 325 MPa

R = 0.95594666 Rsqr = 0.91383402 Adj Rsqr = 0.91383402

Standard Error of Estimate = 0.5569

	Coefficient	Std. Error	t	P
a	-0.8038	0.0467	-17.2111	<0.0001

Analysis of Variance:

	DF	SS	MS	F	P
Regression	0	19.7333	19.7333	63.6331	(NAN)
Residual	6	1.8607	0.3101		
Total	6	21.5940	3.5990		

Table C.2.6 Regression results from Sigma Plot for *E. coli* O157:H7 933 in carrot juice for first-order model at 200 MPa

R = 0.98913962 Rsqr = 0.97839718 Adj Rsqr = 0.97839718

Standard Error of Estimate = 0.0693

	Coefficient	Std. Error	t	P
a	-0.0343	0.0010	-35.3746	<0.0001

Analysis of Variance:

	DF	SS	MS	F	P
Regression	0	1.7407	1.7407	362.3221	(NAN)
Residual	8	0.0384	0.0048		
Total	8	1.7791	0.2224		

Table C.2.7 Regression results from Sigma Plot for *E. coli* O157:H7 933 in carrot juice for first-order model at 250 MPa

R = 0.98213727 Rsqr = 0.96459362 Adj Rsqr = 0.96459362

Standard Error of Estimate = 0.1867

	Coefficient	Std. Error	t	P
a	-0.0754	0.0026	-28.8287	<0.0001

Analysis of Variance:

	DF	SS	MS	F	P
Regression	0	7.5980	7.5980	217.9479	(NAN)
Residual	8	0.2789	0.0349		
Total	8	7.8769	0.9846		

Table C.2.8 Regression results from Sigma Plot for *E. coli* O157:H7 933 in carrot juice for first-order model at 275 MPa

R = 0.94150293 Rsqr = 0.88642776 Adj Rsqr = 0.88642776

Standard Error of Estimate = 0.3767

	Coefficient	Std. Error	t	P
a	-0.1751	0.0158	-11.0840	<0.0001

Analysis of Variance:

	DF	SS	MS	F	P
Regression	0	6.6453	6.6453	46.8298	(NAN)
Residual	6	0.8514	0.1419		
Total	6	7.4967	1.2494		

Table C.2.9 Regression results from Sigma Plot for *E. coli* O157:H7 933 in carrot juice for first-order model at 300 MPa

R = 0.98802182 Rsqr = 0.97618711 Adj Rsqr = 0.97618711

Standard Error of Estimate = 0.2147

	Coefficient	Std. Error	t	P
a	-0.2416	0.0090	-26.8394	<0.0001

Analysis of Variance:

	DF	SS	MS	F	P
Regression	0	11.3339	11.3339	245.9644	(NAN)
Residual	6	0.2765	0.0461		
Total	6	11.6103	1.9351		

Table C.2.10 Regression results from Sigma Plot for *E. coli* O157:H7 933 in carrot juice for first-order model at 325 MPa

R = 0.93299324 Rsqr = 0.87047639 Adj Rsqr = 0.87047639

Standard Error of Estimate = 0.5428

	Coefficient	Std. Error	t	P
a	-0.2847	0.0228	-12.5100	<0.0001

Analysis of Variance:

	DF	SS	MS	F	P
Regression	0	11.8819	11.8819	40.3236	(NAN)
Residual	6	1.7680	0.2947		
Total	6	13.6499	2.2750		

Table C.2.11 Regression results from Sigma Plot for *E. coli* O157:H7 933 in peptone water for Weibull model at 200 MPa

R = 0,98731859 Rsqr = 0,97479799 Adj Rsqr = 0,97119770

Standard Error of Estimate = 0,1807

	Coefficient	Std. Error	t	P
a	14,7313	1,1736	12,5523	<0,0001
b	1,1299	0,1112	10,1626	<0,0001

Analysis of Variance:

	DF	SS	MS	F	P
Regression	1	8,8369	8,8369	270,7556	<0,0001
Residual	7	0,2285	0,0326		
Total	8	9,0654	1,1332		

Table C.2.12 Regression results from Sigma Plot for *E. coli* O157:H7 933 in peptone water for Weibull model at 250 MPa

R = 0,98497913 Rsqr = 0,97018388 Adj Rsqr = 0,96592444

Standard Error of Estimate = 0,2337

	Coefficient	Std. Error	t	P
a	8,7045	1,1696	7,4426	0,0001
b	0,8755	0,0925	9,4632	<0,0001

Analysis of Variance:

	DF	SS	M	F	P
Regression	1	12,4437	12,4437	227,7724	<0,0001
Residual	7	0,3824	0,0546		
Total	8	12,8261	1,6033		

Table C.2.13 Regression results from Sigma Plot for *E. coli* O157:H7 933 in peptone water for Weibull model at 275 MPa

R = 0,98437958 Rsqr = 0,96900316 Adj Rsqr = 0,96383702

Standard Error of Estimate = 0,3482

	Coefficient	Std. Error	t	P
a	1,2122	0,3030	4,0012	0,0071
b	0,7633	0,1030	7,4086	0,0003

Analysis of Variance:

	DF	SS	MS	F	P
Regression	1	22,7468	22,7468	187,5681	<0,0001
Residual	6	0,7276	0,1213		
Total	7	23,4744	3,3535		

Table C.2.14 Regression results from Sigma Plot for *E. coli* O157:H7 933 in peptone water for Weibull model at 300 MPa

R = 0,99258086 Rsqr = 0,98521676 Adj Rsqr = 0,98275288

Standard Error of Estimate = 0,2198

	Coefficient	Std. Error	t	P
a	0,2401	0,0810	2,9658	0,0251
b	0,4295	0,0432	9,9407	<0,0001

Analysis of Variance:

	DF	SS	MS	F	P
Regression	1	19,3267	19,3267	399,8649	<0,0001
Residual	6	0,2900	0,0483		
Total	7	19,6167	2,8024		

Table C.2.15 Regression results from Sigma Plot for *E. coli* O157:H7 933 in peptone water for Weibull model at 325 MPa

R = 0,99060674 Rsqr = 0,98130172 Adj Rsqr = 0,97756207

Standard Error of Estimate = 0,2842

	Coefficient	Std. Error	t	P
a	0,5445	0,1383	3,9373	0,0110
b	0,6473	0,0712	9,0863	0,0003

Analysis of Variance:

	DF	SS	MS	F	P
Regression	1	21,1902	21,1902	262,4043	<0,0001
Residual	5	0,4038	0,0808		
Total	6	21,5940	3,5990		

Table C.2.16 Regression results from Sigma Plot for *E. coli* O157:H7 933 in carrot juice for Weibull model at 200 MPa

R = 0,98938644 Rsqr = 0,97888554 Adj Rsqr = 0,97586918

Standard Error of Estimate = 0,0733

	Coefficient	Std. Error	t	P
a	29,1741	0,8489	34,3684	<0,0001
b	1,0387	0,0927	11,2050	<0,0001

Analysis of Variance:

	DF	SS	MS	F	P
Regression	1	1,7415	1,7415	324,5263	<0,0001
Residual	7	0,0376	0,0054		
Total	8	1,7791	0,2224		

Table C.2.17 Regression results from Sigma Plot for *E. coli* O157:H7 933 in carrot juice for Weibull model at 250 MPa

R = 0,98534860 Rsqr = 0,97091187 Adj Rsqr = 0,96675642

Standard Error of Estimate = 0,1809

	Coefficient	Std. Error	t	P
a	11,8217	1,2406	9,5289	<0,0001
b	0,8768	0,0937	9,3591	<0,0001

Analysis of Variance:

	DF	SS	MS	F	P
Regression	1	7,6478	7,6478	233,6480	<0,0001
Residual	7	0,2291	0,0327		
Total	8	7,8769	0,9846		

Table C.2.18 Regression results from Sigma Plot for *E. coli* O157:H7 933 in carrot juice for Weibull model at 275 MPa

R = 0,96342586 Rsqr = 0,92818940 Adj Rsqr = 0,91382728

Standard Error of Estimate = 0,3281

	Coefficient	Std. Error	t	P
a	7,3041	0,9189	7,9489	0,0005
b	1,5033	0,3167	4,7471	0,0051

Analysis of Variance:

	DF	SS	MS	F	P
Regression	1	6,9583	6,9583	64,6276	0,0005
Residual	5	0,5383	0,1077		
Total	6	7,4967	1,2494		

Table C.2.19 Regression results from Sigma Plot for *E. coli* O157:H7 933 in carrot juice for Weibull model at 300 MPa

R = 0,99170681 Rsqr = 0,98348240 Adj Rsqr = 0,98017888

Standard Error of Estimate = 0,1958

	Coefficient	Std. Error	t	P
a	4,7788	0,4538	10,5312	0,0001
b	1,1606	0,1143	10,1552	0,0002

Analysis of Variance:

	DF	SS	MS	F	P
Regression	1	11,4186	11,4186	297,7075	<0,0001
Residual	5	0,1918	0,0384		
Total	6	11,6103	1,9351		

Table C.2.20 Regression results from Sigma Plot for *E. coli* O157:H7 933 in carrot juice for Weibull model at 325 MPa

R = 0,94340895 Rsqr = 0,89002046 Adj Rsqr = 0,86802455

Standard Error of Estimate = 0,5479

	Coefficient	Std. Error	t	P
a	2,5209	1,0411	2,4213	0,0600
b	0,7808	0,2126	3,6731	0,0144

Analysis of Variance:

	DF	SS	MS	F	P
Regression	1	12,1487	12,1487	40,4630	0,0014
Residual	5	1,5012	0,3002		
Total	6	13,6499	2,2750		

Table C.2.21 Regression results from Sigma Plot for *S. aureus* 485 in peptone water for first-order model at 200 MPa

R = 0.96000326 Rsqr = 0.92160626 Adj Rsqr = 0.92160626

Standard Error of Estimate = 0.1024

	Coefficient	Std. Error	t	P
a	-0.0224	0.0014	-15.6377	<0.0001

Analysis of Variance:

	DF	SS	MS	F	P
Regression	0	0.9869	0.9869	94.0490	(NAN)
Residual	8	0.0840	0.0105		
Total	8	1.0709	0.1339		

Table C.2.22 Regression results from Sigma Plot for *S. aureus* 485 in peptone water for first-order model at 250 MPa

R = 0.97352496 Rsqr = 0.94775084 Adj Rsqr = 0.94775084

Standard Error of Estimate = 0.2142

	Coefficient	Std. Error	t	P
a	-0.0574	0.0039	-14.6857	0.0001

Analysis of Variance:

	DF	SS	MS	F	P
Regression	0	3.3292	3.3292	72.5563	(NAN)
Residual	4	0.1835	0.0459		
Total	4	3.5127	0.8782		

Table C.2.23 Regression results from Sigma Plot for *S. aureus* 485 in peptone water for first-order model at 300 MPa

R = 0.95913884 Rsqr = 0.91994732 Adj Rsqr = 0.91994732

Standard Error of Estimate = 0.3292

	Coefficient	Std. Error	t	P
a	-0.2145	0.0138	-15.5385	<0.0001

Analysis of Variance:

	DF	SS	MS	F	P
Regression	0	7.4734	7.4734	68.9506	(NAN)
Residual	6	0.6503	0.1084		
Total	6	8.1238	1.3540		

Table C.2.24 Regression results from Sigma Plot for *S. aureus* 485 in peptone water for first-order model at 350 MPa

R = 0.69177551 Rsqr = 0.47855335 Adj Rsqr = 0.47855335

Standard Error of Estimate = 0.9605

	Coefficient	Std. Error	t	P
a	-0.3211	0.0403	-7.9712	0.0002

Analysis of Variance:

	DF	SS	MS	F	P
Regression	0	5.0804	5.0804	5.5065	(NAN)
Residual	6	5.5358	0.9226		
Total	6	10.6162	1.7694		

Table C.2.25 Regression results from Sigma Plot for *S. aureus* 485 in peptone water for first-order model at 400 MPa

R = 0.82147412 Rsqr = 0.67481972 Adj Rsqr = 0.67481972

Standard Error of Estimate = 0.8935

	Coefficient	Std. Error	t	P
a	-0.3593	0.0375	-9.5895	<0.0001

Analysis of Variance:

	DF	SS	MS	F	P
Regression	0	9.9414	9.9414	12.4513	(NAN)
Residual	6	4.7905	0.7984		
Total	6	14.7319	2.4553		

Table C.2.26 Regression results from Sigma Plot for *S. aureus* 485 in carrot juice for first-order model at 300 MPa

R = 0.97938265 Rsqr = 0.95919037 Adj Rsqr = 0.95919037

Standard Error of Estimate = 0.3402

	Coefficient	Std. Error	t	P
a	-0.3081	0.0143	-21.5993	<0.0001

Analysis of Variance:

	DF	SS	MS	F	P
Regression	0	16.3233	16.3233	141.0241	(NAN)
Residual	6	0.6945	0.1157		
Total	6	17.0178	2.8363		

Table C.2.27 Regression results from Sigma Plot for *S. aureus* 485 in carrot juice for first-order model at 350 MPa

R = 0.76271565 Rsqr = 0.58173516 Adj Rsqr = 0.58173516

Standard Error of Estimate = 1.0648

	Coefficient	Std. Error	t	P
a	-0.3883	0.0446	-8.6969	0.0001

Analysis of Variance:

	DF	SS	MS	F	P
Regression	0	9.4617	9.4617	8.3450	(NAN)
Residual	6	6.8029	1.1338		
Total	6	16.2647	2.7108		

Table C.2.28 Regression results from Sigma Plot for *S. aureus* 485 in carrot juice for first-order model at 400 MPa

R = 0.15238484 Rsqr = 0.02322114 Adj Rsqr = 0.02322114

Standard Error of Estimate = 1.8954

	Coefficient	Std. Error	t	P
a	-0.4753	0.0795	-5.9802	0.0010

Analysis of Variance:

	DF	SS	MS	F	P
Regression	0	0.5125	0.5125	0.1426	(NAN)
Residual	6	21.5559	3.5927		
Total	6	22.0684	3.6781		

Table C.2.29 Regression results from Sigma Plot for *S. aureus* 485 in peptone water for Weibull model at 200 MPa

R = 0,99190080 Rsqr = 0,98386719 Adj Rsqr = 0,98156250

Standard Error of Estimate = 0,0497

	Coefficient	Std. Error	t	P
a	39,1330	0,9186	42,6000	<0,0001
b	1,5791	0,1285	12,2870	<0,0001

Analysis of Variance:

	DF	SS	MS	F	P
Regression	1	1,0536	1,0536	426,8984	<0,0001
Residual	7	0,0173	0,0025		
Total	8	1,0709	0,1339		

Table C.2.30 Regression results from Sigma Plot for *S. aureus* 485 in peptone water for Weibull model at 250 MPa

R = 0,97389040 Rsqr = 0,94846252 Adj Rsqr = 0,93128336

Standard Error of Estimate = 0,2457

	Coefficient	Std. Error	t	P
a	16,9058	2,9786	5,6757	0,0108
b	0,9535	0,2374	4,0165	0,0277

Analysis of Variance:

	DF	SS	MS	F	P
Regression	1	3,3317	3,3317	55,2101	0,0050
Residual	3	0,1810	0,0603		
Total	4	3,5127	0,8782		

Table C.2.31 Regression results from Sigma Plot for *S. aureus* 485 in peptone water for Weibull model at 300 MPa

R = 0,96489051 Rsqr = 0,93101370 Adj Rsqr = 0,91721644

Standard Error of Estimate = 0,3348

	Coefficient	Std. Error	t	P
a	3,9327	0,9288	4,2340	0,0082
b	0,8415	0,1800	4,6763	0,0055

Analysis of Variance:

	DF	SS	MS	F	P
Regression	1	7,5633	7,5633	67,4782	0,0004
Residual	5	0,5604	0,1121		
Total	6	8,1238	1,3540		

Table C.2.32 Regression results from Sigma Plot for *S. aureus* 485 in peptone water for Weibull model at 350 MPa

R = 0,99109518 Rsqr = 0,98226967 Adj Rsqr = 0,97872360

Standard Error of Estimate = 0,1940

	Coefficient	Std. Error	t	P
a	0,1143	0,0840	1,3614	0,2315
b	0,2768	0,0462	5,9942	0,0019

Analysis of Variance:

	DF	SS	MS	F	P
Regression	1	10,4279	10,4279	277,0026	<0,0001
Residual	5	0,1882	0,0376		
Total	6	10,6162	1,7694		

Table C.2.33 Regression results from Sigma Plot for *S. aureus* 485 in peptone water for Weibull model at 400 MPa

R = 0,99067363 Rsqr = 0,98143424 Adj Rsqr = 0,97772108

Standard Error of Estimate = 0,2339

	Coefficient	Std. Error	t	P
a	0,3561	0,1600	2,2261	0,0765
b	0,4037	0,0546	7,4004	0,0007

Analysis of Variance:

	DF	SS	MS	F	P
Regression	1	14,4584	14,4584	264,3129	<0,0001
Residual	5	0,2735	0,0547		
Total	6	14,7319	2,4553		

Table C.2.34 Regression results from Sigma Plot for *S. aureus* 485 in carrot juice for Weibull model at 300 MPa

R = 0,97941313 Rsqr = 0,95925008 Adj Rsqr = 0,95110009

Standard Error of Estimate = 0,3724

	Coefficient	Std. Error	t	P
a	3,3014	0,6605	4,9983	0,0041
b	1,0136	0,1560	6,4989	0,0013

Analysis of Variance:

	DF	SS	MS	F	P
Regression	1	16,3243	16,3243	117,6996	0,0001
Residual	5	0,6935	0,1387		
Total	6	17,0178	2,8363		

Table C.2.35 Regression results from Sigma Plot for *S. aureus* 485 in carrot juice for Weibull model at 350 MPa

R = 0,99398604 Rsqr = 0,98800825 Adj Rsqr = 0,98560990

Standard Error of Estimate = 0,1975

	Coefficient	Std. Error	t	P
a	0,1527	0,0755	2,0222	0,0991
b	0,3414	0,0407	8,3902	0,0004

Analysis of Variance:

	DF	SS	MS	F	P
Regression	1	16,0696	16,0696	411,9533	<0,0001
Residual	5	0,1950	0,0390		
Total	6	16,2647	2,7108		

Table C.2.36 Regression results from Sigma Plot for *S. aureus* 485 in carrot juice for Weibull model at 400 MPa

R = 0,99689606 Rsqr = 0,99380175 Adj Rsqr = 0,99256210

Standard Error of Estimate = 0,1654

	Coefficient	Std. Error	t	P
a	0,0000	0,0000	0,3043	0,7732
b	0,1082	0,0234	4,6160	0,0058

Analysis of Variance:

	DF	SS	MS	F	P
Regression	1	21,9316	21,9316	801,6788	<0,0001
Residual	5	0,1368	0,0274		
Total	6	22,0684	3,6781		

APPENDIX D

TABLE OF EQUATIONS

Table D.1 Table Curve 3D equation list for *E. coli* O157:H7 933 pressurized in peptone water

Rank	R ²	Equation number	Equation
1	1	302473022	$z^{(-1)}=a+by^2+cy^{(2.5)}+dy/\ln y$
2	1	302473025	$z^{(-1)}=a+by^2+cy^{(2.5)}+d/\ln y$
3	0.9999999998	302467828	$z^{(-1)}=a+be^{(x/wx)}+c/y^{(1.5)}+d\ln y/y^2$
4	0.9999999995	302468540	$z^{(-1)}=a+b(\ln x)^2+c/x+dy^2$
5	0.9999999989	302469029	$z^{(-1)}=a+bx/\ln x+c/x^{(1.5)}+dy^2$
6	0.9999999988	302469849	$z^{(-1)}=a+b\ln x+c/x+dy^3$
7	0.9999999988	302470199	$z^{(-1)}=a+b/\ln x+c\ln x/x+dy^2$
8	0.9999999986	302472732	$z^{(-1)}=a+b\ln y+cy^{(2.5)}+d(\ln y)^2$
9	0.9999999984	302470116	$z^{(-1)}=a+b\ln x+cy/\ln y+d\ln y/y^2$
10	0.9999999981	302472336	$z^{(-1)}=a+be^{(-x)}+cy^2+dy^{(2.5)}$
11	0.9999999945	151243509	$\ln z=a+b\ln y+cy^3+dy/\ln y$
12	0.9999999951	151243204	$\ln z=a+be^{(-x)}+cy/\ln y+de^{(-y)}$
13	0.99999999418	151243228	$\ln z=a+be^{(-x)}+c/\ln y+de^{(-y)}$
14	0.99999999402	151243222	$\ln z=a+be^{(-x)}+c/\ln y+d/y^{(0.5)}$
15	0.99999999319	151243195	$\ln z=a+be^{(-x)}+cy/\ln y+dy^{(0.5)}$

Table D.1 (Continued)

Rank	R²	Equation number	Equation
16	0.9999999216	151243206	$\ln z = a + be^{(-x)} + cy^{(0.5)} + d/\ln y$
17	0.9999998778	151243512	$\ln z = a + by \ln y + cy^3 + d/\ln y$
18	0.9999998755	151243197	$\ln z = a + be^{(-x)} + cy/\ln y + d/\ln y$
19	0.9999998364	151243198	$\ln z = a + be^{(-x)} + cy/\ln y + d/y^{(0.5)}$
20	0.9999998071	151238484	$\ln z = a + be^{(x/wx)} + cy^{(2.5)} + d/y^{(0.5)}$
21	0.9999996703	302462187	$z^{(-1)} = a + by^2 + cy^3$
22	0.9999994762	302462259	$z^{(-1)} = a + be^{(y/wy)} + ce^{(-y)}$
23	0.9999992994	302462186	$z^{(-1)} = a + by^2 + cy^{(2.5)}$
24	0.9999992969	302462150	$z^{(-1)} = a + by \ln y + cy^2 \ln y$
25	0.9999986216	302462170	$z^{(-1)} = a + by^{(1.5)} + cy^3$
26	0.9999982816	302462250	$z^{(-1)} = a + be^{(y/wy)} + cy^{(0.5)}$
27	0.9999970467	302462251	$z^{(-1)} = a + be^{(y/wy)} + c \ln y$
28	0.9999958653	302462234	$z^{(-1)} = a + by^3 + cy^{(0.5)} \ln y$
29	0.9999952924	302462218	$z^{(-1)} = a + by^{(2.5)} + cy^3$
30	0.9999947449	302462121	$z^{(-1)} = a + be^{(-x)} + c/y^{(0.5)}$
31	0.9999907637	151233014	$\ln z = a + be^{(y/wy)} + c/\ln y$
32	0.9999867304	151233011	$\ln z = a + be^{(y/wy)} + cy/\ln y$
33	0.9999644371	9187	$z = a + be^{(x/wx)} + cy^{(1.5)} + dy^2$
34	0.99995876	151232882	$\ln z = a + be^{(-x)} + c/\ln y$
35	0.9999286044	151232876	$\ln z = a + be^{(-x)} + ce^{(y/wy)}$
36	0.9999277734	151232879	$\ln z = a + be^{(-x)} + cy/\ln y$
37	0.9999217599	9258	$z = a + be^{(x/wx)} + cy^3 + d \ln y$
38	0.999899947	9209	$z = a + be^{(x/wx)} + cy^2 + dy^{(0.5)} \ln y$
39	0.9998741399	13552	$z = a + b \ln x/x^2 + c/y^{(0.5)} + d/y^{(1.5)}$

Table D.1 (Continued)

Rank	R²	Equation number	Equation
40	0.9997611428	151232998	$\ln z = a + by^3 + cy / \ln y$
41	0.9997574203	151232531	$\ln z = a + be^{(x/wx)} + c / \ln y$
42	0.9997520326	151233001	$\ln z = a + by^3 + c / \ln y$
43	0.9997434092	13308	$z = a + b/x^{(1.5)} + c/y + d/y^{(1.5)}$
44	0.9997335032	9192	$z = a + be^{(x/wx)} + cy^{(1.5)} + dy^{(0.5)} \ln y$
45	0.9997268337	151232528	$\ln z = a + be^{(x/wx)} + cy / \ln y$
46	0.999622123	9252	$z = a + be^{(x/wx)} + cy^{(2.5)} + de^{(-y)}$
47	0.9994248513	9152	$z = a + be^{(x/wx)} + cy + dy^{(2.5)}$
48	0.9991631675	2087	$z = \text{LORCUMX}(a, b, c) * \text{LORCUMY}(1, d, c)$
49	0.9991199109	13542	$z = a + b \ln x / x^2 + c \ln y + de^{(-y)}$
50	0.9991104422	151232972	$\ln z = a + by^2 \ln y + c / \ln y$
51	0.9991023261	9243	$z = a + be^{(x/wx)} + cy^{(2.5)} + dy^{(0.5)}$
52	0.999075517	162	$z = a + b/x + c/y + d/y^2$
53	0.9983751826	2135	$z = \text{LDRX}(a, b, c) * \text{LDRY}(1, d, c)$
54	0.998100508	2111	$z = \text{SIGX}(a, b, c) * \text{SIGY}(1, d, c)$
55	0.9980833934	2099	$z = \text{LNCUMX}(a, b, c) * \text{LNCUMY}(1, d, c)$
56	0.9979492053	2027	$z = \text{LOGNORMX}(a, b, c) * \text{LOGNORMY}(1, d, c)$
57	0.9979164095	2075	$z = \text{GCUMX}(a, b, c) * \text{GCUMY}(1, d, c)$
58	0.9876374676	3734	$z = a + by^2 \ln y + c / \ln y$
59	0.987414581	3731	$z = a + by^2 \ln y + cy / \ln y$
60	0.9794621311	3641	$z = a + be^{(-x)} + cy / \ln y$
61	0.9768670568	3290	$z = a + be^{(x/wx)} + cy / \ln y$
62	0.9766492975	3644	$z = a + be^{(-x)} + c / \ln y$
63	0.9762919445	3293	$z = a + be^{(x/wx)} + c / \ln y$

Table D.1 (Continued)

Rank	R²	Equation number	Equation
64	0.9733450501	87	$z=a+b\ln x+c/y+d/y^2$
65	0.9703070359	3773	$z=a+be^{(y/wy)}+cy/\ln y$
66	0.9688967846	3776	$z=a+be^{(y/wy)}+c/\ln y$
67	0.9649129072	3279	$z=a+be^{(x/wx)}+ce^{(-x)}$
68	0.9641007489	12	$z=a+bx+c/y+d/y^2$
69	0.9622249499	3635	$z=a+be^{(-x)}+cy^2\ln y$
70	0.9451064074	7	$z=a+bx+c\ln y+d(\ln y)^2$
71	0.944893277	157	$z=a+b/x+c\ln y+d(\ln y)^2$
72	0.9448197403	82	$z=a+b\ln x+c\ln y+d(\ln y)^2$
73	0.9387886029	16	$z=a+bx+cx^2+dy$
74	0.9385951212	21	$z=a+bx+cx^2+d\ln y$
75	0.9381795143	26	$z=a+bx+cx^2+d/y$
76	0.9357662135	6	$z=a+bx+cy+dy^2$
77	0.933699203	2151	$z=a+by+\text{EXPX}(c,d)$
78	0.9328842784	2164	$z=a+bx+\text{POWY}(c,d)$
79	0.9309868008	151	$z=a+b/x+cy$
80	0.9289281547	156	$z=a+b/x+c\ln y$
81	0.9276916181	161	$z=a+b/x+c/y$
82	0.9266475585	2161	$z=\text{POWX}(a,b)+\text{POWY}(c,d)$
83	0.9235924665	76	$z=a+b\ln x+cy$
84	0.9229516999	2148	$z=a+\text{EXPX}(b,c)*\text{EXPY}(1,c)$
85	0.918889865	81	$z=a+b\ln x+c\ln y$
86	0.9164614548	86	$z=a+b\ln x+c/y$
87	0.9110894423	1	$z=a+bx+cy$

Table D.1 (Continued)

Rank	R²	Equation number	Equation
88	0.9110894423	2169	$z=a+bx+cy$ [Robust None, Least Squares]
89	0.911089415	2152	$z=a+bx+EXPY(c,d)$
90	0.9010339274	6	$z=a+bx+clny$
91	0.9001824428	2170	$z=a+bx+cy$ [Robust Low, Least Abs Deviation]
92	0.899562605	2163	$z=a+by+POWX(c,d)$
93	0.895876318	11	$z=a+bx+c/y$
94	0.8893846521	2172	$z=a+bx+cy$ [Robust High, Pearson VII Limit]
95	0.8893206595	2171	$z=a+bx+cy$ [Robust Medium, Lorentzian]
96	0.8889115086	2147	$z=EXPX(a,b)*EXPY(1,b)$
97	0.6214565972	2039	$z=LOGISTICX(a,b,c)*LOGISTICY(1,d,c)$
98	0.616196891	2015	$z=LORX(a,b,c)*LORY(1,d,c)$
99	0.5942135679	2051	$z=EXTRVALX(a,b,c)*EXTRVALY(1,d,c)$
100	0.5304258721	2003	$z=GAUSSX(a,b,c)*GAUSSY(1,d,c)$
101	0.2178812618	2146	$z=a+EXPX(b,c)*EXPY(1,d)$
102	0.1646809597	2123	$z=EXVCUMX(a,b,c)*EXVCUMY(1,d,c)$

Table D.2 Table Curve 3D equation list for *E. coli* O157:H7 933 pressurized in carrot juice

Rank	R ²	Equation number	Equation
1	0.9999999941	13018	$z=a+b/x+c/\ln y+d\ln y/y^2$
2	0.9999999256	12694	$z=a+b\ln x/x+cy/\ln y+d\ln y/y^2$
3	0.9999994339	12994	$z=a+b/x+cy/\ln y+d\ln y/y^2$
4	0.9999986262	12718	$z=a+b\ln x/x+c/\ln y+d\ln y/y^2$
5	0.9999975476	12369	$z=a+b/x^{(0.5)}+cy/\ln y+d\ln y/y^2$
6	0.9999951205	12018	$z=a+b/\ln x+cy/\ln y+d\ln y/y^2$
7	0.9999939627	13294	$z=a+b/x^{(1.5)}+c/\ln y+d\ln y/y^2$
8	0.999993489	12393	$z=a+b/x^{(0.5)}+c/\ln y+d\ln y/y^2$
9	0.9999902478	13270	$z=a+b/x^{(1.5)}+cy/\ln y+d\ln y/y^2$
10	0.9999895247	12042	$z=a+b/\ln x+c/\ln y+d\ln y/y^2$
11	0.999858993	3232	$z=a+bx^3+ce^{(x/wx)}$
12	0.9998561863	3197	$z=a+bx^{(2.5)}+ce^{(x/wx)}$
13	0.9998541227	3161	$z=a+bx^2\ln x+ce^{(x/wx)}$
14	0.9998531336	3124	$z=a+bx^2+ce^{(x/wx)}$
15	0.9998498763	3086	$z=a+bx^{(1.5)}+ce^{(x/wx)}$
16	0.9998474742	3047	$z=a+bx\ln x+ce^{(x/wx)}$
17	0.9998464697	3007	$z=a+bx+ce^{(x/wx)}$
18	0.999845531	3269	$z=a+be^{(x/wx)}+cx/\ln x$
19	0.9998438716	3267	$z=a+be^{(x/wx)}+cx^{(0.5)}\ln x$
20	0.9998429868	3270	$z=a+be^{(x/wx)}+cx^{(0.5)}$
21	0.9998132284	176	$z=a+b/x+c/x^2+d/y$
22	0.9998078439	171	$z=a+b/x+c/x^2+d\ln y$
23	0.9998054583	166	$z=a+b/x+c/x^2+dy$

Table D.2 (Continued)

Rank	R²	Equation number	Equation
24	0.9998014461	151232470	$\ln z = a + bx^3 + ce^{(x/wx)}$
25	0.9998008628	151232482	$\ln z = a + bx^3 + c/x^2$
26	0.9998002066	151232481	$\ln z = a + bx^3 + c \ln x / x^2$
27	0.9997997298	2151	$z = a + by + \text{EXPX}(c, d)$
28	0.9997986581	151232480	$\ln z = a + bx^3 + c/x^{(1.5)}$
29	0.9997969257	2146	$z = a + \text{EXPX}(b, c) * \text{EXPY}(1, d)$
30	0.9997965447	151232435	$\ln z = a + bx^{(2.5)} + ce^{(x/wx)}$
31	0.999794444	151232479	$\ln z = a + bx^3 + c/x$
32	0.9997917662	151232478	$\ln z = a + bx^3 + c \ln x / x$
33	0.9997900558	151232447	$\ln z = a + bx^{(2.5)} + c/x^2$
34	0.9997892181	2148	$z = a + \text{EXPX}(b, c) * \text{EXPY}(1, c)$
35	0.9997887101	151232446	$\ln z = a + bx^{(2.5)} + c \ln x / x^2$
36	0.9997879655	151232477	$\ln z = a + bx^3 + c/x^{(0.5)}$
37	0.9997170735	2099	$z = \text{LNCUMX}(a, b, c) * \text{LNCUMY}(1, d, c)$
38	0.9997145542	2149	$z = \text{EXPX}(a, b) + \text{EXPY}(c, d)$
39	0.9996579562	101	$z = a + b \ln x + c(\ln x)^2 + d/y$
40	0.9995999262	96	$z = a + b \ln x + c(\ln x)^2 + d \ln y$
41	0.9995430155	91	$z = a + b \ln x + c(\ln x)^2 + dy$
42	0.9995142706	2145	$z = \text{EXPX}(a, b) * \text{EXPY}(1, c)$
43	0.9995095505	2147	$z = \text{EXPX}(a, b) * \text{EXPY}(1, b)$
44	0.9993362229	2161	$z = \text{POWX}(a, b) + \text{POWY}(c, d)$
45	0.9992776782	2111	$z = \text{SIGX}(a, b, c) * \text{SIGY}(1, d, c)$
46	0.9992355594	302461672	$z^{(-1)} = a + bx^{(2.5)} + cx^3$
47	0.9992091894	2163	$z = a + by + \text{POWX}(c, d)$

Table D.2 (Continued)

Rank	R²	Equation number	Equation
48	0.999204326	302461636	$z^{(-1)}=a+bx^2\ln x+cx^3$
49	0.9991839124	302461599	$z^{(-1)}=a+bx^2+cx^3$
50	0.9991617119	26	$z=a+bx+cx^2+d/y$
51	0.9991410281	302461635	$z^{(-1)}=a+bx^2\ln x+cx^{(2.5)}$
52	0.9991321397	302461561	$z^{(-1)}=a+bx^{(1.5)}+cx^3$
53	0.9991097709	302461598	$z^{(-1)}=a+bx^2+cx^{(2.5)}$
54	0.9990975201	302461522	$z^{(-1)}=a+bx\ln x+cx^3$
55	0.9990805278	302461482	$z^{(-1)}=a+bx+cx^3$
56	0.9990754547	2015	$z=LORX(a,b,c)*LORY(1,d,c)$
57	0.9990653063	302461711	$z^{(-1)}=a+bx^3+cx/\ln x$
58	0.9990458112	302461560	$z^{(-1)}=a+bx^{(1.5)}+cx^{(2.5)}$
59	0.9989299683	21	$z=a+bx+cx^2+d\ln y$
60	0.9986849261	16	$z=a+bx+cx^2+dy$
61	0.9979415329	2027	$z=LOGNORMX(a,b,c)*LOGNORMY(1,d,c)$
62	0.9975771331	2087	$z=LORCUMX(a,b,c)*LORCUMY(1,d,c)$
63	0.9970296298	2075	$z=GCUMX(a,b,c)*GCUMY(1,d,c)$
64	0.9955926978	2123	$z=EXVCUMX(a,b,c)*EXVCUMY(1,d,c)$
65	0.9813192827	152	$z=a+b/x+cy+dy^2$
66	0.9803497618	151	$z=a+b/x+cy$
67	0.9800924638	156	$z=a+b/x+c\ln y$
68	0.9799024489	161	$z=a+b/x+c/y$
69	0.9582010776	76	$z=a+b\ln x+cy$
70	0.9576174961	2158	$z=a+POWX(b,c)*POWY(1,d)$
71	0.9576174959	81	$z=a+b\ln x+c\ln y$

Table D.2 (Continued)

Rank	R²	Equation number	Equation
72	0.957160436	86	$z=a+b\ln x+c/y$
73	0.9280761608	2169	$z=a+bx+cy$ [Robust None, Least Squares]
74	0.9280761608	1	$z=a+bx+cy$
75	0.9280761315	2152	$z=a+bx+EXPY(c,d)$
76	0.9269387105	6	$z=a+bx+clny$
77	0.9269072093	2164	$z=a+bx+POWY(c,d)$
78	0.9259886306	11	$z=a+bx+c/y$
79	0.9198753055	2170	$z=a+bx+cy$ [Robust Low, Least Abs Deviation]
80	0.8873529592	2171	$z=a+bx+cy$ [Robust Medium, Lorentzian]
81	0.8846783152	2172	$z=a+bx+cy$ [Robust High, Pearson VII Limit]
82	0.5848981867	2039	$z=LOGISTICX(a,b,c)*LOGISTICY(1,d,c)$
83	0.5591057859	2051	$z=EXTRVALX(a,b,c)*EXTRVALY(1,d,c)$
84	0.4978922658	2003	$z=GAUSSX(a,b,c)*GAUSSY(1,d,c)$
85	0.3533105825	2160	$z=a+POWX(b,c)*POWY(1,c)$
86	0.1690800763	2159	$z=POWX(a,b)*POWY(1,b)$

Table D.3 Table Curve 3D equation list for *S. aureus* 485 pressurized in peptone water

Rank	R ²	Equation number	Equation
1	1	302463575	$z^{(-1)}=a+bx\ln x+c/x^{(0.5)}+d(\ln y)^2$
2	1	151243363	$\ln z=a+by+cy^{(0.5)}\ln y+dy/\ln y$
3	1	151243366	$\ln z=a+by+cy^{(0.5)}\ln y+d/\ln y$
4	0.999999995	151241275	$\ln z=a+b/\ln x+c\ln y+de^{(-y)}$
5	0.999999994	302465153	$z^{(-1)}=a+bx^2+ce^{(-x)}+dy^{(1.5)}$
6	0.999999988	302465760	$z^{(-1)}=a+bx^2\ln x+c/x^{(1.5)}+d(\ln y)^2$
7	0.999999987	151243848	$\ln z=a+by^2+cy/\ln y+d/y^{(0.5)}$
8	0.999999981	302472730	$z^{(-1)}=a+b\ln y+cy^{(2.5)}+de^{(y/wy)}$
9	0.999999998	151243872	$\ln z=a+by^2+c/\ln y+d/y^{(0.5)}$
10	0.999999977	151233867	$\ln z=a+bx+cy/\ln y+d/\ln y$
11	0.999999944	302465094	$z^{(-1)}=a+bx^2+c/x^{(1.5)}+d(\ln y)^2$
12	0.999999942	302464342	$z^{(-1)}=a+bx^{(1.5)}+c\ln x/x+d(\ln y)^2$
13	0.999999941	4145	$z=a+bx+cx^{(0.5)}\ln x+d\ln y$
14	0.999999931	302463751	$z^{(-1)}=a+bx\ln x+c\ln y+dy^{(2.5)}$
15	0.999999928	302464367	$z^{(-1)}=a+bx^{(1.5)}+c/x+d(\ln y)^2$
16	0.999999928	302463819	$z^{(-1)}=a+bx\ln x+cy^{(2.5)}+de^{(y/wy)}$
17	0.999999917	302462795	$z^{(-1)}=a+bx+c/x^{(0.5)}+d(\ln y)^2$
18	0.999999893	9546	$z=a+bx^{(0.5)}\ln x+c\ln x/x+dy^3$
19	0.999999803	151243559	$\ln z=a+b\ln y+cy/\ln y+d/y^{(0.5)}$
20	0.999999803	12767	$z=a+b/x+c\ln x/x^2+de^{(-x)}$
21	0.999999802	151240032	$\ln z=a+bx/\ln x+cy/\ln y+d/\ln y$
22	0.99999978	151243583	$\ln z=a+b\ln y+c/\ln y+d/y^{(0.5)}$
23	0.999999762	11421	$z=a+b\ln x+c\ln x/x^2+de^{(y/wy)}$

Table D.3 (Continued)

Rank	R²	Equation number	Equation
24	0.9999999673	151244097	$\ln z = a + by^{(2.5)} + c/\ln y + d/y^{(0.5)}$
25	0.9999999584	9432	$z = a + bx^{(0.5)} \ln x + cx^{(0.5)} + dy^{(1.5)}$
26	0.9999999511	4367	$z = a + bx + c/x + dy^3$
27	0.9999999183	11776	$z = a + b/\ln x + c/x^{(1.5)} + de^{(y/wy)}$
28	0.9999997446	9420	$z = a + bx^{(0.5)} \ln x + cx/\ln x + de^{(-y)}$
29	0.9999997331	4337	$z = a + bx + c \ln x/x + dy \ln y$
30	0.9999997175	12467	$z = a + b \ln x/x + c \ln x/x^2 + de^{(-x)}$
31	0.9999980216	151233047	$\ln z = a + by/\ln y + c/\ln y$
32	0.9999975482	302462243	$z^{(-1)} = a + by^3 + c/y^{(1.5)}$
33	0.9999975179	302462254	$z^{(-1)} = a + be^{(y/wy)} + c \ln y/y$
34	0.9999974129	302462214	$z^{(-1)} = a + by^2 \ln y + c/y^{(1.5)}$
35	0.9999969548	302462122	$z^{(-1)} = a + be^{(-x)} + c \ln y/y$
36	0.9999961257	302462180	$z^{(-1)} = a + by^{(1.5)} + c/y$
37	0.9999954193	302462295	$z^{(-1)} = a + by^{(0.5)} + c/y^{(0.5)}$
38	0.9999953712	302462162	$z^{(-1)} = a + by \ln y + c/y$
39	0.9999953478	302462256	$z^{(-1)} = a + be^{(y/wy)} + c/y^{(1.5)}$
40	0.9999952562	151233056	$\ln z = a + by^{(0.5)} + c/\ln y$
41	0.9999951907	151233045	$\ln z = a + by/\ln y + cy^{(0.5)}$
42	0.9999950181	302462276	$z^{(-1)} = a + b(\ln y)^2 + c/y^{(0.5)}$
43	0.9999945102	302462197	$z^{(-1)} = a + by^2 + c/y$
44	0.9999808629	151232875	$\ln z = a + be^{(-x)} + cy^3$
45	0.9999777331	3641	$z = a + be^{(-x)} + cy/\ln y$
46	0.9999387058	151232902	$\ln z = a + by + c/\ln y$
47	0.9999375172	151232899	$\ln z = a + by + cy/\ln y$

Table D.3 (Continued)

Rank	R²	Equation number	Equation
48	0.9999095125	3644	$z=a+be^{(-x)}+c/\ln y$
49	0.9999037964	151233026	$\ln z=a+by^{(0.5)}\ln y+c/\ln y$
50	0.99990176	151233023	$\ln z=a+by^{(0.5)}\ln y+cy/\ln y$
51	0.999873303	2135	$z=LDRX(a,b,c)*LDRY(1,d,c)$
52	0.9998732761	2027	$z=LOGNORMX(a,b,c)*LOGNORMY(1,d,c)$
53	0.9998552392	2123	$z=EXVCUMX(a,b,c)*EXVCUMY(1,d,c)$
54	0.9998326013	151232876	$\ln z=a+be^{(-x)}+ce^{(y/wy)}$
55	0.9996539836	2111	$z=SIGX(a,b,c)*SIGY(1,d,c)$
56	0.9995388533	26	$z=a+bx+cx^2+d/y$
57	0.9995016381	3334	$z=a+b(\ln x)^2+cx/\ln x$
58	0.9994982172	3009	$z=a+bx+c(\ln x)^2$
59	0.9994978647	3303	$z=a+bx^{(0.5)}\ln x+cx^{(0.5)}$
60	0.9994931017	3052	$z=a+bx\ln x+c\ln x$
61	0.9994819065	3049	$z=a+bx\ln x+c(\ln x)^2$
62	0.9994813722	3012	$z=a+bx+c\ln x$
63	0.9994653488	3301	$z=a+bx^{(0.5)}\ln x+c(\ln x)^2$
64	0.9994583066	3367	$z=a+bx/\ln x+c\ln x$
65	0.9992714789	151232513	$\ln z=a+be^{(x/wx)}+c/x$
66	0.999209666	91	$z=a+b\ln x+c(\ln x)^2+dy$
67	0.9991965287	2075	$z=GCUMX(a,b,c)*GCUMY(1,d,c)$
68	0.9991932921	21	$z=a+bx+cx^2+d\ln y$
69	0.9989854937	96	$z=a+b\ln x+c(\ln x)^2+d\ln y$
70	0.998943818	101	$z=a+b\ln x+c(\ln x)^2+d/y$
71	0.9980293549	16	$z=a+bx+cx^2+dy$

Table D.3 (Continued)

Rank	R²	Equation number	Equation
72	0.9967949452	2087	$z=\text{LORCUMX}(a,b,c)*\text{LORCUMY}(1,d,c)$
73	0.9949019467	176	$z=a+b/x+c/x^2+d/y$
74	0.9946781822	171	$z=a+b/x+c/x^2+d\ln y$
75	0.9946123941	166	$z=a+b/x+c/x^2+dy$
76	0.9945448583	2151	$z=a+by+\text{EXPX}(c,d)$
77	0.9945261593	2148	$z=a+\text{EXPX}(b,c)*\text{EXPY}(1,c)$
78	0.9912679443	2163	$z=a+by+\text{POWX}(c,d)$
79	0.9901028172	2147	$z=\text{EXPX}(a,b)*\text{EXPY}(1,b)$
80	0.9810182383	162	$z=a+b/x+c/y+d/y^2$
81	0.9751550417	2161	$z=\text{POWX}(a,b)+\text{POWY}(c,d)$
82	0.9666760954	2164	$z=a+bx+\text{POWY}(c,d)$
83	0.9584598456	2039	$z=\text{LOGISTICX}(a,b,c)*\text{LOGISTICY}(1,d,c)$
84	0.9409682039	161	$z=a+b/x+c/y$
85	0.9404442165	151	$z=a+b/x+cy$
86	0.9399171597	156	$z=a+b/x+c\ln y$
87	0.9348368157	2099	$z=\text{LNCUMX}(a,b,c)*\text{LNCUMY}(1,d,c)$
88	0.9170362279	2051	$z=\text{EXTRVALX}(a,b,c)*\text{EXTRVALY}(1,d,c)$
89	0.9113476988	76	$z=a+b\ln x+cy$
90	0.89875028	1	$z=a+bx+cy$
91	0.89875028	2169	$z=a+bx+cy$ [Robust None, Least Squares]
92	0.8981472326	2146	$z=a+\text{EXPX}(b,c)*\text{EXPY}(1,d)$
93	0.8956320246	2170	$z=a+bx+cy$ [Robust Low, Least Abs Deviation]
94	0.8823677282	86	$z=a+b\ln x+c/y$

Table D.3 (Continued)

Rank	R²	Equation number	Equation
95	0.8810794331	81	$z=a+b\ln x+c\ln y$
96	0.8805139147	2171	$z=a+bx+cy$ [Robust Medium, Lorentzian]
97	0.872617373	2015	$z=LORX(a,b,c)*LORY(1,d,c)$
98	0.8661824525	2172	$z=a+bx+cy$ [Robust High, PearsonVII Limit]
99	0.8188555503	6	$z=a+bx+c\ln y$
100	0.8079279139	11	$z=a+bx+c/y$
101	0.7748433646	2003	$z=GAUSSX(a,b,c)*GAUSSY(1,d,c)$
102	0.222766084	2145	$z=EXPX(a,b)*EXPY(1,c)$

Table D.4 Table Curve 3D equation list for *S. aureus* 485 pressurized in carrot juice

Rank	R ²	Equation number	Equation
1	1	151239201	$\ln z = a + b(\ln x)^2 + c \ln x + d y^{(0.5)} \ln y$
2	0.9999999995	302469445	$z^{(-1)} = a + b x^{(0.5)} + c/x + d y^{(0.5)} \ln y$
3	0.9999999992	302462837	$z^{(-1)} = a + b x + c/x + d y$
4	0.9999999942	302469386	$z^{(-1)} = a + b x^{(0.5)} + c/x^{(0.5)} + d y$
5	0.9999999863	302468520	$z^{(-1)} = a + b(\ln x)^2 + c \ln x/x + d y^{(0.5)} \ln y$
6	0.9999999824	151232334	$\ln z = a + b x^{(1.5)} + c/x^{(1.5)}$
7	0.9999999814	151232607	$\ln z = a + b x/\ln x + c/x^{(0.5)}$
8	0.9999999811	151240521	$\ln z = a + b \ln x + c/\ln x + d \ln x/x$
9	0.9999999809	151239186	$\ln z = a + b(\ln x)^2 + c \ln x + d/x^{(0.5)}$
10	0.9999999808	151239185	$\ln z = a + b(\ln x)^2 + c \ln x + d/\ln x$
11	0.9999999805	151240548	$\ln z = a + b \ln x + c/x^{(0.5)} + d \ln x/x$
12	0.9999999802	151240522	$\ln z = a + b \ln x + c/\ln x + d/x$
13	0.9999999797	151240523	$\ln z = a + b \ln x + c/\ln x + d/x^{(1.5)}$
14	0.9999999796	151233108	$\ln z = a + b x + c x \ln x + d x/\ln x$
15	0.9999999787	151233360	$\ln z = a + b x + c x^{(0.5)} \ln x + d x/\ln x$
16	0.9999999756	151241655	$\ln z = a + b \ln x/x + c/x + d/x^{(1.5)}$
17	0.9999999744	151232253	$\ln z = a + b x + c \ln x/x$
18	0.999999972	151232635	$\ln z = a + b x^{(0.5)} + c \ln x$
19	0.9999999661	302467990	$z^{(-1)} = a + b x^{(0.5)} \ln x + c/x^{(0.5)} + d y$
20	0.9999999634	151232294	$\ln z = a + b x \ln x + c/x$
21	0.9999999614	151232606	$\ln z = a + b x/\ln x + c/\ln x$
22	0.9999999561	151232293	$\ln z = a + b x \ln x + c \ln x/x$
23	0.9999999234	151232252	$\ln z = a + b x + c/x^{(0.5)}$

Table D.4 (Continued)

Rank	R²	Equation number	Equation
24	0.9999999125	151232542	$\ln z = a + bx^{(0.5)} \ln x + c \ln x$
25	0.9999999019	10283	$z = a + b(\ln x)^2 + cy^3 + d/\ln y$
26	0.9999998761	11183	$z = a + bx^{(0.5)} + cy^3 + d/\ln y$
27	0.9999997379	302470555	$z^{(-1)} = a + b/x^{(0.5)} + c \ln x/x + dy^{(0.5)} \ln y$
28	0.9999996891	302462200	$z^{(-1)} = a + by^2 + c/y^2$
29	0.9999996576	302462165	$z^{(-1)} = a + b \ln y + c/y^2$
30	0.9999996095	302462281	$z^{(-1)} = a + b(\ln y)^2 + c/y^2$
31	0.9999996086	9787	$z = a + bx^{(0.5)} \ln x + cy^3 + d/\ln y$
32	0.9999996026	302462231	$z^{(-1)} = a + by^{(2.5)} + c/y^2$
33	0.9999995812	302462183	$z^{(-1)} = a + by^{(1.5)} + c/y^2$
34	0.9999995665	14089	$z = a + by + cy^{(2.5)} + d/\ln y$
35	0.9999995607	11589	$z = a + b \ln x + cy^3 + d/\ln y$
36	0.9999995366	12329	$z = a + b/x^{(0.5)} + ce^{(y/wy)} + dy^{(0.5)}$
37	0.9999995335	14398	$z = a + by^{(1.5)} + cy^2 \ln y + d/\ln y$
38	0.9999993934	14669	$z = a + by^2 \ln y + cy^{(2.5)} + d/\ln y$
39	0.9999993767	302462306	$z^{(-1)} = a + b \ln y + c/y^{(1.5)}$
40	0.9999993203	14413	$z = a + by^{(1.5)} + cy^{(2.5)} + d/\ln y$
41	0.9999992275	302462304	$z^{(-1)} = a + b \ln y + c \ln y/y$
42	0.9999989742	302462296	$z^{(-1)} = a + by^{(0.5)} + c \ln y/y$
43	0.9999989508	302462324	$z^{(-1)} = a + b \ln y/y + c/y^{(1.5)}$
44	0.9999987747	10748	$z = a + bx/\ln x + cy^3 + d/\ln y$
45	0.9999986171	302462318	$z^{(-1)} = a + b/y^{(0.5)} + c/y$
46	0.9999976349	171	$z = a + b/x + c/x^2 + d \ln y$
47	0.9999967199	302462344	$z^{(-1)} = a + bx + cx \ln x + dx^{(0.5)} \ln x$

Table D.4 (Continued)

Rank	R²	Equation number	Equation
48	0.9999958517	302469786	$z^{(-1)}=a+b\ln x+c/x^{(0.5)}+d\ln x/x$
49	0.999995761	302470164	$z^{(-1)}=a+b/\ln x+c/x^{(0.5)}+d\ln x/x$
50	0.999995435	302470542	$z^{(-1)}=a+b/x^{(0.5)}+c\ln x/x+d/x$
51	0.9999944403	2149	$z=\text{EXPX}(a,b)+\text{EXPY}(c,d)$
52	0.9999882773	2135	$z=\text{LDRX}(a,b,c)*\text{LDRY}(1,d,c)$
53	0.9999871124	151233009	$\ln z=a+be^{(y/wy)}+cy^{(0.5)}\ln y$
54	0.9999799617	2111	$z=\text{SIGX}(a,b,c)*\text{SIGY}(1,d,c)$
55	0.9999644999	2075	$z=\text{GCUMX}(a,b,c)*\text{GCUMY}(1,d,c)$
56	0.9999630455	2027	$z=\text{LOGNORMX}(a,b,c)*\text{LOGNORMY}(1,d,c)$
57	0.9999577643	2039	$z=\text{LOGISTICX}(a,b,c)*\text{LOGISTICY}(1,d,c)$
58	0.9999532488	3760	$z=a+by^3+cy/\ln y$
59	0.999950908	3763	$z=a+by^3+c/\ln y$
60	0.9999259194	2161	$z=\text{POWX}(a,b)+\text{POWY}(c,d)$
61	0.9998205564	3746	$z=a+by^{(2.5)}+cy/\ln y$
62	0.9998082	3749	$z=a+by^{(2.5)}+c/\ln y$
63	0.9994042209	3739	$z=a+by^2\ln y+c\ln y/y^2$
64	0.9993519755	3740	$z=a+by^2\ln y+c/y^2$
65	0.9992479724	3738	$z=a+by^2\ln y+c/y^{(1.5)}$
66	0.9992351454	3736	$z=a+by^2\ln y+c\ln y/y$
67	0.9990262825	3737	$z=a+by^2\ln y+c/y$
68	0.9989897784	3730	$z=a+by^2\ln y+c(\ln y)^2$
69	0.9982701175	2087	$z=\text{LORCUMX}(a,b,c)*\text{LORCUMY}(1,d,c)$
70	0.9972002219	2123	$z=\text{EXVCUMX}(a,b,c)*\text{EXVCUMY}(1,d,c)$
71	0.9898567036	2	$z=a+bx+cy+dy^2$

Table D.4 (Continued)

Rank	R²	Equation number	Equation
72	0.9881821473	77	$z=a+b\ln x+cy+dy^2$
73	0.9872825933	152	$z=a+b/x+cy+dy^2$
74	0.9689586076	96	$z=a+b\ln x+c(\ln x)^2+d\ln y$
75	0.9518459291	176	$z=a+b/x+c/x^2+d/y$
76	0.9407925907	101	$z=a+b\ln x+c(\ln x)^2+d/y$
77	0.9328257221	26	$z=a+bx+cx^2+d/y$
78	0.9263516597	7	$z=a+bx+c\ln y+d(\ln y)^2$
79	0.9219982887	16	$z=a+bx+cx^2+dy$
80	0.910790682	2164	$z=a+bx+POWY(c,d)$
81	0.9103430595	11	$z=a+bx+c/y$
82	0.8909855948	86	$z=a+b\ln x+c/y$
83	0.8848455147	2151	$z=a+by+EXPX(c,d)$
84	0.8807974252	6	$z=a+bx+c\ln y$
85	0.8761270918	151	$z=a+b/x+cy$
86	0.8757829065	2163	$z=a+by+POWX(c,d)$
87	0.8722259141	81	$z=a+b\ln x+c\ln y$
88	0.8666201205	2148	$z=a+EXPX(b,c)*EXPY(1,c)$
89	0.865727858	161	$z=a+b/x+c/y$
90	0.8640345684	76	$z=a+b\ln x+cy$
91	0.8591687885	156	$z=a+b/x+c\ln y$
92	0.838765792	1	$z=a+bx+cy$
93	0.838765792	2169	$z=a+bx+cy$ [Robust None, Least Squares]
94	0.8348458351	2170	$z=a+bx+cy$ [Robust Low, Least Abs Deviation]
95	0.8124809272	2147	$z=EXPX(a,b)*EXPY(1,b)$

Table D.4 (Continued)

Rank	R²	Equation number	Equation
96	0.7873833042	2171	$z=a+bx+cy$ [Robust Medium, Lorentzian]
97	0.7857901012	2172	$z=a+bx+cy$ [Robust High, PearsonVII Limit]
98	0.4779221756	2051	$z=\text{EXTRVALX}(a,b,c)*\text{EXTRVALY}(1,d,c)$
99	0.3833097412	2015	$z=\text{LORX}(a,b,c)*\text{LORY}(1,d,c)$
100	0.2211151685	2003	$z=\text{GAUSSX}(a,b,c)*\text{GAUSSY}(1,d,c)$

APPENDIX E

VIEW AREA AND VOLUME CALCULATIONS

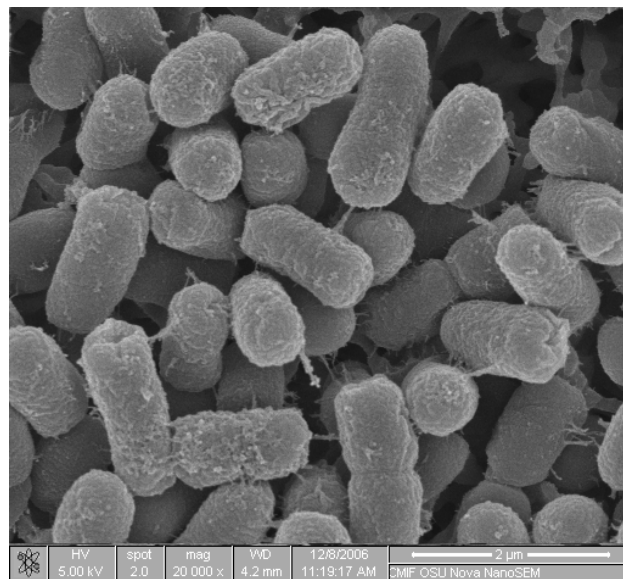


Figure E.1 SEM micrograph of unpressurized *E. coli* O157:H7 933

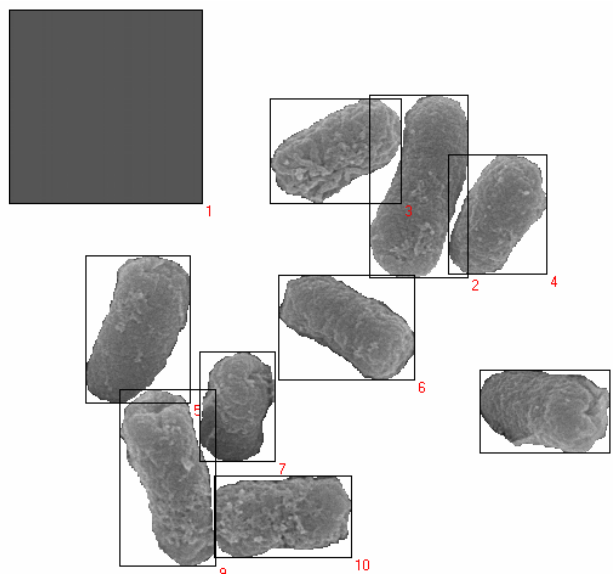


Figure E.2 Isolated organisms of unpressurized *E. coli* O157:H7 933 as area objects, with size reference square

Table E.1 View area results *E. coli* O157:H7 933 cells calculated by LenseEye Software from Fig. E.2

Object #	View Area (pixels)	View Area (user units)
1	25600	4
2	8101	1.265781
3	5852	0.914375
4	5265	0.822656
5	7026	1.097813
6	5889	0.920156
7	4303	0.672344
8	5846	0.913438
9	7466	1.166563
10	6321	0.987656

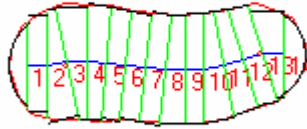


Figure E.3 Rotated (rotation angle= 0°) volume image of object 2 from Fig. E.2



Figure E.4 Rotated (rotation angle= -16°) volume image of object 3 from Fig. E.2

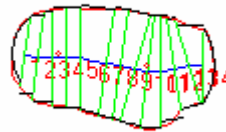


Figure E.5 Rotated (rotation angle= -14°) volume image of object 4 from Fig. E.2

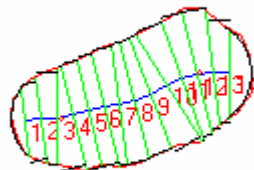


Figure E.6 Rotated (rotation angle= 10°) volume image of object 5 from Fig. E.2

Table E.2 Volume results of *E. coli* O157:H7 933 cells calculated by LenseEye Software from Fig. E.2

Object #	Rotation Angle	Scale factor	Cuts	Scaled Volume
2	0	80	15	0.6301
3	-16	80	15	0.4479
4	-14	80	15	0.3951
5	10	80	15	0.5812
6	-3	80	15	0.4202
7	3	80	15	0.3118
8	-24	80	15	0.4768
9	5	80	15	0.5649
10	0	80	15	0.5185

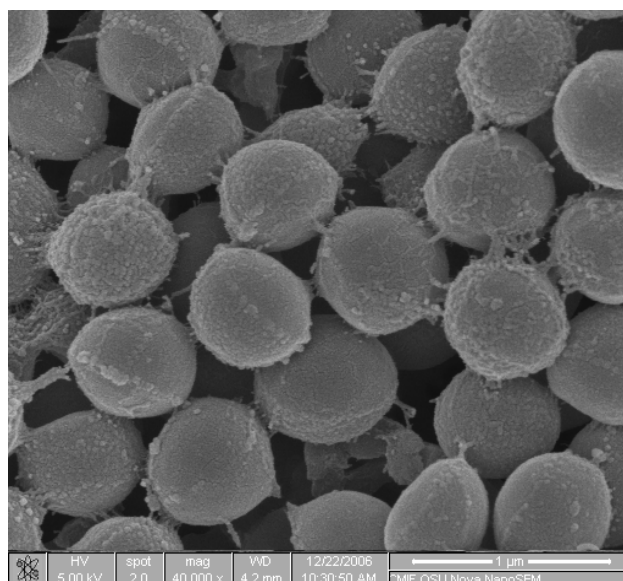


Figure E.7 SEM micrograph of pressurized (300 MPa- 5 min- 40°C) *S. aureus*
485

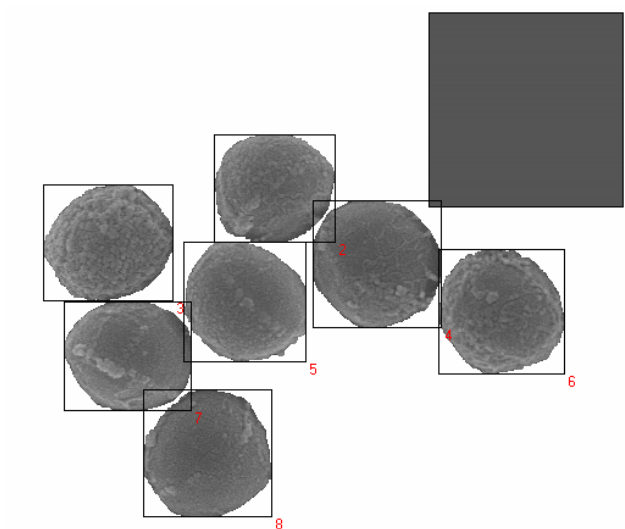


Figure E.8 Isolated organisms of pressurized (300 MPa- 5 min- 40°C) *S. aureus* 485 as area objects, with size reference square

Table E.3 View area results of *S. aureus* 485 cells calculated by LenseEye Software from Fig. E.8

Object #	View Area (pixels)	View Area (user units)
1	25600	1
2	7050	0.275391
3	7670	0.299609
4	8813	0.344258
5	7766	0.303359
6	8163	0.318867
7	7566	0.295547
8	8584	0.335313

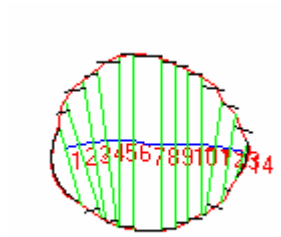


Figure E.9 Rotated (rotation angle=5°) volume image of object 2 from Fig. E.8

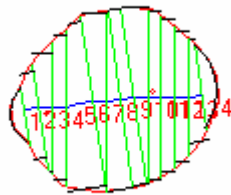


Figure E.10 Rotated (rotation angle=1°) volume image of object 3 from Fig. E.8

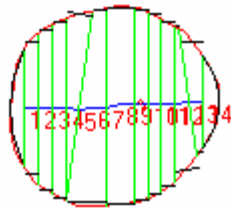


Figure E.11 Rotated (rotation angle=17°) volume image of object 4 from Fig. E.8

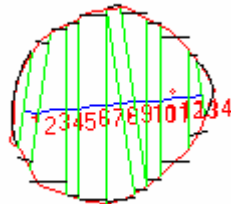


Figure E.12 Rotated (rotation angle=14°) volume image of object 5 from Fig. E.8

Table E.4 Volume results of *S. aureus* 485 cells calculated by LenseEye Software from Fig. E.8

Object #	Rotation Angle	Scale factor	Cuts	Scaled Volume
2	5	160	15	0.0964
3	1	160	15	0.1087
4	17	160	15	0.1404
5	14	160	15	0.1147
6	-16	160	15	0.1215
7	-21	160	15	0.1065
8	-20	160	15	0.1346

Table F.2 Tukey's pairwise comparisons for view area values of *E. coli* O157:H7 933

Family error rate = 0.0500
 Individual error rate = 0.00447
 Critical value = 4.07
 Intervals for (column level mean) - (row level mean)

	0 MPa	200 MPa	250 MPa	275 MPa	300 MPa
200 MPa	-0.4524 -0.1647				
250 MPa	-0.2499 0.0217	0.0644 0.3244			
275 MPa	-0.1136 0.1642	0.2006 0.4671	0.0150 0.2639		
300 MPa	-0.1079 0.1755	0.2061 0.4785	0.0203 0.2755	-0.1225 0.1394	
325 MPa	-0.2968 -0.0207	0.0174 0.2822	-0.1682 0.0789	-0.3110 -0.0571	-0.3226 -0.0625

Table F.3 One-way ANOVA results for transformed volume (log volume) values of *E. coli* O157:H7 933

Analysis of Variance for log volume

Source	DF	SS	MS	F	P
Power level	5	0.35361	0.07072	18.43	0.000
Error	185	0.70989	0.00384		
Total	190	1.06350			

Individual 95% CIs for Mean
 Based on Pooled StDev

Level	N	Mean	StDev	CI
0 MPa	25	0.77002	0.06301	(----*----)
200 MPa	29	0.86750	0.05106	(----*----)
250 MPa	39	0.80765	0.07541	(----*----)
275 MPa	33	0.73916	0.06231	(----*----)
300 MPa	31	0.74981	0.04412	(----*----)
325 MPa	34	0.81584	0.06581	(----*----)

Pooled StDev = 0.06195

0.750 0.800 0.850

Table F.4 Tukey's pairwise comparisons for transformed volume (log volume) values of *E. coli* O157:H7 933

Family error rate = 0.0500
 Individual error rate = 0.00447
 Critical value = 4.07
 Intervals for (column level mean) - (row level mean)

	0 MPa	200 MPa	250 MPa	275 MPa	300 MPa
200 MPa	-0.14614 -0.04884				
250 MPa	-0.08331 0.00804	0.01614 0.10357			
275 MPa	-0.01641 0.07812	0.08297 0.17372	0.02632 0.11066		
300 MPa	-0.02772 0.06813	0.07164 0.16375	0.01494 0.10074	-0.05524 0.03394	
325 MPa	-0.09280 0.00114	0.00660 0.09672	-0.05002 0.03364	-0.12025 -0.03312	-0.11030 -0.02176

Table F.5 One-way ANOVA results for area values of *S. aureus* 485

Analysis of Variance for area

Source	DF	SS	MS	F	P
Power level	5	0.02608	0.00522	3.22	0.007
Error	322	0.52131	0.00162		
Total	327	0.54739			

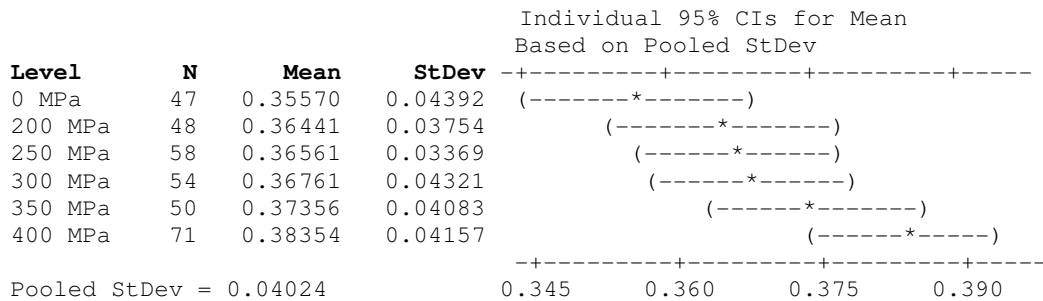


Table F.6 Tukey's pairwise comparisons for area values of *S. aureus* 485

Family error rate = 0.0500
 Individual error rate = 0.00466
 Critical value = 4.03
 Intervals for (column level mean) - (row level mean)

	0 MPa	200 MPa	250 MPa	300 MPa	350 MPa
200 MPa	-0.03223 0.01482				
250 MPa	-0.03241 0.01260	-0.02358 0.02117			
300 MPa	-0.03478 0.01097	-0.02595 0.01955	-0.02368 0.01969		
350 MPa	-0.04115 0.00544	-0.03232 0.01402	-0.03008 0.01418	-0.02846 0.01655	
400 MPa	-0.04940 -0.00628	-0.04056 0.00229	-0.03822 0.00236	-0.03664 0.00477	-0.03115 0.01119

Table F.7 One-way ANOVA results for transformed volume (log volume) values of *S. aureus* 485

Analysis of Variance for log volume

Source	DF	SS	MS	F	P
Power level	5	0.004042	0.000808	3.47	0.005
Error	319	0.074267	0.000233		
Total	324	0.078310			

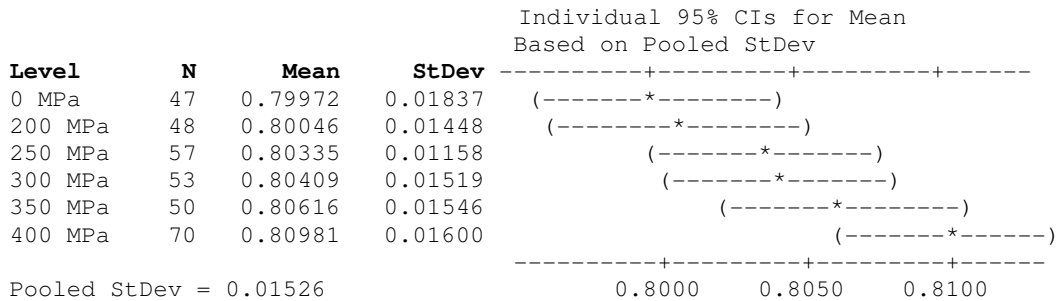


Table F.8 Tukey's pairwise comparisons for transformed volume (log volume) values of *S. aureus* 485

Family error rate = 0.0500
 Individual error rate = 0.00466
 Critical value = 4.03
 Intervals for (column level mean) - (row level mean)

	0 MPa	200 MPa	250 MPa	300 MPa	350 MPa
200 MPa	-0.00965 0.00819				
250 MPa	-0.01219 0.00494	-0.01141 0.00563			
300 MPa	-0.01308 0.00435	-0.01230 0.00503	-0.00904 0.00756		
350 MPa	-0.01527 0.00240	-0.01449 0.00308	-0.01124 0.00561	-0.01064 0.00650	
400 MPa	-0.01828 -0.00188	-0.01750 -0.00120	-0.01421 0.00130	-0.01363 0.00220	-0.01170 0.00441

CURRICULUM VITAE

Name Surname : Mutlu Pilavtepe
Date of Birth : November 20, 1978
Nationality : Turkish
e-mail : mpilavtepe@gmail.com

Education

Doctor of Philosophy (Integrated Ph. D. Program, applying with a Bachelor's degree), Food Engineering Department, Middle East Technical University (METU), Ankara, 2002- 2007

Bachelor of Science, Food Engineering Department, Hacettepe University, Beytepe, Ankara, 1996-2000

Research Experience

- M.S. Student, Food Engineering Department, Microbiology Lab, Hacettepe University, Ankara, Beytepe, 2000-2001.
- Research Assistant, Food Engineering Department, METU, Ankara, 2002- 2007.
- Research Scholar, Food Science and Human Nutrition Department, University of Florida, Gainesville, Florida, February- August 2006, January- February 2007 (Supervised by Prof. Dr. M. O. Balaban).

- Research Scholar, Food Science and Technology Department, Ohio State University, Columbus, Ohio, August 2006- January 2007 (Supervised by Prof. Dr. Ahmed Yousef).

Project Work

Effect of ultra high pressure (uhp), bacteriocins and low temperature on preservation of low acid foods, M.E.T.U Research Fund Project, BAP-08-11-DPT.2002K120510-GT-4, Researcher, 2003-2007.

Publications

- 1) **Pilavtepe, M.**, Alpas, H., and Bozoğlu, F. Inactivation of *Escherichia coli* O157:H7 and *Staphylococcus aureus* by High Hydrostatic Pressure (HHP) in Carrot Juice (Submitted to Journal of Food Safety).
- 2) **Pilavtepe, M.**, Balaban, M. O., Alpas, H., and Yousef, A. E. Machine Vision Based Quantification of Bacterial Volume Change with High Hydrostatic Pressure (Submitted to Journal of Food Science)
- 3) **Pilavtepe, M.**, Alpas, H., and Bozoğlu, F., 2005. High hydrostatic pressure (HHP) inactivation kinetics of *Escherichia coli* O157:H7 and *Listeria monocytogenes* in broth and low acid foods. TUBITAK, 1st International Food and Nutrition Congress, Poster No. 54. 15-18 June, Istanbul, Turkey.
- 4) **Pilavtepe, M.**, Alpas, H., and Bozoğlu, F., 2006. Effect of high hydrostatic pressure (HHP) for sensitizing *Listeria monocytogenes* in carrot juice. IFT,

Annual Meeting and Food Expo, Poster Session (039J- 20), June 24th-28th, Orlando, Florida, US.

- 5) **Pilavtepe, M.**, Alpas, H., and Bozoğlu, F., 2006. Evaluation of structural changes induced by high hydrostatic pressure (HHP) in pressure resistant foodborne pathogens. IFT, Annual Meeting and Food Expo, Poster Session (039J- 22), June 24th-28th, Orlando, Florida, US.

- 6) **Pilavtepe, M.**, Balaban, M. O., and Alpas, H., 2007. Machine vision based quantification of bacterial volume change with high hydrostatic pressure. IFT, Annual Meeting and Food Expo, Oral Session (092- 04), July 28th- August 1st, Chicago, Illinois, US.

- 7) **Pilavtepe, M.**, Alpas, H., Bozoğlu, F., and Balaban, M. O., 2007. Use of Weibull Model for the inactivation of foodborne pathogens in carrot juice by high hydrostatic pressure (HHP). Joint 21st AIRAPT and 45th EHRPG International Conference on High Pressure Science and Technology, Catania, Italy, September 17-21.